FLAVIA
FLexible Architecture
for Virtualizable wireless future Internet Access

Grant Agreement: FP7 - 257263

Specific Targeted Research Project

FLAVIA
FLexible Architecture for Virtualizable wireless future Internet Access

Deliverable Report

D5.2Novel approaches and solutions for scheduled technology enhancements

Deliverable title	Novel approaches and solutions for scheduled technology enhancements
Version	1.1
Due date of deliverable (month)	14 (30 AUG 2011)
Actual submission date of the deliverable (dd/mm/yyyy)	21 NOV 2011
Start date of project (dd/mm/yyyy)	01 JUL 2010
Duration of the project	36 months
Work Package	WP5
Tasks	5.2 and 5.3
Leader for this deliverable	BGU
Other contributing partners	ALV, CNIT, IITP, IMD, NEC, NUIM
Authors	O. Gurewitz, E. Biton (BGU), A. Krasilov, A. Lyakhov (IITP), D. Malone, P. Patras (NUIM), V. Mancuso (IMD), A. Maeder, P. Rost (NEC), P. Pileggi (CNIT)
Deliverable reviewers	V. Mancuso (IMD)
Deliverable abstract	The Document describes novel approaches and solutions developed in the FLAVIA project for enhancement of IEEE 802.16scheduled access technology.
Keywords	802.16, MAC, Radio Resource Management

FLAVIA
FLexible Architecture
for Virtualizable wireless future Internet Access

Grant Agreement: FP7 - 257263

Project co-funded by the European Commission within the Seventh Framework Programme		
DISSEMINATION LEVEL		
PU	Public	**X**
PP	Restricted to other programme participants (including the Commission Services)	
RE	Restricted to a group specified by the consortium (including the Commission Services)	
CO	Confidential, only for members of the consortium (including the Commission Services)	

STATEMENT OF ORIGINALITY
This deliverable contains original unpublished work except where clearly indicated otherwise. Acknowledgement of previously published material and of the work of others has been made through appropriate citation, quotation or both.

TABLE OF CONTENTS

Executive summary

In order to understand and derive the requirement for flexible but yet robust architecture for next-generation wireless networks platform, FLAVIA suggests and examines the limitation of existing platforms to support innovative solutions which improve the performance over wireless communication. In this report we summarize the first year main research activities on designing and evaluating novel approaches to enhance the performance of existing schedule-based OFDMA systems. Since, these research activities induce on FLAVIA architecture and design, and serve as an ongoing assessment for the developed architecture, this document also presents FLAVIA's architectural support for each suggested solution.

After a brief introduction, which provides an overview of the topics tacked in this document, the report is split into four different research areas, each corresponding to a Section or an Appendix:

(i) Section 1 focuses on radio resource allocation, in which we study both intra cell resource allocation, i.e., how resources should be distributed within a cell (between the MSs) as well as inter-cell resource allocation, i.e., how resources should be distributed between the cells (between the BSs), and a mixture of the two (joint inter/intra cell allocation).

(ii) Cellular architecture and scenarios is the topic of Section 2, in which we examine new paradigms for organizing cellular systems which benefit from the future cellular deployments.

(iii) Power-save schemes are addressed in Section 3, in which, based on a comprehensive measurement study of the power consumption of different operational modes (e.g., transmission mode, IDLE mode) on widely deployed WiMAX network cards, we analyze the performance and tradeoffs between various power-save modes, examine the limitations of existing devices and suggest protocols and algorithms to reduce the power consumption of mobile devices and base stations.

(iv) Eventually, we report in Appendix about a schedule-based solution for contention-based technologies, which suggest enhancements that support schedule-based operations over contention-based technologies.

Introduction

Work Package 5 (WP5) focuses on the design of novel approaches to enhance the performance of schedule based OFDMA systems, regardless of the employed technology. The suggested novel solutions should exploit FLAVIA's architecture, and prove its flexibility.
As detailed in Deliverable D3.1.1 [59], FLAVIA's high level MAC architecture for scheduled systems is composed of modules, each representing a service that a scheduled access technology is expected to provide. Services can have common functions, i.e., a function can be reused by multiple services. The high-level FLAVIA functionalities for scheduled access systems (e.g., 802.16 and LTE) are depicted in Figure **1**. In particular, the figure below shows the main services needed for the implementation of scheduled access.

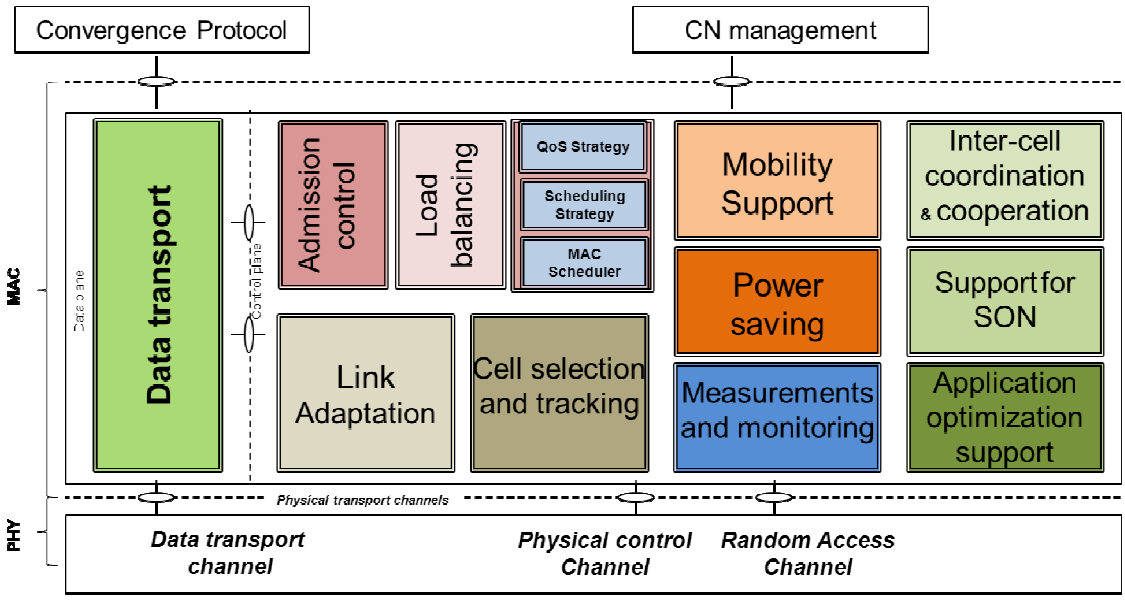

Figure 1: FLAVIA scheduled MAC functional architecture.

The figure describes a generic architecture for schedule access entity (e.g., base station, relay stations and mobile stations) and its interfaces. The modules can be differently implemented for different entities (e.g., the base station implementation is not necessarily the same as the mobile station implementation), furthermore some of the models can even be degenerate for some entities. A detailed description of each service and the decomposition of each such service into one or more functions can be found in D3.1.1 [59]. Throughout this document we will highlight the FLAVIA services that support each suggested solution.

In particular, we divide the first year research results into four different aspects of schedule access technology, namely (i) radio resource allocation, (ii) cellular architecture and scenarios, (iii) power-save schemes, (iv) scheduled solutions for contention-based technology.

(i) Radio Resource Allocation (Section 1),

Resource allocation plays a significant role in communication networks and particularly in modern wireless cellular networks. While the traffic in traditional cellular networks (i.e., voice) is mostly homogeneous emerging cellular networks are expected to carry a highly heterogeneous payload mixing voice, video, internet browsing, file transfer and more, with variable service requirements. Still, current scheduling schemes are optimized to support a single set of service preferences. Under this research field we study both intra cell resource allocation, i.e., how resources should be distributed within a cell (between the MSs), inter-cell resource allocation, i.e., how resources should be distributed between the cells (between the BSs), and a mixture of the two (joint inter/intra cell allocation). In particular we have three ongoing studies:

Flexible auction-based framework for heterogeneous traffic scheduling in wireless networks (Subsection 1.1)

We present a novel framework for wireless scheduling that supports multiple service requirements. Our framework is based on auctions, where each user bids for the wireless resources based on service requirements and channel state. We show that the proposed framework allocates resources based on each user's private set of preferences, while maintaining a notion of fairness and efficiency. The framework flexibility to schedule users' packets based on various sets of considerations opens new possibilities that are currently unavailable with state of the art scheduling schemes. Using simulations we show that the proposed framework matches the performance of existing state of the art schemes for the simple homogenous service type scenarios for which they were designed. On the other hand, our scheme outperforms alternative schemes with heterogeneous services and maintains good spectral efficiency where the other schemes fail to work.

Joint scheduling and power control with noise rise constraints (Subsection 1.2**)**

Frequency-Division Multiple Access (FDMA) based schemes, such as Orthogonal-FDMA (OFDMA) and Single-Carrier FDMA (SC-FDMA) have been endorsed in most emerging broadband wireless standards such as IEEE 802.16e/m and LTE (Long Term Evolution). Resource allocation in such systems is quite challenging, in particular the uplink power allocation due to the diverse transmission power of the subscriber stations (SS). In this study we consider the joint uplink scheduling and power allocation problem. Common techniques for the uplink resource allocation adopt the classic power control schemes in which all users are received with the same Signal to Interference-plus-Noise Ratio (SINR). Nonetheless, these techniques are less appropriate to OFDMA based channel access that suffers mostly from inter-cell interference. Our approach suggests a novel scheduling approach in which each base station (BS) besides distributing the ordinary resources (time and frequency band) according to some fairness criterion and channel condition, also manages its uplink power budget, such that the aggregate noise rise caused by its subscribers at its neighboring cells is bounded. Using a comprehensive set of simulations, we show that the suggested approach increases dramatically the overall throughput achieved in each cell, while maintaining a high level of fairness.

Traffic-Centric modeling methodology for studying connection admission control (CAC) and scheduling synergy in WiMAX/LTE systems (Subsection 0)

Much work has been and is still being done on scheduling and connection admission control (CAC) in WiMAX/LTE system. However, these are typically studied independently or without considering a strong interrelationship between these functions. By allowing both scheduler and CAC to consider the current quality of service (QoS) status in the network, it would be ideal to exploit the synergy that is evident. The initial problem with developing a joint scheduling and CAC mechanism is having a reasonable performance modeling methodology. The resource requirement and intricacies and complexities of the exercise and the system respectively, demands a different more efficient approach. We describe our novel performance modeling methodology and the generalizing 4G framework to be used to develop hybrid analytic-simulation performance models. Resulting hybrid models will aid the development of such joint QoS management mechanisms and evaluation of different system scenarios in a highly extensible and credible manner.

(ii) Cellular Architecture and Scenarios (Section 2)

Currently deployed cellular networks still rely on a macro- and micro-cellular architecture without advanced cooperation and coordination possibilities. However, this changes with the development and deployment of next-generation mobile communication systems such as IEEE 802.16m and 3GPP LTE-A. These systems rely on the support of relay nodes, femto-cells, as well as multi-cell cooperation. Furthermore, future deployments will be characterized by a tremendous increased cell density. This requires new approaches to organize cellular systems in order to benefit from the future cellular deployments. These approaches will heavily rely on novel MAC protocols and coordination techniques supporting the operation of cellular networks. Among others, those protocols will allow for more inter-BS coordination and information-exchange. Furthermore, they provide more flexibility which is a pre-requisite to implement future-proof algorithms. The FLAVIA framework shows one way to provide the means to implement scalable and flexible algorithm for future cellular networks. This section presents algorithms that exploit FLAVIA's flexibility and provide significant benefits in future cellular networks.

A flexible assignment of the uplink and downlink of mobile stations to base stations (Subsection 2.1)

Energy costs became a major part of operational expenditure of mobile operators. At the same time, wireless broadband services require increasing throughput. In this section, we present and evaluate a novel asymmetric user assignment scheme, which allows for major energy savings while guaranteeing a minimum quality-of-service. This scheme separates the association of users to base stations in uplink and downlink, such that in overlay deployments parts of the radio access network can be switched off. System-level simulations show that the novel scheme enables energy savings of up to 15% and 60% over typical macro and micro cell deployments, respectively. All numerical results are obtained in accordance with the guidelines and requirements of IMT-Advanced systems and based on the system definitions of IEEE 802.16m.

Dynamic assignment of UL/DL sub-frames in TDD systems in order to increase system capacity (Subsection 2.2)

A prerequisite to obtain full spatial reuse is to cancel or mitigate inter-cell interference, which is limiting the cell throughput. In order to derive new strategies for cellular interference-mitigation, this section analyzes achievable uplink-downlink data rates for different inter-cell interference

scenarios. Among others, this section discusses an asymmetric protocol exploiting cross-uplink-downlink interference, i.e. two adjacent cells do not operate simultaneously in uplink or downlink but only one of both is active in uplink and one is active in downlink. Using analytical results, it is shown that under specific conditions this approach provides performance gains over conventional approaches and close to multi-cell MIMO. Although this approach is not able to improve the performance under all channel conditions, it provides a new degree of freedom which might be exploited if inter-cell interference significantly impairs the performance.

Reliable multicast (Subsection 2.3)
IEEE 802.16 considers multicast as unreliable service, which is inappropriate for many multimedia applications making strict QoS demands. We propose and study new reliable multicast mechanism to support multimedia QoS. This mechanism is based on the concept of multiple ACK-leaders, that is, multicast recipients responsible for acknowledging data packets. Specifically, we propose assigning some recipients as ACK-leaders by allocating ACK slots in the ACK-CH part of the uplink sub-frame for the recipients. We develop a mathematical method to select ACK-leaders for a given multicast stream so that specific QoS requirements can be met and consumed bandwidth is minimized.

(iii) Power-save schemes (Section 3)
One of the biggest advantages of next generation cellular technology (3.5G going on 4G) is their ability to provide widespread coverage providing connectivity all over. Users in such networks are expected to be mobile. The mobility of the devices in such cellular network implies not only limited accessibility to power but also portability (small and light with small batteries), hence, power-saving mechanisms are crucial for conserving the power of the mobile terminals. Former cellular technology (e.g. 2G and 3G) utilized power-save mechanisms. However, unlike these technologies which were mainly designed for voice applications, 4th generation cellular technology will integrate voice and data, supporting a variety of applications wherein traditional telephony will only play a secondary role. Accordingly, next generation power-save mechanisms are expected to be more challenging as more applications need to stay tuned regularly (periodically or non-periodically). In this study we examine analytically the performance and tradeoffs between various power-save modes. We also measure the power consumption of the regular operational mode and the IDLE and SLEEP modes, and suggest protocols and algorithms to improve the power consumption of the mobile devices. In particular in this document we describe two studies.

Experimental assessment of power-save behavior of commercial IEEE 802.16e network cards (Subsection 3.1)
IEEE 802.16e (WiMAX) network cards are widely used in today's pre-4G cellular networks worldwide. These devices, either embedded as cards in hosts such as laptops and smart phones or USB dongles, provide mobile wireless broadband access to users within the cellular network coverage area. In this study we provide a comprehensive set of measurements of five leading commercial WiMAX network cards, a comparison between the power consumption of the regular operational mode and the IDLE and SLEEP modes. We further identify the power consumption distribution of the different operational modes (e.g., data reception and transmission, map reception, HARQ, CQI, passive listening, etc.) within the common working mode. We show that even though

theoretically power consumption can be dramatically reduced by employing an efficient algorithm which alternates between power-save and operational modes, lack of cross layer coordination between the applications, the operating system and the network card prevents efficient power save implementation. Accordingly power-save protocols which are defined by the IEEE 802.16 standard are rarely applied, and when applied they are inefficiently implemented. We present a different approach for power-save operation termed Intra Frame Power Save (IFPS), which is supported by the standard and does not require any cross layer coordination. We evaluate IFPS on two of the examined devices and show that IFPS operation mode can save 90% of the power saved by the standard IDLE mode even when the device is completely idle. We further show how IFPS can dramatically reduce the power consumption even while the device is in operational mode, and suggest ways for further reducing power consumption by taking into consideration MS supporting IFPS mode while performing the schedule by the base station (BS).

Power save analysis for base stations and mobiles with continuous connectivity (Subsection 3.2)
In this study, we analyze the power save and its impact on web traffic performance when customers adopt the continuous connectivity paradigm. To this aim, we provide a model for packet transmission and cost. We model each mobile user's traffic with a realistic web traffic profile, and study the aggregate behavior of the users attached to a base station by means of a processor-shared queueing system. In particular, we evaluate user access delay, download time and expected economy of energy in the cell. The model is validated through packet-level simulations. Our model shows that dramatic energy savings can be achieved by both mobile users and base stations, e.g., as much as 70% of the energy cost due to packet transmission at the base station.

(iv) Scheduled solutions for contention-based technology (Appendix A)
Scheduled MAC approaches cannot only provide quality of service guarantees but potentially can also provide better physical resource utilization over traditional contention-based technologies, especially under heavy traffic loads. Such better channel utilization is attained by efficiently distributing resources such as time, frequency and power, between the users, in a manner that avoids transmission conflicts (i.e., "collisions") and channel idle periods. Nonetheless, in order to attain such high utilization, in contrast to contention-based access schemes which are decentralized, schedule-based MAC schemes usually require a central controller and non-negligible signaling overhead for acquiring complete information about the demand of the users and the network conditions. Furthermore, in contrast to contention-based access schemes such as 802.11 WLANs, traditional schedule-based protocols such as 802.16 or LTE are typically deployed in licensed spectral bands, hence involve significant deployment costs. In this study we suggest hybrid solutions that combine the best features of contention-based and scheduled-based schemes. We assess how such contention-free MAC protocol can be implemented in the context of FLAVIA architecture. Even though scheduled solutions for contention-based technology relate to the contention based architecture, we bring it as part of the scheduled based research, as it was discussed and was examined by the schedule access working group.

1. Radio resource allocation

1.1 Flexible auction based framework for heterogeneous traffic scheduling in wireless networks

Radio resource scheduling is one of the most important parts in modern cellular networks. The scheduler is required to carefully balance between the network operator's desire to maximize revenue and the user's demand for satisfactory *Quality of Service* (*QoS*) or *Quality of Experience* (*QoE*). To maximize their revenue, operators seek to minimize the resources allocated to a single user and to maximize the number of supported users. Users, on the other hand, strive to receive a satisfactory service level.

In early generations of cellular networks the meaning of satisfactory level of service was quite simple as all users got basically the same service, namely, voice. However, as technology evolves voice traffic no longer dominates the cellular networks and the data traffic volume constantly increases. Indeed, 4th generation cellular standards like LTE and WiMAX focus on delivering a more efficient data transmission.

Unlike homogenous voice networks, cellular data networks are heterogeneous in nature, serving a multitude of applications like web browsing, video streaming, Voice over IP (VoIP), file sharing, gaming, and more.

The diversity of applications translates into diversity in users' requirements from the network. While a user that downloads a large file is interested in the sustained throughput, a user playing an interactive game would focus mostly on the system's latency when passing singled-out packets. Furthermore, we need also consider the diversity in channel conditions among users, and the change of these conditions over time.

The importance of radio resource scheduling has drawn much industry and academic attention. Most of these works focused on balancing two requirements, namely, fairness and resource efficiency. Although receiving much attention, most of the work done did not capture the true diversity of the problem, giving a single dimension solution. The commonly proposed solutions include, (i) rate fairness – maximizing the equality of rate between users, usually at the cost of overall efficiency, (ii) *Proportional Fairness* (*PF*) - focusing on efficient allocation of resources based on current channel conditions, considering fairness in resources instead of rate [1], and (iii) *Earliest Deadline Due* (*EDD*) – prioritizing packets based on their due deadline trying to efficiently meet the deadline, not considering fairness at all. Little work has been done to consider all traffic types (e.g., [2], [3]), where the dominant approach was to impose strict priority between the service types. That is, schedule according to the EDD discipline to support delay requirements, then employ the GPS (Generalized Processor Sharing) discipline to support rate fairness, and finally use the PF scheme to support best effort traffic. However, such an approach hardly explores the potential user diversity gain of the wireless channels (which is obtained here solely for the best effort traffic). Some limited approach for supporting best effort traffic together with delay sensitive traffic has been proposed in [4]. However, a comprehensive framework for the efficient wireless scheduling of heterogeneous traffic is an open challenge.

The problem of maximizing the satisfaction of a varied set of users, with different motivations and goals, is not unique to the world of radio resource scheduling. A similar problem is one of the basic

problems of economics, where one aims at distributing goods (i.e., resources) between different people/companies (i.e., users). The value of the goods may change from user to user. A mechanism to define the way to distribute the goods to the users while maximizing the social welfare is called for.

This work exploits results in game theory to solve the above-mentioned economic challenge. Specifically, it defines a novel economic framework for radio resource allocation with heterogeneous service requirements. The economic framework includes: (i) monetary resources (money) management, (ii) allocation of goods in exchange to monetary resources, user selection and price setting (2^{nd} price auction), (iii) A system to record the amount of money each user has in its disposal, keeping account of both payments paid in exchange for goods and money allocated.

While auction mechanism was already suggested as a means for radio resource allocation ([5,6,7,8,9,10,11]), it was mostly considered as an alternative fairness scheme, termed 'competitive fairness' in [5]. Careful examination may reveal that proportional fair scheduling could be formulated as a 1^{st} price auction, while the novelty of the introduction of 'competitive fairness' based on 2^{nd} price auction is limited. None of the above works considered heterogeneous scenarios, or paid real attention to the importance of the monetary system.

The novelty of this work, in contrast to prior work done on auction based scheduling, is twofold. The first major novelty is the usage of the auction mechanism and concept of money to mix diverse valuation functions representing different sets of considerations and requirements. The second difference is the definition of the supporting monetary system, implementing fairness, service differentiation, priority and Quality of Service (QoS) considerations through monetary allocation functions.

We further show that the differences highlighted above make the heterogeneous auction based scheduling scheme unique in its abilities to implement efficiently mixed scheduling schemes. The scheme flexibility to support each packet of each user with a different set of considerations (e.g. priority, deadline, and/or budget) opens new possibilities to the way scheduling and applications are interacting.

To further demonstrate the advantages of the proposed framework, we compare via simulations the performance of the heterogeneous scheduling scheme to that of the classic scheduling schemes. We consider scenarios with various levels of traffic heterogeneity. The simulation results show that while the proposed scheduling scheme matches the performance of traditional schemes at homogenous scenarios, it efficiently allocates resources at heterogeneous cases, where other schemes fail to meet the minimal requirements.

1.1.1 Problem formulation

We consider the resource allocation problem in a single base station connected to a set of users through time and frequency varying wireless channels.

We assume that the base station controls the medium access by assigning subsets of its sub-carriers to users, such as in OFDMA systems. In other words, the transmission resource is partitioned into frequency over time rectangles, termed resource blocks or slots. We shall use the terms resource blocks and slots interchangeably. We assume that a resource block can be used by a single user. We index the slots in an increasing order and denote the index of the t-th slot with t.

We consider a communication channel between each user and the base station that may vary in time and frequency. The communication channels of the different users are independently distributed. Let $r_i(t)$ denote the instantaneous channel rate in terms of number of bits that the i-th user can transmit over the t-th resource block.

We model the channel of user i as a random process R_i, and the channel rate, $R_i(t)$ at slot index t, as a random variable with a generalized probability density function (which may include the Dirac delta function) $b(r) = f_{R_i(t)}(r)$

$$\boldsymbol{b(r) = f_{R_i(t)}(r) = \frac{d}{dr} F_{R_i(t)} = \frac{d}{dr} Pr[R_i(t) \leq r].} \qquad \textbf{(1.1.1)}$$

We assume the user has information about its channel rate distribution at each slot. We further assume that the user knows its channel rate at slot $t - \tau$. Given its channel rate at slot $t - \tau$ was r^* (i.e., $R_i(t-\tau) = r^*$). We denote this conditional distribution with $b(r/r^*, \tau)$:

$$\boldsymbol{b(r/r^*, \tau) = f_{R_i(t)/R_i(t-\tau)}(r/R_i(t-\tau) = r^*).} \qquad \textbf{(1.1.2)}$$

For ease of presentation, we shall omit the user index i.

1.1.2 Proposed framework

1.1.2.1 Overview

Our auction-based framework is constructed on three pillars: (i) auction based resource arbitration mechanism, (ii) bidding agents representing the users preferences, and (iii) monetary system (see Figure 2).
The first building block, i.e., the auction, is responsible for the actual scheduling. That is, selection of the user to win the allocation and the price paid. The auction mechanism allows all users to compete over all allocations. The allocation process by itself is very simple, and fair, i.e., allocating the resources based solely on the bid placed by the users.
The second part of the scheduling mechanism is the user bidding agent. The bidding agent goal is to convert the user value for an allocation to a monetary value used for bidding. This translation considers both the usage the user is intending for the allocation and the monetary resources at the user's disposal.
As an output from the bidding agent we get the user valuation of the resource block. The valuation is derived in a way that will maximize the user aggregated value taking into account the roles of the game and the user's private knowledge**.**
The third part of the scheme is the monetary system. The monetary system controls the long term behavior of the scheduling mechanism. As part of the monetary system, each user has a 'bank account'. In the bank account we record all allocation of monetary resources to the user, and all payments for won resources. The monetary system may influence the user bidding-agent bid, using a regulation function based on the user bank account balance.

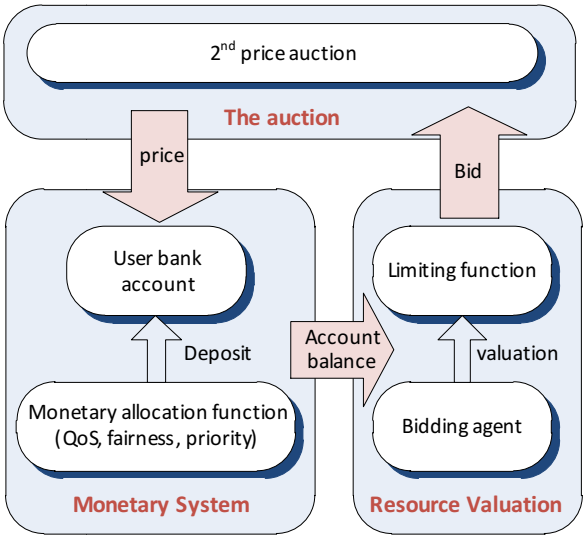

Figure 2: Structure of auction-based heterogeneous scheduler.

Logically, the scheduling functionality is presented as distributed between three entities, the auction representing the resource owner (the base-station), the bidding agent representing the user, and the monetary system that may represent a centralized network entity. In practical implementation we may either exploit this logical split to implement a distributed scheduler, or select to implement a unified scheduler, implementing all elements at the base-station.

1.1.2.1.1 The auction

In our framework, users compete for resources sequentially for an infinite number of resource blocks. Each user is assumed to have a certain amount of money. This money can only be used for bidding for resources and has no value outside the allocation mechanism. For each resource block users have their private valuation of the resource, which is translated into a "bid".
These characteristics give rise to an auction. We consider the second-price auction, where users submit a bid and the scheduler allocates the resource block to the user that made the highest bid. The price of the resource block is determined by the second highest bid. This price is deducted from the winning user's bank account.
We note that our auction mechanism is a modified version of a game of N players with independent private values and incomplete information [12].
The second price auction mechanism is adopted here since its incentive compatibility feature (a.k.a. truth telling) make the strategic problem confronting bidders in second-price auctions very simple. The user's optimal strategy is to bid the true value, further allowing a distributed implementation of the mechanism [9]. The fact that the second price auction maximizes the social welfare (aggregated value) makes it the optimal mechanism to maximize the users' aggregated value.

1.1.2.1.2 Resource valuation

We assume that 'the user' holds a truthful valuation of the allocation unit for auction. This valuation is private and is based on its (private) knowledge of its channel conditions $r(t)$ and other private information like the amount of information needed to be sent, QoS considerations, and the amount of monetary resources held.
As the money granted can only be used to pay for won auctions, it is desirable for each user to spend all money on hand.
Let Y denote the highest valuation all other users. The probability density function of Y is given by

$$\boldsymbol{\phi(y) = \frac{d}{du} F_Y(y) = \frac{d}{dy} Pr\left[max_{j \neq i}\, v_j \leq y\right].} \qquad \textbf{(1.1.3)}$$

We will generally assume that $\phi(y)$ represents a steady state that takes into account the bidding strategy of the user.
In practice, we can first calculate the user's bidding strategy using $\phi(y)$ that represents the steady–state without our user, and then recalculate the function $\phi(y)$ with the impact of the new user. After this we iteratively calculate the user's new bidding strategy and the new $\phi(y)$ reflecting changes in strategies.
It can be shown that this process is monotonic as in each iteration the difference between the aggregated user-budget and the money paid for auctions decrease as a result of the users' increasing their bids. The proof of the above is omitted for space considerations.
We additionally assume that while the user knows $R(t)$ just before the auction, the probability density functions $b(r)$ or $b(r/r^*, \tau)$ is also known

1.1.2.1.3 The Monetary system and fairness mechanisms

While the arbitration mechanism for resource allocation has received much attention in the literature, the monetary system that supports it has been hardly explored. In this section, we provide the basic definitions of the monetary system and lay its foundations. The monetary system is further explored in Section 1.1.2.3.

The auction mechanism manages the short term 'competitive' fairness, allowing all users to compete on each allocation. Nevertheless, the auction is a singled out event in time, with no notion of long term fairness. Providing a whole solution, the monetary system copes with long term fairness as well as with service differentiation. For this purpose, each user has a virtual "bank account". The bank account keeps the monetary resources allocated to the user balanced with the money spent on won bids.

The user's bank account balance at time t may impose limitations on the user bid for the t-th auction. This is obtained via a monetary regulation function f_m. We have,

$$\boldsymbol{\bar{v} = f_m\left(v, w(t)\right);} \qquad \textbf{(1.1.4)}$$

where $\bar{v}$ denotes the actual bid used in the auction mechanism, v denotes the real valuation of the slot, f_m is a monetary regulation function, and $w(t)$ is the bank account balance at time t. For example, the regulation function can take the form

$$f_m(v, w(t)) = min(v, w(t)). \quad (1.1.5)$$

Here, the user's bid is limited by the money the user has at its disposal, or in other words, **no credit is allowed** for the user. Another form of a monetary limitation function may be:

$$f_m(v, w(t)) = min(v, w(t) + C). \quad (1.1.6)$$

Here, C denotes the credit the auction mechanism is granting the user.
In the auction mechanism, the money goes only in one direction, from the user bank account to the auction manager. Now, a mechanism that allocates money back into the user bank account should be defined. In our framework, this functionality is managed by the monetary allocation function.
The monetary allocation function can take various forms. We shall refer to the simplest form as the constant *paycheck*. The constant *paycheck* function is defined as follows:

$$w(t^-) = w((t-1)^+) + M_{avg}. \quad (1.1.7)$$

The notations $(t-1)^+$and t^-, denote that the user bank account is granted a constant amount of money after the $t-1$ auction and just before the t-th auction.
Based on this simple monetary allocation mechanism and on a regulation function (e.g., (1.1.5)), the auction mechanism can enforce the average amount of money limitation used in the derivation of the resource valuation functions.
By setting different values of M_{avg} to different users, we can simply differentiate the service provided to various users.
One shortcoming of the above definition arises when dealing with the case where the user transmit queue is not always full. In this case, user that has data to send only a small fraction of time, may block other users, each time they have data to send.
One way to reduce the blocking effect is to modify the pay-check function to include limitations on the amount of saving allowed. The modified function in this case will be

$$w(t) = min(w((t-1)^+) + M_{avg}, SL); \quad (1.1.8)$$

where *SL* denotes the saving limit allowed.
Other monetary allocation functions may be based on data queue state, the amount of data to be sent, priority, strictness of deadlines, etc.

1.1.2.2 Resource valuation

In this section we discuss the user valuation of a resource block according to its required service. Typically, a user is interested either in throughput (rate) or in delay (deadlines). In both cases we derive the user valuation of a resource based on (i) the user knowledge of the channel, (ii) the distribution of the highest bid of other users, and (iii) the available "money" at the user's disposal.
We focus on rate and delay demands, which are commonly required by most applications. However, the valuation of other service demands, such as jitter (single allocation every few slots), could be derived using a similar methodology. Clearly, with valuation at hand, these services can be easily incorporated to our framework.

1.1.2.2.1 Throughput maximization

Consider users with best effort traffic, such as web browsing, file transfer and emails. In this case, the user will optimize the experience when the long term throughput is maximized. The user is only interested in maximizing the throughput and has no gain from any other requirements such as delay guarantees.

Next we devise the user valuation of an allocation unit (resource block) that maximizes its throughput. Although, we obtain a closed form for the resource valuation, its computation could be prohibitively complex. Accordingly, we devise a practical scheme for approximating the valuation.

As discussed above, we assume that the user can spend on average M_{avg} money units, and gain nothing from spending less. The user valuation of the resource unit, as in real market is based on two things, namely, (i) the market view or how other users evaluate the good ('street price'), and (ii) the private value of the good to the user. The private value depends on the usage the user designates for the good. In our case, the user seeks to maximize throughput; therefore, the user valuation will be based on the transmission rate (or number of bits) over the resource block.

The user seeks to maximize throughput; accordingly, the user is motivated to buy bits at the lowest price possible. Assuming an offline allocation, the user would buy bits in ascending price order until budget was consumed. Assume that budget is consumed when the price per bit reaches a value of $q^{\max}$. For a lower price per bit, the user would be left with some money. Clearly the user valuation of a bit should follow a similar approach. That is, the price per bit for which the user is left out of money (on the average). We note that there might not be a price per bit for which the user exactly consumes the budget. In that case, the user valuation per bit should be that $q^{\max}$ for some auctions and a bit less for others, such that the entire budget is consumed.

The following proposition devises the user resource valuation for maximizing its throughput.

Proposition 1: Given the user instantaneous transmission rate over resource block t - $r(t)$, the user resource valuation for maximizing its long term throughput is given by

$$\boldsymbol{v(t) = r(t) \cdot q^{max}}, \qquad \textbf{(1.1.9)}$$

where

$$q^{\max} = \arg\min_q (P^{\text{avg}}(q) \geq M^{\text{avg}}) - h \cdot \delta;$$

$$P^{\text{avg}}(q) = \int_0^{\infty} b(r) \int_0^{r \cdot q} y \cdot \phi(y)\, dy\, dr.$$

δ is a constant as small as we wish, and $h = \{0,1\}$ is a dithering function.

Proof: Assume that the user is biding with a price per bit of q, and let P be a random variable denoting the price paid by the user for a slot. Let V denote the user bid, and Y denote a random variable that is the maximal bid of other users with a probability density function $\phi(y)$. The user channel rate R is a random variable with probability density function $b(r)$.

Given the slot rate r, we have that:

$$\boldsymbol{P} = \begin{cases} \boldsymbol{Y} & \textit{if } \boldsymbol{r \cdot q} > Y; \\ \boldsymbol{0} & \textit{otherwise.} \end{cases} \qquad \textbf{(1.1.10)}$$

Accordingly, the mean price per slot is given by:

$$\boldsymbol{E[P/R=r]=\int_0^{r\cdot q} y\cdot \phi(y)\,dy.} \qquad \textbf{(1.1.11)}$$

Averaging over all possible values of r, we have

$$\boldsymbol{P^{avg}(q)=\int_0^{\infty} b(r)\int_0^{r\cdot q} y\cdot \phi(y)\,dy\,dr.} \qquad \textbf{(1.1.12)}$$

Now, the user would bid for a price per bit q as low as possible but such that $P^{avg}(q)\geq M^{avg}$, accordingly:

$$\boldsymbol{q^{max}=arg\,min_q(P^{avg}(q)\geq M^{avg})-h\cdot\delta.} \qquad \textbf{(1.1.13)}$$

Here, we set a random variable $h=\{0,1\}$ with probabilities such that

$$\boldsymbol{E[h]=\frac{P^{avg}(q^{max})-M^{avg}}{P^{avg}(q^{max})-P^{avg}(q^{max}-\delta)}}. \qquad \textbf{(1.1.14)}$$

□

We note that our result differs from that of [5] since we do not assume continuous distribution of other users' bids and continuous distribution of the channel rate. This allows working in real life conditions (e.g. quantized channel rate), and with mixed user scenarios (e.g. with and without delay requirements).
Since the evaluation of the price per bit according to Proposition 1 is not straightforward, in the following we propose a more practical blind adaptive scheme for the approximation of $q^{\max}$.
Every N auctions derive a new approximation of $q^{\max}$ according to:

$$\boldsymbol{\hat{q}_{i+1}^{max}=\hat{q}_i^{max}+\Delta\cdot sign\big(w(t)-w(t-1)+\alpha w(t)\big),} \qquad \textbf{(1.1.15)}$$

where Δ is the adaptation step and α is a constant ($\alpha<1$).
The above approximation is designed with two objectives, (i) estimating $q^{\max}$, and (ii) deriving a long term budget balance 0 (and therefore the inclusion of the component $\alpha w(t)$).

1.1.2.2.2 Delay guarantees

Next, we consider users with real time traffic such as voice, gaming, video streaming, etc. These applications require some delay guarantees to maintain a satisfactory user experience.
Each packet is associated with a deadline and the user aim at transmitting the packet within the deadline. The traffic sensitivity to a packet deadline violation is quantified by a penalty $p_{penalty}$.
For simplicity, we assume that at any time instance only one packet is pending for transmission. This model can be extended to include queues with multiple packets. It is omitted here due to space constraints.
To derive the truthful valuation of a resource block for delay sensitive traffic, we follow three steps. First, we consider the resource valuation of a single slot packet over a fixed channel. Next, we consider packets that span multiple slots over a fixed channel. Finally, we obtain the valuation of multiple slots packets over a time varying channel.

Packets with deadline over a fixed channel

Here, we analyze the valuation of a resource block to a user that is required to pass a single packet before its deadline expires. We assume that a packet spans exactly one resource block.
Denote a packet deadline by D. Consider the user i valuation $v_i(\theta)$ of the resource block allocation at time index $t_\theta = D - \theta$.
Denote by $p^{\text{avg}}(\theta)$ the average price the user is expected to pay, including possible penalty payments, when facing the auction on slot t_θ. Bidding for that allocation, the user may win the auction, transmit its packet, and pay the second highest price. Alternatively, the user may lose the auction. In that case, the user is left with $\theta - 1$ auctions to retry and transmit the packet within its deadline. The expected price then is $p^{\text{avg}}(\theta - 1)$.
Proposition 2: Given a single allocation packet with a deadline D, the user i valuation of resource block $t_\theta = D - \theta$ is given by:

$$\boldsymbol{v_i(\theta) = p^{avg}(\theta - 1)}, \qquad \textbf{(1.1.16)}$$

where

$$p^{avg}(\theta) = \int_0^{p^{avg}(\theta-1)} y \cdot \phi(y)dy + p^{avg}(\theta - 1) \int_{p^{avg}(\theta-1)}^{\infty} \phi(y)dy \,,$$

and $p^{avg}(-1) = p_{penalty}$.

Proof: Bidding for resource block t_θ the user may win the auction, transmit its packet and pay the auction second price. Alternatively, the user may lose the auction. In that case, the user is left with θ auctions to retry and transmit the packet meeting its deadline. If the user loses the auction, then its new expected price is $p^{avg}(\theta - 1)$. On the other hand, if the user wins the auction the price is bounded by the user bid $v(\theta)$. By setting $v(\theta) = p^{avg}(\theta - 1)$, the user can insure that the second alternative will be selected only if the price of winning the auction is lower than the expected price of the alternative. For negative values of θ, since the deadline expired, the expected price is equal to $p_{penalty}$.

□

Multiple slots packets

Consider the case where more than one resource block is required to transmit a single packet. Here, we assume that $p_{penalty}$ is paid if the whole packet was not transmitted before its deadline expired.
To find the valuation in this case, we adopt the following concept, evaluating the attractiveness of an investment, one should disregard money already spent, and should evaluate only future costs with future gains.
We assume that the channel is fixed. Thus, the number of resources required to transmit a packet is known. Let s denote the number of resource allocations left to send the packet, $v_s(\theta)$ the valuation, and $p_s(\theta)$ the expected cost at time index t_θ.
Proposition 3: Given a packet with a deadline D and with s resource blocks left to transmit the packet, the user i valuation of resource block $t_\theta = D - \theta$ is given by:

$$\boldsymbol{v_s(\theta) = p_s^{avg}(\theta - 1) - p_{s-1}^{avg}(\theta - 1),} \quad \textbf{(1.1.17)}$$

where, for $\theta < s - 1$:

$$\boldsymbol{p_s^{avg}(\theta) = p_{penalty};} \quad \textbf{(1.1.18)}$$

otherwise,

$$\boldsymbol{p_s^{avg}(\theta) = \int_0^{v_S(\theta)} \left(y + p_{s-1}^{avg}(\theta - 1)\right) \cdot \phi(y) dy + p_s^{avg}(\theta - 1) \int_{v_s(\theta)}^{\infty} \phi(y) dy.} \quad \textbf{(1.1.19)}$$

Proof: The proof of Proposition 3 goes along similar lines to the proof of Proposition 2.
□

Packets with Deadlines over a time varying channel

We proceed with the case that the channel connecting the user to the base-station is varying in time. Now, we don't have exact information on the number of slots needed, we only know the number of bits left to be sent.

Proposition 4: Given a packet with a deadline D and with l bits left to transmit, at time $t_\theta = D - \theta_0$, with channel rate r^{θ_0}, the user valuation of the resource block t_θ can be derived iteratively as follows:
For $\theta = -1$:

$$\boldsymbol{p^{avg}(-1, l, r) = \begin{cases} P_{penalty} & l > 0; \\ 0 & otherwise. \end{cases}} \quad \textbf{(1.1.20)}$$

For $\theta \geq 0$

$$\boldsymbol{v(\theta, l, r) = h(\theta, l, r) - h(\theta, l - r, r).} \quad \textbf{(1.1.21)}$$

In the two above expressions we have:

$$h(\theta, l, r) = \int_0^{\infty} p^{avg}(\theta - 1, l, g)\, b(g/r, 1) dg;$$

$$p^{avg}(\theta, l, r) = \int_0^{v(\theta,l,r)} \big(y + h(\theta, l - r, r)\big) \phi(y) dy + h(\theta, l, r) \int_{v(\theta,l,r)}^{\infty} \phi(y) dy.$$

Proof: The proof of Proposition 4 goes along similar lines to the proof of Proposition 2.

□

The above set of equations should be recalculated for every slot. To reduce the complexity, we outline a lower complexity heuristic. The heuristic is composed of two steps: (i) estimation of the expected number of required allocation $\hat{s}$, and (ii) calculation of resource valuation function $v_s(\theta)$ according toa simpler form of proposition 3.

Consider the estimation of s. For large values of θ_0, the expected average rate is approximately the expected average rate without the knowledge of r^{θ_0}, denoted here by R^{avg}. Therefore,

$$\hat{s} = l/R^{avg}. \qquad (1.1.22)$$

For small values of θ_0(in the order of s) the expected average rate approaches r^{θ_0}.
Hence,

$$\hat{s} = l/r^{\theta_0}. \qquad (1.1.23)$$

Since $\hat{s}$ may take a non-integer value, while$P_s^{avg}(\theta)$was developed (in the previous section) for integer values of s, we shall utilize linear interpolation. That is, define $P_s^{avg}(\theta)$ for non-integer values of s as a linear interpolation between$P_{\lceil s \rceil}^{avg}(\theta)$ and $P_{\lfloor s \rfloor}^{avg}(\theta)$, where $\lceil s \rceil$ stands for the nearest integer which is not less than s, and $\lfloor s \rfloor$ stands for the nearest integer which is not greater than s.

1.1.2.3 Fairness, QoS, and the monetary system

In the following section we show that, similarly to the world of economics, the monetary system is an essential part of the auction based heterogeneous traffic scheduling mechanism. We demonstrate that, while its basic functionality is to maintain fairness and stability in traffic heterogeneity scenarios, it also allows the flexibility to control and redefine the notion of fairness. Furthermore, it allows the operator to measure the effort required to comply with the user's SLA (Service Lever Agreement).
In previous sections we presented the monetary system as a fairness enforcing mechanism. As the valuation functions were developed to meet the average money constraint, one can ask if enforcing the constraint is really needed. A closer look at the valuation function derivation will quickly show that it is essential.
Deriving the valuation functions we assumed that the users know the channel statics, the biddings statistics of all other users, and, lastly, the preferences of the user at future time (e.g. to maximize rate with no limitation on latency). In practice, this is not the case due to the dynamic nature of mobile wireless. The channel conditions constantly vary in time and, additionally, the user preferences may also vary with changes in its payload. Consequently the user bidding statistics may vary. Under this set of conditions, the valuation function may seek to keep its budget balanced, but possibly it cannot ensure it. Accordingly, the monetary system can serve not only as an enforcing mechanism, but also as a tool to derive practical adaptive valuation functions similar to the case of (1.1.15). Based on the bank account balance, the user further adapts its target rates, packet drop rate, and latency constraints to meet its monetary budget.
While the above functionality expresses the user freedom to use its allocated budget in order to optimize its satisfaction, the monetary system serves as an important tool for the operator. While proportional fairness may seem quite logical to the operator, users will seldom perceive it as a fair service. The user would prefer, for instance, to receive a minimal rate to be able to get an acceptable level of service. In this section we shall demonstrate how the monetary system can be used to implement such a requirement, while maintaining efficiency. In this example, we translate the preference in resource block allocation to weak users (with low transmission rate) to preference in monetary resource allocation. Preference in the allocation of monetary resources may also be the

results of different packages sold to the user at different prices. In both cases the operator is given a mean to measure the relative effort to support each user. Such a measure is beneficial when the operator seeks to maximize return on assets.

1.1.2.3.1 Minimal rate guarantee

In the following discussion, we assume that the user QoS contract includes: (i) a constant pay-check of at least $M_{\min}$, and (ii) a minimal throughput of $R_{\min}$, assuming that $R_{\min}$is lower than $R_{\max}$, with $R_{\max}$ being the user throughput if granted all allocations.
According to the above contract, we assume that the monetary system allocates salary of Mmoney units to the user such that its minimal throughput demand is provided. The following proposition states some property of the system behavior.
Proposition 5:

a. The user's achievable throughput R is monotonically increasing in M, as long as $R < R_{\max}$.
b. If the user bids the true valuation function of Section IV.A, it is given M_{opt} money units such that its throughput is exactly $R_{\min}$, and all users' aggregated valuation is the maximal possible over all allocations that grant the user $R_{\min}$.

Proof: Consider the first part of the proposition; Assume that the user bids with average money constraint of M; if we increase its budget by δ, the user will increase its per bit valuation$q^{\max}$ and therefore its bid prices (up toP^{avg}) are increased by δ. We note that, for the second price auction the price paid for a won auction does not change as a result of increasing the bids. Therefore, increasing the spent money can only be the result of winning more auctions, and thus increasing the throughput.
Consider, now, the second part of the proposition; based on the first part, we can conclude that M_{opt} is the minimal (and only) value that allows a throughput of $R_{\min}$. As the price the user pays in 2nd price auction (M_{opt} in our case) is the loss of value to the other users, by minimizing the price paid we minimize the loss to the other users and therefore maximize the social welfare (aggregated valuation).
□
Next we present a simple heuristic for the implementation of an efficient minimal rate mechanism.
Consider the auction mechanism that allocates a single slot at a time. Divide the sequential auctions into observation periods of N consecutive auctions. With the construction of these observation periods at hand, denote by T_i the i-th observation period. For each observation period T_i measure $R(i)$, which denotes the actual rate the user achieves over the observation period T_i. To meet the minimal rate guarantee, exploiting the monotony of the throughput as a function of M, we use the following adaptive scheme to search for the optimal value of M:
Initialization (i = 0):

$$M(0) = M_{\min}.$$

For following time intervals:

$$m = M(i-1) + d \cdot \text{sign}\big(R_{\min} - R(i)\big);$$
$$M(i) = \max(\min(m, M_{\max}), M_{\min}).$$

In the above algorithm, $M(i)$denotes the average constant paycheck for the time period T_i, and $M_{\max}$ the maximal pay-check the mechanism is willing to allocate, before it gives up trying to meet the QoS contract, and d is the search step.

1.1.3 Simulation results

In this section, we investigate the performance of the auction based heterogeneous scheduling framework, at scenarios with various levels of traffic heterogeneity. The simulation baseline includes a single base-station connected to ten users through a single path Rayleigh fading channel, with users' average SNR varied from 2 to 18dB. In the simulation 1 Mhz bandwidth was assumed.
We simulated the following scenarios:

- Scenario I – rate maximization with no latency requirements. All users use same average money constraint.
- Scenario II – rate maximization with minimal rate guarantee. Like first scenario with the addition of minimal rate guarantee.
- Scenario III – rate maximization and packet with deadline mix, single priority. Users divided into two groups first five users with no latency constraint, other five user need to transmit packets with deadline using the same priority.
- Scenario IV – rate maximization and packet with deadline of two priority levels. Like Scenario III with one more user (of the first group) given deadline and higher priority than the other users.
- Scenario V – rate maximization with minimal rate guarantee and packet with deadline mix, multiple priorities. Like Scenario IV with each of the users with deadlines given different priority (six in total) and the addition of minimal rate requirement for the four user with no latency constraints.

We set the packet drop rate goal of packets with deadline to lower than 1%. For the highest priority level we assume a target packet drop rate of 0%.Prioritization of the delay sensitive packets was implemented via differentiating the packet drop penalties. The minimum rate provisioning was obtained using the method presented in section V.
We compared the performance of our framework with that of a strict priority (between traffic types) scheduling scheme. In this scheme, resources are first allocated to delay sensitive packets. These packets are selected according to their priority, and then according to the EDD scheme, which differentiates between packets of the same priority level. Resource not assigned in the first phase are allocated to the remaining users (referred here as low priority users). In cases where a minimal rate is specified resources are initially allocated to users to satisfy their minimal rate. Finally, remaining resources are allocated to the lowest priority users based on the proportional fair scheme.
Figure 3 depicts the aggregated throughput in bits per allocation. The figure presents both, the aggregated throughput of all users as well as the aggregated throughput of the low priority users.

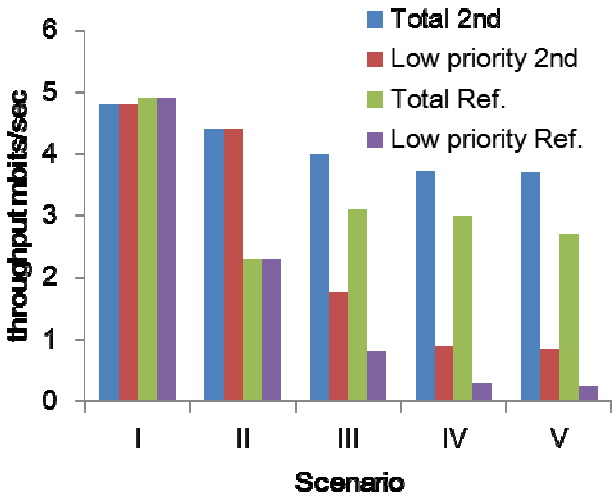

Figure 3: Total and low priority users aggregated throughput.

Consider the first (homogenous) scenario, here, no deadline or minimal rates are required, one can see that both the proportional fair scheduling and the auction based scheme perform similarly.
Considering the more complex scenarios, we can see that our auction based scheme outperforms the strict priority scheduling scheme in all parameters. In the simple, minimal rate scenario, one can see that the traditional scheduling scheme fails to efficiently deliver the minimal rate, causing a reduction of the aggregated throughput by more than 50%. The auction based scheduling scheme, on the other hand, succeeds to deliver a minimal rate of 350Kb/sec with only 10% degradation in the aggregated throughput, and a minimal rate of 400Kb/sec with less than 20% degradation. Overall, the proposed scheme allowed a minimal rate higher than the reference scheme by more than 70%.
In the third and fourth scenarios, we investigated the performance of the two schemes in the presence of delay sensitive packets, with one and two priority levels. The results in these two scenarios reveals that, while the heterogeneous scheduling scheme achieves 25-30% higher total aggregated throughput than the reference scheme, the contribution to the low priority users is dramatic, i.e., more than doubling the capacity allocated to these users.
Yet another important performance indicator is the packet drop rate due to missed deadlines. In the first, single priority level, scenario, both scheduling schemes meet the packet drop goal of 1% easily. However, in the 4th scenario, the results of the reference scheme deteriorate. In this case, the reference scheme fails to meet the target packet drop rate for the 2nd priority users, achieving a packet drop rate of approximately 4%. This high packet drop rate may be unsatisfactory for some applications. On the other hand, the heterogeneous scheduling scheme met the packet drop goal quite easily.
The result of the highly heterogeneous 5th scenario, continue on the same lines with the proposed heterogeneous scheduling scheme continuing to perform well, with an aggregated throughput of 3.7 Mb/sec (only 25% less than the peak performance of scenario I), minimal rate of 200 Kb/sec, and a packet drop rate that easily exceeds the set goals. Moreover, scenario V turned out to be too complex for the reference scheduling scheme. Not only that the strict priority scheduling scheme delivered 27% less aggregated throughput and 72% less capacity for the low priority users, it

completely failed to deliver acceptable packet drop rates for four out of the six users with delay sensitive packets, reaching packet drop rates as high as 30%.

1.1.4 FLAVIA architecture support

The proposed auction based scheduler can be realized by two main services namely (i) QoS scheduler and (ii) scheduling strategy. These services implements the following algorithms.

***Algorithm 1:* QoS scheduler**

1) At the beginning of each time interval (parameter_
   a) Allocate tokens to each active connection according to its QoS requirements

and

***Algorithm 2:* scheduling strategy**

1) For each resource block
   a) Compute the connection resource valuation ("bid") – based on (i) the connection QoS requirements, (ii) channel rate, (iii) available tokens
   b) **Allocate** the resource block to the connection with the highest bid
   c) Deduct tokens from connection "bank" according to the second highest bid

We can see that these services can be easily mapped into FLAVIA's architecture as defined in D3.1.1 (depicted in the following figure).

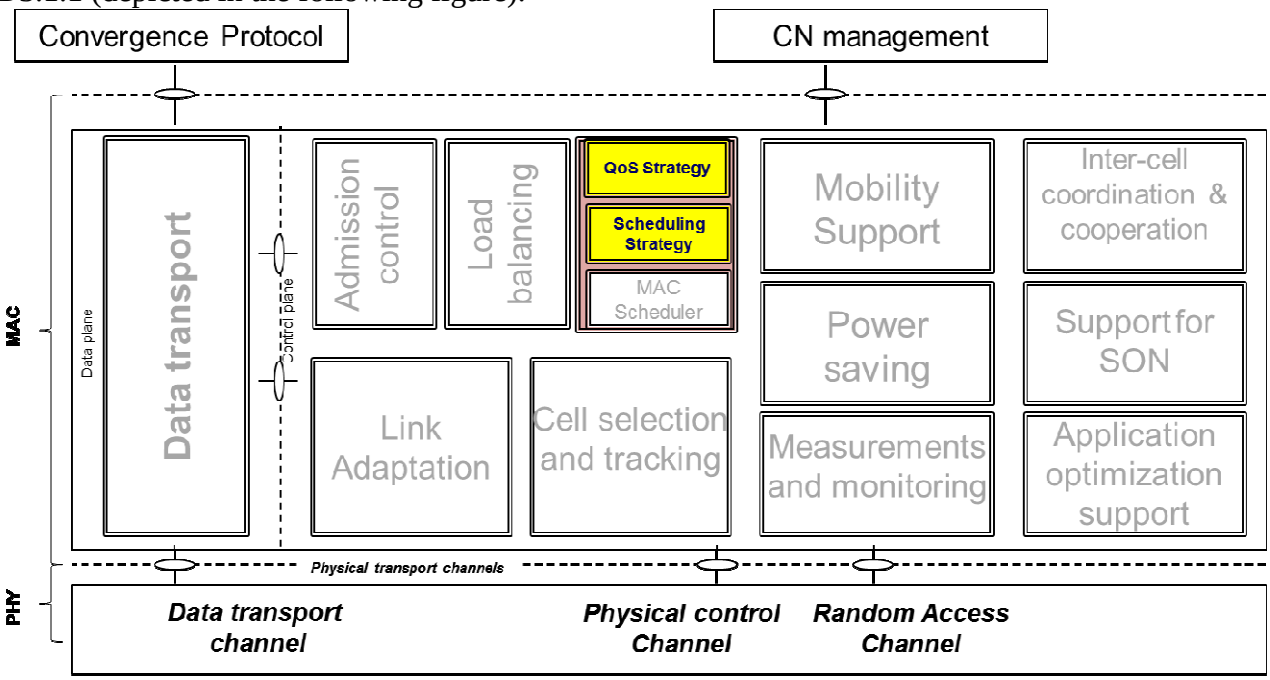

Figure 4: FLAVIA architecture support for auction based scheduling.

1.2 Joint scheduling and power control with noise rise constraints

The desire to provide integrated broadband services while maintaining quality of service (QoS) guarantees bestows growing interest in schedule access techniques used in multiple-access protocols for future broadband radio systems. Hence for example, IEEE 802.16e/m (WiMAX) adopted Orthogonal Frequency-Division Multiple Access (OFDMA) as the access mechanism, and 3GPP Long Term Evolution (LTE) choose OFDMA and Single-Carrier FDMA (SC-FDMA) as the downlink and uplink channel access methods respectively. The design of scheduling algorithms for mobile communication networks which supports the high bandwidth demands while maintaining some type of fairness is challenging due to the high variability in link-quality.

In this research we consider the joint uplink scheduling and power allocation problem for OFDMA and SC-FDMA wireless access networks. Two common approaches for the uplink resource allocation are either to assign transmission power to the Mobile Stations (MSs) such that all users are received at the Base Station (BS) with the same Signal to Interference-plus-Noise Ratio (SINR), or to allow users to transmit at their maximal available power while distributing the resources (time and bandwidth) according to the fairness notion. Although the orthogonality between different frequency bands (sub-channels) in OFDMA as well as in SC-FDMA, removes the intra-cell interference and the near-far problem typical of the CDMA-based systems (i.e., the transmission on one sub-channel will not contribute to the SINR received on a different sub-channel), both of these techniques optimize the user/cell throughput neglecting the interference injected to neighboring cells. However, since the system is still sensitive to inter-cell interference, the interference from neighboring cells can dramatically decrease the SINR received at the BS hence reduce the MS throughput. As a result, the role of the Power Control (PC) becomes decisive in providing the required SINR while controlling at the same time the interference caused to neighboring cells. This is challenging as on the one hand MS near BS is expected to have high quality link hence high throughput even when transmitting in low power while distant MS needs to transmit in much higher power to attain the same throughput, and on the other hand as far as inter-cell interference is concerned, MSs near BS can transmit in high power since they are not in the proximity of other BSs, while distant MSs which can be in the proximity of other BSs should not transmit in high power as they can interfere with other (neighboring) BSs.

In order to limit the interference to neighboring cells, 3GPP has recently approved the use of Fractional Power Control (FPC). This new proposal makes users with a higher path-loss operate at a lower SINR requirement so that they will more likely generate less interference to neighboring cells. According to this approach to preserve fairness properties most of the resources should be allocated to far-away MSs. The 3GPP LTE standard suggests a different approach for inter-cell interference handling termed Inter-cell interference coordination (ICIC). ICIC provides tools for dynamic inter-cell-interference coordination of the scheduling in neighboring cells such that cell-edge users in different cells are preferably scheduled in complementary parts of the spectrum when required. However, ICIC requires coordination between neighboring cells both in terms of exchanging information regarding subscribers at one cell and their interference level on other neighboring cells, as well as coordination in the resource allocation which further complicates the scheduling process. Furthermore ICIC requires synchronization between neighboring cells.

In this research we suggest a different novel scheduling approach which controls the inter-cell interference and does not require any cross deployment communication or coordination. Based on this approach the uplink intercell interference that each BS is allowed to contribute with its neighboring cells is limited. Accordingly, the average interference level sensed by each BS due to transmissions on its neighboring cells is bounded, which sequentially enables the transmission reception at each BS with higher SINR, hence higher throughput.

First, we introduce the noise-rise level concept for which each cell should be allowed to contribute a limited amount of interference (noise) with its neighboring cells. Accordingly each BS distributes the ordinary resources (time frequency band) according to some fairness criterion and channel condition and in addition under the constraint that the average noise it allows on its uplink transmissions into the neighboring cells is below a given limit. Obviously, the noise rise caused by each MS relates to its location with respect to neighboring cells and the transmission power assigned to it by the BS. Next, we formalize the scheduling problem under the noise rise constraint as a convex optimization problem and suggest a simple heuristics to solve it. Specifically, instead of bounding the average noise rise over all the channels allowing some sub-channels to contribute more noise rise at the expense of further limiting the noise rise on other channels, our heuristic bounds the noise rise on each sub-channel to the exact same value.

1.2.1 Problem formulation

We consider the problem of scheduling and resource allocation for the uplink of an OFDM cell, where a set $\mathcal{M} = \{1, \dots, M\}$of users transmit to the same base station. The total frequency band is divided into a set $\mathcal{N} = \{1, \dots, N\}$ of subchannels (e.g., frequency bands).

We shall assume that a permutation scheme is employed, which is the most commonly implemented scheme in WiMAX (i.e., PUSC zone). With permutations, sub-carriers from all the system bandwidth are grouped to logical sub-channels. Since each logical sub-channel is composed of sub-carriers of all frequencies, we can assume that the channel conditions over all the logical sub-channel are identically distributed.

Let x_i be the fraction of the resources (i.e., all subchannels) allocated to user i, where the total allocation across all users should be no larger than 1, i.e.

$$\sum_{i \in \mathcal{M}} x_i \leq 1. \qquad (1.2.1)$$

In practical systems (considering a single user MIMO), x_i is constrained to a fraction of the number of subchannels, i.e., a single user could transmit in a subchannel. Initially, we ignore this constraint, and consider a system in which users can share subchannels, or alternatively a system with a very large number of subchannels.

Denote by $p_i$the transmission power of user i overall subchannels, which is subject to a per-user power constraint: $p_i < P$. Let L_i be the pathloss from user i to the base station. Let r_i be the instantaneous uplink rate of user i. We assume that r_i is the achievable rate of user i in a Gaussian Multiple Access Channel using time-sharing. That is:

$$\boldsymbol{r_i = x_i\, log_2\left(1 + \frac{p_i}{x_i}\frac{L_i}{(I+N_0)}\right)}. \qquad \textbf{(1.2.2)}$$

The rate of a user depends on the subchannel radio conditions and the power allocations.
In common scenarios users have limited choices of modulation and coding schemes with a maximal rate value.

Since we consider a permutation zone, it is reasonable to assume that both the average interference per subchannel, I, as well as the average pathloss, L_i, are independent of the subchannel index j. Accordingly, the interference per subchannel is the average interference caused by all other MSs in the deployment, according to their power and subchannel allocations

$$\boldsymbol{I^{k^*} = \frac{1}{N}\sum_{k\in neighboring\ cells}\sum_{i(k)\in M(k)}\frac{L^{k^*}_{i(k)}p_{i(k)}}{x_{i(k)}}}. \qquad \textbf{(1.2.3)}$$

The first summation in ***(1.2.3)*** is over all neighboring cells except the serving cell $\boldsymbol{k^*}$, and the second summation is over all users in neighboring cell $\boldsymbol{k}$.

The optimal joint scheduling and power control allocation is a complicated task since the interference depends on the behavior of all neighboring cells. In other words, the optimal uplink resource allocation requires full coordination across the deployment. However, it is desired that resource allocation would be performed per cell without taking account of the allocation in neighboring cells. To that end, we introduce the concept of limited noise rise resource allocation as explained next.

1.2.1.1 Limited Noise Rise concept

We shall exploit two reasonable assumptions:

(i) all base stations implement the same resource allocation scheme, and
(ii) the deployment is homogenous.

Accordingly, on the average all base stations operate with the same intercell interference level$I$. Let N_r denote the noise rise above the thermal noise caused by the intercell interference, that is: $I = N_r \cdot N_0$.
By symmetry, we argue that on the average the interference the entire deployment injects to a base station equals to the interference injected by the base station to the entire deployment.
That is:

$$N_r N_0 = \frac{1}{N}\sum_{k\neq k^*}\sum_{i(k)\in M(k)} L^{k^*}_{i(k)}\sum_{j(k)}\frac{p_{i(k)j(k)}}{x_{i(k)j(k)}}$$
$$= \frac{1}{N}\sum_{k\neq k^*}\sum_{i(k^*)\in M(k^*)} L^{k}_{i(k^*)}\sum_{j(k^*)}\frac{p_{i(k^*)j(k^*)}}{x_{i(k^*)j(k^*)}} \quad . \qquad \textbf{(1.2.4)}$$

Let l_i denote the amount a user i uplink transmission increases the noise rise in its neighboring cells. More formally:

$$l_i = \sum_{k\neq k^*} L^{k}_{i(k^*)} \quad . \qquad \textbf{(1.2.5)}$$

Accordingly, all base stations should keep the noise rise they cause in neighbor cells limited. More formally, the power control and scheduling in each base station should keep:

$$\frac{1}{N}\sum_{i(k)\in M(k)}\sum_{j(k)}\frac{p_{i(k)j(k)}l_{i(k)}}{x_{i(k)j(k)}} \leq I, \forall k \quad . \qquad \textbf{(1.2.6)}$$

where, I is the interference budget for each base station.In the following, we propose a method to estimate l_i from the downlink SNR measurements, which are typically reported by the users. The downlink SNR measured by a user is given by

$$SNR^{DL}_{i(k^*)} = \frac{L^{k^*}_{i(k^*)}P_{Tx}}{\sum_{k\neq k^*} L^{k}_{i(k^*)}P_{Tx} + N_0} \quad , \qquad \textbf{(1.2.7)}$$

where P_{Tx} is the base station downlink transmission power. In interference-limited scenarios, which are typical in cellular networks, the thermal noise can be neglected relatively to the interference. Accordingly, we have:

$$SNR^{DL}_{i(k^*)} \approx \frac{L^{k^*}_{i(k^*)}}{\sum_{k\neq k^*} L^{k}_{i(k^*)}} \quad . \qquad \textbf{(1.2.8)}$$

Therefore,

$$l_i = \sum_{k\neq k^*} L^{k}_{i(k^*)} \approx \frac{L^{k^*}_{i(k^*)}}{SNR^{DL}_{i(k^*)}} \quad . \qquad \textbf{(1.2.9)}$$

1.2.1.2 Gradient-based scheduling framework

Our scheduling approach is based on the gradient-based scheduling framework [13,14,15], Each user i is assigned a utility function $U_i(W_{i,t}, Q_{i,t})$depending on their average throughput $W_{i,t}$ up to time t and their queue-length $Q_{i,t}$at time$t$. This is used to quantify fairness and ensure stability of the queues. At the beginning of each time slot t, the scheduler chooses an allocation that maximizes a weighted sum of the user's rates, where the weights are determined by the gradient of the sum utility across all users, i.e., it solves

$$\max_{r_t \in R(SINR_t)} \left(\nabla_w U(W_t, Q_t) - \nabla_q U(W_t, Q_t)\right)^T r_t, \qquad \textbf{(1.2.10)}$$

where $U(W_t, Q_t) = \sum_{i=1}^{M} U_i(W_{i,t}, Q_{i,t})$.

Further assuming that for each user i, $U_i(W_{i,t}, Q_{i,t}) = u_i(W_{i,t}) - \frac{d_i}{p}(Q_{i,t})^p$, then(1.2.10) is equivalent to

$$\max_{r_t \in R(SINR_t)} \sum_i \left(\frac{\partial u_i(W_{i,t})}{\partial W_{i,t}} + d_i (Q_{i,t})^{p-1} \right) r_{i,t}, \qquad \textbf{(1.2.11)}$$

where, $u_i(W_{i,t})$is a increasing concave function used to represent elastic data applications, $d_i \geq 0$ is a QoS weight for user i's queue length, and $p > 1$is a fairness parameter associated with the queue length.
The broad class of policies in (1.2.11) can be tuned to yield good operating points by a proper choice of parameters. If $d_i = 0$ for all $i \in M$, the resulting policy has been shown to yield utility maximizing solutions (see [13,14,15]). If $u_i(\cdot) \equiv 0$ with $d_i > 0$ for all $i \in M$, then the policy has been shown to be stabilizing in a variety of settings. The weights can also be adapted so as to maximize sum utility subject to stability or (feasible) minimum throughput constraints.
More generally, the optimization in (1.2.11) can be written as

$$\max_{r_t \in R(SINR_t)} \sum_i \omega_{i,t} r_{i,t}, \qquad \textbf{(1.2.12)}$$

where $\omega_{i,t} \geq 0$ is a time-varying weight assigned to the i-th user at time t. Our focus is on solving such a problem for an uplink ODFMA (and SC-FDMA) system, i.e., when $R(SINR_t)$ is given by (1.2.2). Note that (1.2.12) must be re-solved at each scheduling instant because of changes in both the subchannel state as well as the weights.

1.2.1.3 The Optimization Problem

Next, we formulate the resource allocation problem under the noise-rise constraint as an optimization problem. The decision the scheduler takes at the beginning of each frame is twofold, namely: (i) match a subset of the backlogged users with the available subchnnels, and (ii) assign a

rate (transmission power) to each scheduled user. The scheduling challenge in hand is to allocate the resources (subchannels and rates) to the users, aiming at maximizing the achievable rate yet maintaining a fair share of the bandwidth over time (based on a predefined fairness metric) and under the restriction that the overall interference with neighboring cells will not exceed the threshold. In other words, the scheduler needs to select the backlogged users that are eligible to be scheduled based on the fairness criterion, and distribute the power between them based on the rate each one is entitled to and the interference it causes to the neighbor cells. Note the trade-off between rate and contribution to the overall *Noise Rise* when assigning transmission powers to users. Furthermore, usually user that are far from the BS are required to transmit in a high power in order to maintain a reasonable rate, yet these users are closer to other cells, hence are also required to decrease their transmission power in order to minimize the interference to the neighboring cells.
Our suggested scheduling decision employed at each BS relies on the gradient-based scheduling framework as previously suggested in [13,14,15]. Specifically, at the beginning of each frame $k$the scheduler picks a rate vector $r(k) = (r_1, r_2, \dots, r_M)$ that is compliant with the power constraints induced by the noise-rise limitation, and that maximizes the time-varying weight assigned to each user at the beginning of the k-th frame, i.e.,

$$\boldsymbol{max_{r(k)\in\mathcal{R}} \sum_{i=1}^{M} \omega_i(k) r_i}, \qquad \textbf{(1.2.13)}$$

where $\omega_i(k) \geq 0$is the time-varying weight assigned to the i-th user at the beginning of the k-th allocation. These weights are the gradient of the increasing concave utility function of each user. We shall concentrate on utility functions that depend on the average throughput attained by each user up to the k-th frame, and capture some fairness notation (e.g., $\omega_i = \frac{1}{T_i(k)}$, where $T_i(k)$ is the average throughput at frame k, which captures proportional fairness).

Taking r_i as indicated in (1.2.2) we can formulate the joint uplink power control and scheduling optimization problem as follows:

$$\boldsymbol{max_{\underline{x},\underline{p}} \left\{ \sum_{i=1}^{M} \omega_i(k) x_i \, log\left(1 + \frac{p_i e_i}{x_i}\right) \right\}}, \qquad \textbf{(1.2.14)}$$

subject to

$$\boldsymbol{0 \leq x_i \leq 1;} \qquad \textbf{(1.2.15)}$$

$$\boldsymbol{0 \leq p_i \leq P;} \qquad \textbf{(1.2.16)}$$

$$\boldsymbol{\sum_{i=1}^{M} x_i \leq 1;} \qquad \textbf{(1.2.17)}$$

$$\boldsymbol{\sum_{i=1}^{M} l_i p_i \leq I.} \qquad \textbf{(1.2.18)}$$

Notice that the above optimization aim at finding both the fraction of channel allocated to each user, denoted by $\underline{x} = \{x_1, x_2, \dots, x_M\}$, as well as the set of powers assigned to each user and denoted by $\underline{p} = \{p, p_2, \dots, p_M\}$.Obviously the total fraction of the channel (frequency band) distributed among

the users cannot exceed one (hence (1.2.17)). Finally, inequality (1.2.18) denotes the noise rise constraint.

The derived optimization problem is a convex optimization problem (can be easily shown through the calculation of the Hessian), and thus an optimal solution exists.

To solve the joint scheduling and power allocation optimization problem we shall exploit the Lagrange multiplier method.
Associating (1.2.17) and (1.2.18) with the Lagrange multipliers $\lambda$and μ respectively, we can write the Lagrangian as:

$$\mathcal{L}\left(\underline{x},\underline{p},\lambda,\mu\right)=\left\{\sum_{i=1}^{M}\omega_i(k)x_i\,log\left(1+\frac{p_ie_i}{x_i}\right)\right\}+\lambda\left(1-\sum_{i=1}^{M}x_i\right)+\mu\left(I-\sum_{i=1}^{M}l_ip_i\right), \quad (1.2.19)$$

and solve:

$$\nabla_{\underline{x},\underline{p},\lambda,\mu}\mathcal{L}\left(\underline{x},\underline{p},\lambda,\gamma,\mu\right)=0; \quad (1.2.20)$$

which gives:

$$\frac{\partial\mathcal{L}}{\partial x_i}=\left(\omega_i\,log\left(1+\frac{p_ie_i}{x_i}\right)-\omega_i\frac{1}{1+\frac{p_ie_i}{x_i}}\frac{p_ie_i}{x_i}\right)-\lambda=0,\ \ \forall i; \quad (1.2.21)$$

$$\frac{\partial\mathcal{L}}{\partial x_i}=\frac{\omega_ie_ix_i}{x_i+p_ie_i}-\mu l_i=0,\forall i; \quad (1.2.22)$$

$$\frac{\partial\mathcal{L}}{\partial\lambda}=1-\sum_{i=1}^{M}x_i=0; \quad (1.2.23)$$

$$\frac{\partial\mathcal{L}}{\partial\mu}=I-\sum_{i=1}^{M}l_ip_i=0. \quad (1.2.24)$$

While the above equations provide the optimal solution, a closed form solution cannot be obtained. Accordingly, in the following sub-section we shall provide a heuristic that provide a low complexity sub-optimal solution (of closed form).

1.2.2 Proposed scheme

To devise a closed form sub-optimal solution we shall narrowing the solution space such that the assigned rate is configured independently of the power and frequency allocations. More precisely, instead of constraining the total noise rise over all the bandwidth, we shall assume a constrained *noise rise density*. In that case, the power and rate are determined by the constrained noise rise density. More formally, we shall assume that

$$l_i\cdot\frac{p_i}{x_i}\le I,\ \ \forall i. \quad (1.2.25)$$

Clearly, resource allocation $\{p_i, x_i\}$ that complies with (1.2.25) will not exceed the noise rise constraint in (1.2.18). Accordingly, the optimization problem can be rewritten as follows:

$$\boldsymbol{max_{\underline{x},\underline{p}} \left\{ \sum_{i=1}^{M} \omega_i(k) x_i \, log\left(1 + \frac{p_i e_i}{x_i}\right) \right\}}, \qquad \textbf{(1.2.26)}$$

subject to

$$\boldsymbol{0 \le x_i \le 1}; \qquad \textbf{(1.2.27)}$$

$$\boldsymbol{0 \le p_i \le P}; \qquad \textbf{(1.2.28)}$$

$$\boldsymbol{\sum_{i=1}^{M} x_i \le 1;} \qquad \textbf{(1.2.29)}$$

$$\boldsymbol{l_i \cdot \frac{p_i}{x_i} \le I, \ \forall i.} \qquad \textbf{(1.2.30)}$$

We are now ready to present the joint scheduling and power control scheme.

Algorithm 3: **joint scheduling and power allocation**

1) set $x_i = 0, \ \forall i, \underline{y} = \{\}$
2) repeat until all queues are empty or $\sum_{i=1}^{M} x_i = 1$ (all frequency band was allocated)
   a) let $i^* = \arg\max_{i \notin \underline{y}} \left\{ \omega_i(k) \log\left(1 + \frac{I e_i}{l_i}\right) \right\}$
   b) set $x_i = \begin{cases} \min\left(\frac{l_i P}{I}, 1\right) & \text{if } i = i^* \\ 0 & \text{otherwise} \end{cases}$
   c) set $p_{i^*} = \frac{I x_{i^*}}{l_{i^*}}, r_{i^*} = x_{i^*} \log\left(1 + \frac{p_{i^*} e_{i^*}}{x_{i^*}}\right)$
   d) $\underline{y} = \left\{\underline{y}, i^*\right\}$

1.3 Traffic-Centric Modelling methodology for studying CAC and Scheduling Synergy in WiMAX/LTE systems

Performance quality management of the more complicated 4G technologies, such as IEEE 802.16m and 3GPP LTE-advanced, depends much on the Connection Admission Control (CAC) and scheduling mechanisms used to control connection- and packet-level activities within the network, respectively. By allowing both mechanisms to consider the variable quality of service (QoS) delivered by the system, a synergy is evident [16]. Much work is still to be done on this work.

In a collaboration between FLAVIA partners CNIT and BGU, a preliminary investigation of statistical CAC confirmed that simulation through the consolidation of connection- and packet-level activities is extremely difficult, particularly due to the many orders of magnitude different in timing of events and amount of physical resource required. One typically needs to generalize or make oversimplified assumptions of the behavior of either of the levels involved.
We therefore set out to develop a modeling methodology that would allow us to study this synergy with a model that performs reasonably well. The technique is called Traffic-Centric Modeling (TCM). We have verified that the approach works for a less-complex system, by corroborating results with that of widely-accepted models. Also, we showed that the model is extensible for different scenarios and system assumptions.
A 4G modeling framework was developed that we intend to use to develop hybrid analytic-simulation models of various scenarios. This will allow the evaluation of algorithm features, particularly studying CAC and scheduler synergy, before committing them to FLAVIA implementation and deployment.

1.3.1 Traffic-centric modeling

Traffic-Centric modeling (TCM) is a modeling paradigm different from traditional modeling paradigms. Even though both paradigms include the workload model (WLM) and machine model (MM) components, TCM shifts the focus of the exercise to that which requires service from that which serves. As evident in the following figure, the generalizing traffic abstraction, called the t-unit, becomes the core of the system model.

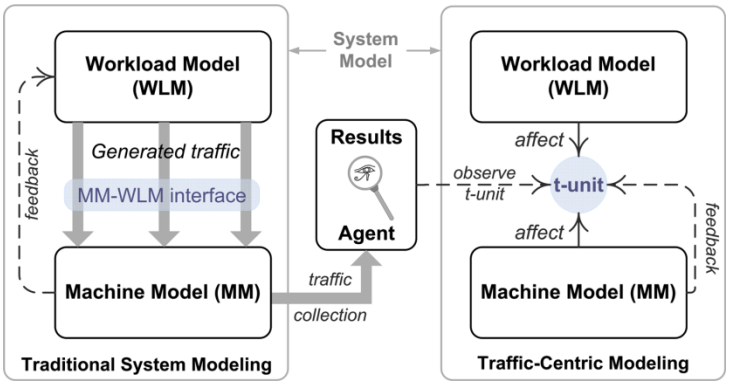

Figure 5: Comparison of traditional and traffic-centric modeling approaches.

In the TCM approach, we have both WLM and MM affect the t-unit directly, where feedback is applied to the unit, as opposed to the traditional case where the WLM feeds traffic into the MM and feedback must be explicitly communicated directly from the MM to the WLM.
Traditionally, traffic elements served by the MM are collected in some trace file that is post-processed to obtain performance estimates. On the contrary, in TCM, the t-unit stores experience, such as transmission failures, within the structure used to represent itself, making experience self-contained. Thereafter, mathematical formulation allows direct conversion from experience to desired performance metrics.
A particular methodology for developing TCM models serves as a guideline. The resulting model is hybrid, borrowing the useful features from analytic and simulation approaches but does not exclude the possibility of incorporating other modeling techniques such as hardware experimentation. Here we specify 4 steps for developing the hybrid model:

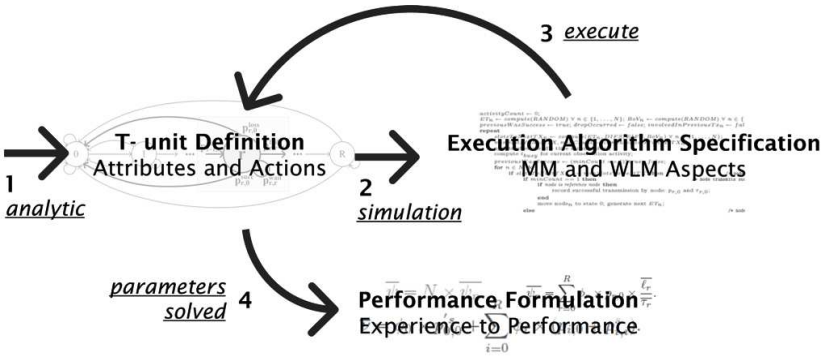

Figure 6: The 4 steps of the TCM methodology guideline.

The first step is to outline the t-unit as some mathematical structure. So far, we have identified a semi-Markov Process (SMP) and chain (SMC) as the analytic structures for the systems studied. This was convenient and effective since the possible and permissible behaviors of the traffic can be seen as a some state machine. The formulation of transition and sojourn parameters of the SMC are left undefined in this definition.
Thereafter, the WLM and MM are incorporated as an execution algorithm, i.e., an iterative process that is executed to determine the parameter values of the t-unit structure. Step 2 therefore involves defining the algorithm.
In the third step, the execution algorithm is executed until parameter values are converged upon. The convergence condition depends on the modeler. The parameter values therefore represent the actual experience of a general t-unit belonging to some category of traffic.
Finally, the experience needs to be translated into performance measures. A formulation of the performance indices required from analytic parameters are therefore the forth step.

1.3.2 Preliminary proof-of-concept work

As proof of concept, we applied TCM to a wireless local area network [17]. We found that we were able to obtain performance statistics. Furthermore, we verified our hybrid model's results to those of a widely-accepted analytic model. We were also able to show how easily other performance statistics, such as channel efficiency, we obtained. The basic model was also easily extended by changing an assumption on the workload of the system. The following figures are reproduced from the work already reported: To the left we have the normalized mean throughput reported for a system operating in basic access mode of the distributed coordination function (DCF) under 1 saturated and 2 unsaturated traffic conditions. To the right we show the mean channel efficiency for the same configuration. In both figures, we vary the number of participating nodes in the system.

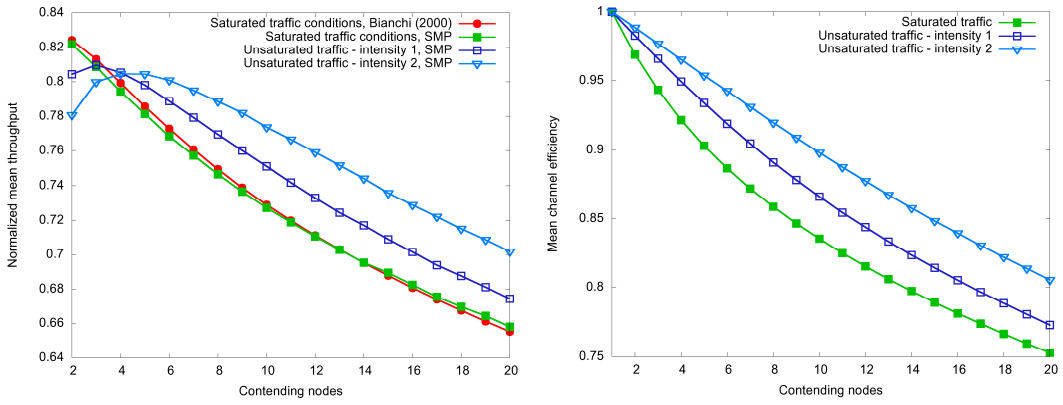

Figure 7: IEEE 802.11 DCF basic access mode verification and extensibility results for a varying number of contending nodes showing the mean normalized throughput (left) and mean channel efficiency (right).

Consequently, we have shown how effective TCM can be, even though we believe that there is much work to be done to understand the paradigm better. The resulting model is very credible and, since it is highly extensible and has a low resource intensity requirement, it is highly useful.

1.3.3 Generic modeling framework for 4G scenarios

We have presented a generic modeling framework [18] to develop 4G performance models that we shall use in FLAVIA when developing CAC and scheduling algorithms. The framework involves a hierarchical analytic structure, one level for packet-level activity and another for connection-level activity.

The packet-level activity, as shown in the following figure, involves success of transmission activities, failure of transmission activities, discarding of traffic due to whichever reason activities and idle activities. This structure is per connection and therefore each device in a system could have zero or more of these structures.

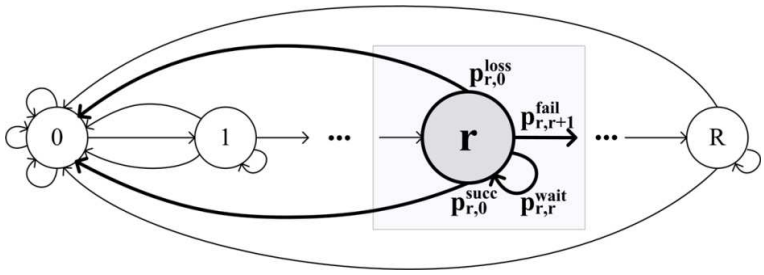

Figure 8: Packet-level per-connection structure for the TCM 4G framework.

The connection-level structure is different from the packet-level one. It is a TC-dimensional SMC, where there are TC types of service categories available in the system. Each device has one of these structures and there is a limit C_{TC} for each type of service per device. Transitions involve connections admitted by the CAC, connections refused by the CAC and no connection requests made, i.e., idle cases. These transitions are furthermore per service category.

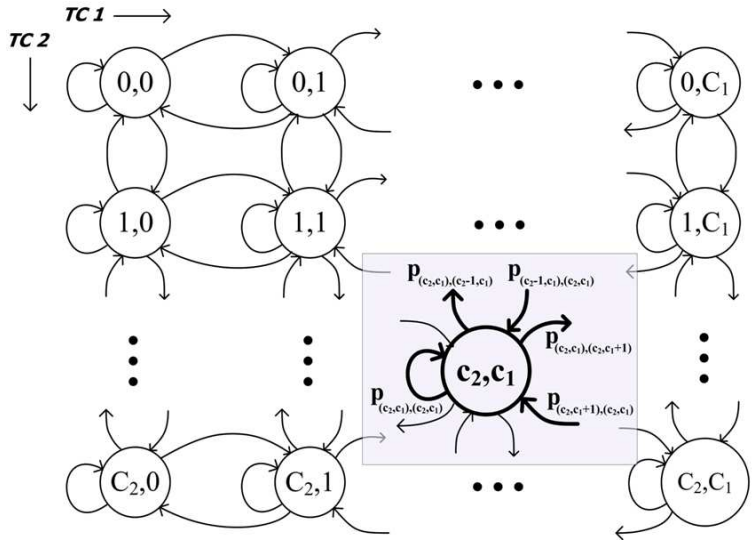

Figure 9: Connection-level per-user device chain structure for the TCM 4G framework.

The framework also specifies the execution algorithm as a set of system functions. In doing so, we make the framework highly modular, allowing quick and easy modification to the model. We should therefore be able to change the scenario as we evaluate different system configurations.

1.3.4 Future work

Ultimately, as already mentioned, we aim to develop the 4G models to develop joint CAC and Scheduler resource and connection management (RaCM). However, in order to achieve our goal, we shall develop a baseline model using the framework. It would then be safe to include more complicated system functions, i.e., more realistic channel, mobility, etc., descriptions. A more accurate workload definition should also be defined and included. The WLM must account for both connection- and packet-level activity.

2 Novel cellular architectures and scenarios

2.1 A flexible assignment of the uplink and downlink of mobile stations to base stations

Mobile communication systems face the challenge of reducing the energy-consumption while guaranteeing the required Quality-of-Service of applications. In order to achieve this, we exploit the fact that traffic patterns and link budget are different for UL and DL such that depending on the use case, either DL traffic (e.g. web traffic) or UL traffic (e.g. M2M metering services) dominates. Furthermore, constraints in the UEs, e.g. limited transmit power, imply that the UL determines the coverage area. The common approach to save energy is to turn off BSs, which, however, affects both UL and DL coverage. In order to avoid user drops and insufficient QoS though, BSs may not be turned off as otherwise either UL or DL may not be able to provide the required QoS. The section evaluates the energy-saving potential of existing cellular networks in load conditions below the maximum capacity while guaranteeing a minimum QoS.

2.1.1 System model

The analysis discussed in this section applies the guidelines of the ITU-R, which were developed as requirements and baseline assumptions for IMT-Advanced systems. We investigate two scenarios, which are typical for metropolitan areas: UMa and UMi. The UMa scenario assumes that BSs are mounted well above rooftop level in order to provide continuous coverage in rather large cells. The UMi scenario focuses on provisioning high throughput in areas with high user densities. Cell sizes are small such that the spatial reuse is increased and the number of users per cell is reduced. Micro-BSs are assumed to be installed below rooftop to increase the isolation between cells.

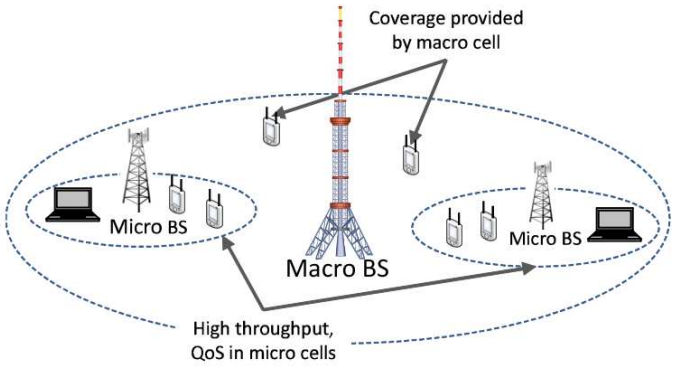

Figure 10: UMa/UMi overlay deployment concept.

In order to guarantee both continuous coverage and high data throughput, operators may choose to deploy macro- and micro-BSs in a hierarchical or overlay manner as illustrated in Figure 10.

2.1.2 Asymmetric traffic routing

This section discusses the approach of asymmetric traffic routing in cellular networks. It selectively turns off UL and DL at BSs in order to guarantee a minimum QoS in both UL and DL. Our evaluation focuses on the application of this approach to M2M communication, which has different requirements than traditional communication towards UEs with an interactive interface. For instance, M2M communication is likely to involve a higher density of terminals with infrequent, very short bursts. However, the approach can also be applied to scenarios with asymmetric traffic demands such as hotspots where a high spatial reuse of DL resources is required and the UL mainly carries signaling and controlling information.

An advantage of overlay deployments is the possibility to switch off micro-BSs for the purpose of energy saving in situations with low or no traffic load. However, many terminals, e.g. M2M devices, are deployed indoors and therefore experience high path-loss towards macro-BSs and therefore may experienced significantly worse QoS. This implies that in order to ensure a minimum QoS also to indoor users, micro-BSs cannot be completely switched off.

One solution to this problem is to assign a UE to different BSs in UL and DL. This solution relies on the assumption that BSs are inter-connected for instance through X2 in 3GPP LTE. This allows micro-BSs to turn off their DL module in order to save energy. The UL-bottleneck in a network using only macro-BSs can be avoided while the energy-saving benefits are still preserved. In addition, also the energy-consumption at the UEs is reduced as their transmit power is lower and the active time-period is shorter than in a system using only macro-BSs. We refer to this network operation as *asymmetric UL/DL assignment*.

2.1.3 Implementation aspects

In order to implement an asymmetric UL/DL assignment, we need to distinguish between logical and physical BSs. Conventional cellular networks manage each physical BS as an own logical entity, while in the asymmetric assignment a logical BS assigned to a UE might consist of different physical BSs, e.g., one for UL and one for DL.

An implementation of the asymmetric assignment involves changes on the physical and medium-access layer. However, most of these changes can be transparent to UEs and be applied only to the BS and inter-BS communication. Regarding the site selection process, let each UL-BS (which refers to the uplink-serving BS) be assigned to a DL-BS (downlink-serving BS) in order to form a logical BS. Each UL-BS forwards the received connection requests as well as the CQI to the assigned DL-BS, which then selects the UL-BS serving each UE. This implies that we can implement the proposed asymmetric assignment by only forwarding signaling and controlling information between UL-BSs and DL-BSs. Alternatively, UL-BSs could quantize their received signal and forward it to the DL-BS. However, this implementation requires significantly more backhaul while offering an additional array gain in the case of multi-cell MIMO detection. Finally, the power control at UEs is affected as micro-BSs usually have a lower path loss towards a particular UE than the macro-BS. Hence, using a distributed power control by sending CQI values from UL-BSs to DL-BSs, we can

obtain further energy-saving benefits at the terminal side. Most of these implementation changes require a flexible and adaptive MAC implementation in order to forward and process UE data correctly.

2.1.4 Test scenarios

The benefits of the introduced deployment and user assignment approaches are demonstrated for two different traffic models, each reflecting a different application scenario. The first model represents a scenario where each terminal has one single file, which needs to be delivered. Such a scenario might appear in metering applications, where nodes regularly execute measurement tasks and aggregate information over a long period of time. We model these scenarios using a Poisson arrival process of nodes which aim on transmitting one single file to the assigned BS. The Poisson arrival process reflects the case of sporadically active terminals, which do not maintain a permanent context with the assigned BS over a long period of time but only request a connection once enough data has been aggregated and the data buffer has been filled. Each UE delivers a single file originating from a typical FTP stream such that the size of each file is distributed according to a truncated log-normal distribution with mean $\mu = 0.9385$ and standard deviation $\sigma = 2.0899$. Furthermore, the file-size is lower-bounded by 500 bytes and upper-bounded by 500 kBytes.

In contrast to the previous use case, the packet arrival traffic model represents scenarios where terminals regularly need to deliver information through a mobile network. A relevant example would be, for instance, a health care data monitoring system for elderly people in order to identify any significant degradation of health status at an early stage. Another example is regular road state information about traffic density in order to avoid traffic jams.

We model the second scenario using a Poisson arrival process for each UE.A fixed packet-size is considered since most of these applications regularly transmit the same amount of information. More specifically, we assume that 210 users are uniformly distributed over the system area such that exactly 10 users are connected to each BS in the case of UMa, as defined by the IMT-Advanced guidelines, and at most 10 users are assigned to each BS in the case of UMi and asymmetric assignment. The packet size taken as representative for some of the use cases is 1024 bytes.

2.1.5 Evaluation setup

This section discusses numerical results for the previously introduced asymmetric assignment as well as for networks deploying either macro-BSs or micro-BSs. Our evaluation focuses on showing how the system is capable to maintain the required QoS under different system load.

Our results are obtained using a SLS, which has been calibrated against the channel models defined by IMT-Advanced. In the case of Uma we deploy one central site with one tier of macro-BSs using wrap-around and inter-site distance $d_{is,\ uma} = 500$m. In the case of UMi we deploy three tiers of micro-BS with one central site and inter-site distance $d_{is,\ umi} = 200$min order to simulate the same

area in both cases. For the asymmetric assignment we apply an overlay of both deployments where only micro-BSs serve the UL and only macro-BSs serve the DL.

The assignment of UEs to BSs is done based on the path-loss. Depending on the assigned BSs and whether it is a macro-BS or micro-BS, the UMa or UMi channel model according to IMT-Advanced is applied. The frame structure is implemented according to the IEEE 802.16m draft standard operating in TDD and using 10 MHz bandwidth. We further employ a proportional fair scheduler operating at frequency reuse 3 where the scheduling utility is chosen as the ratio of the expected throughput on a resource block and the previous average throughput achieved so far. BSs use four antennas and UEs use one antenna while at maximum two UEs are served on one resource block.

2.1.6 Evaluation results

At first we discuss the performance for the previously introduced high-rate user arrival model, where each UE transmits one single file. Numerical results were obtained after a simulation of 1000 super frames, i.e., overall 20s.

In order to evaluate the ability of the individual assignment approaches to handle the required load, we show in Figure 11 the actually achieved normalized cell data rate R_{cell} (dashed lines) as well as the required normalized cell data rate R_{min} (solid lines) according to Little's law. Figure 11(a) shows the results for UL and illustrates that for $\lambda > 80$, the macro-only assignment does not suffice to satisfy the demand of UEs as $R_{cell} < R_{min}$. By contrast, both the asymmetric assignment and the micro-only assignment provide sufficiently high data rates to satisfy the demands. This picture slightly changes for the DL in Figure 11(b) where all three approaches provide sufficiently high data rates in order to serve all UEs. However, the macro-only assignment outperforms the other two approaches in terms of R_{cell} due to the higher multi-user diversity. This demonstrates that in the case of using only macro-BSs, we primarily face a serious bottleneck in the UL, which can be avoided using the asymmetric UL/DL assignment.

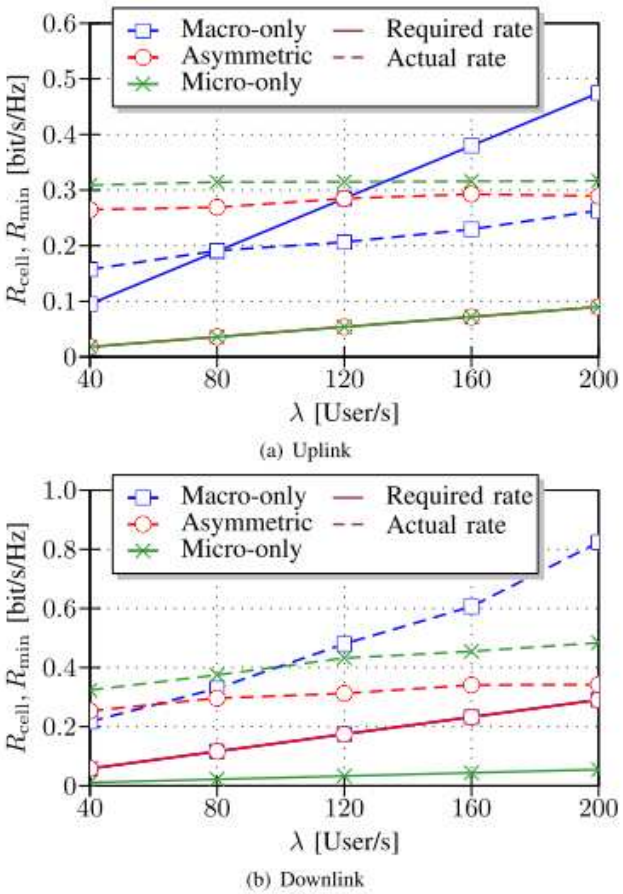

Figure 11 Required (solid lines) cell normalized cell data rate according to Little's law and actual normalized cell data rates (dashed lines).

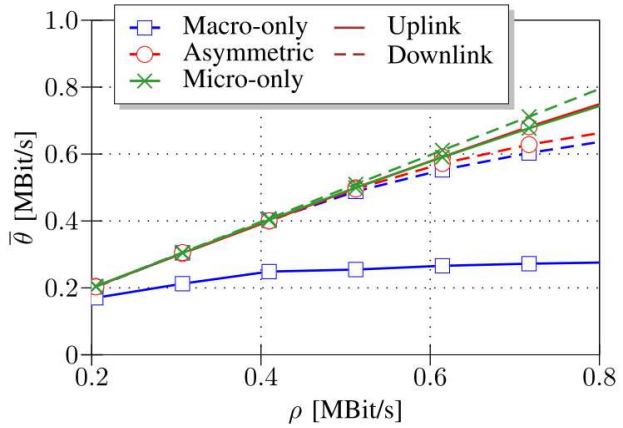

Figure 12 Average throughput θ in uplink (solid lines) and DL (dashed lines) depending on the required average load per user ρ.

Figure 12 shows the achieved average throughput in UL (solid lines) and DL (dashed lines) depending on the packet arrival rate λ= [25, ... 100] (packets/s). The results are shown depending on the required average load ρ per user given by the product of packet arrival rate λ and packet size (1024 bytes). In order to guarantee a stable system the achieved average throughput per user must not be lower than the required average load per user, represented by a bisecting line. We can immediately see that the macro-only mode is not able to cope with the required load in the UL, and in the DL only for loads below 0.6MBit/s. By contrast to UMa, a micro-only and the asymmetric assignment achieve sufficient UL rates for up to ρ≈0.6Mbit/s and in the case of micro-only assignment also the DL rates suffice for the simulated packet arrival rates. This shows that for high UL and moderate DL load, the asymmetric assignment achieves sufficient performance figures compared to the macro-only assignment, which is unable to support sufficient UL rates. The best performance is provided by the micro-only assignment at the cost of higher energy consumption as shown in the next part.

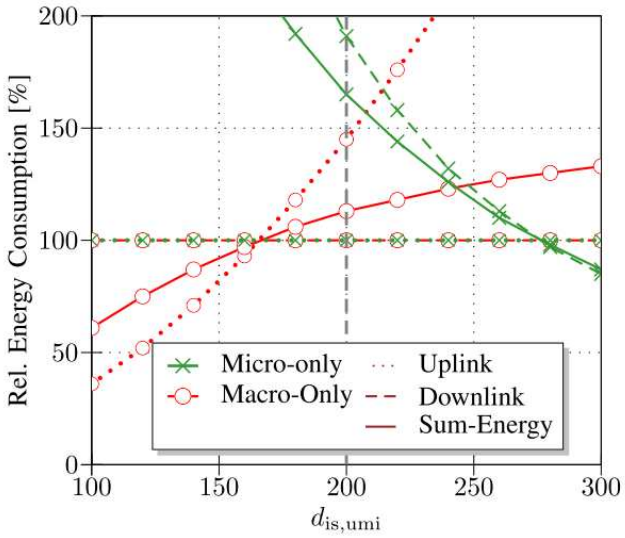

Figure 13: Energy consumption relative to the proposed asymmetric assignment in the uplink (dotted lines), downlink (dashed lines), and the sum of both (solid lines).

The energy-saving potential is emphasized with an exemplary energy budget based on the model given in [19], where an energy model has been proposed. This energy model separates the flexible energy-consumption depending on the transmit-power and the static energy-consumption depending on signal processing, power loss, battery backup and other factors. We apply the macro-BS and micro-BS model of [19] (using the UMTS1 configuration) and assume that micro-BSs require air conditioning due to the high transmit-power of 41dBm. Based on these specifications, Figure 13 shows the required energy in a network using only micro-BSs and using only macro-BSs relative to the energy-consumption of a network using our proposed asymmetric assignment.

For very short inter-site distances, the macro-cellular deployment is more energy-efficient as the high number of BSs and the static energy in UL/DL dominate in the case of micro-cellular deployments. However, the asymmetric assignment already outperforms the macro-cellular model

for about $d_{is,umi}$>170m. By contrast, the micro-cellular assignment only provides energy-saving benefits for about $d_{is,umi}$>240m. Only for very large values of inter-site distance of about $d_{is,umi}$>280m a micro-only assignment is more energy-efficient than the asymmetric assignment. However, for higher inter-site distance the performance also drops and the demand for high data rates cannot be satisfied anymore. In the case of $d_{is,umi}$=200m, which is the suggested value by IMT-Advanced, the asymmetric assignment is about 15% more energy-efficient than the macro-cellular assignment and about 60% more energy-efficient than the micro-cellular assignment.

2.2 Dynamic assignment of UL/DL subframes in TDD systems in order to increase system capacity

2.2.1 Multi-cell MIMO

The majority of existing work on multi-cell MIMO assumes perfect compound Channel State Information (CSI) and unlimited inter-site connections for which high-speed low-latency backhaul solutions are mandatory. There is the need to either improve existing backhaul technologies allowing for multi-cell MIMO implementations, or to introduce more practical approaches providing similar gains but avoiding the stringent requirements of multi-cell MIMO.

Conventional mobile communication systems align uplink (UL) and downlink (DL) transmission, i.e., adjacent BSs simultaneously transmit or receive. Furthermore, multi-cell MIMO is realized by exchanging either quantized signals (after modulation) or en-/decoded data (before modulation). Exchanging quantized signals offers diversity-gains but requires significant backhaul-resources. By contrast, exchanging en-/decoded data is more backhaul-efficient but suffers from error propagation. Furthermore, CSI must be acquired and exchanged among BSs, which requires low-latency backhaul to avoid out-dated CSI. These requirements render multi-cell MIMO across different sites as a less feasible and highly resource-consumptive method.

2.2.2 A redesigned cell-layout

We introduce a setup in which BSs do not align their UL and DL but intentionally create an asymmetric operation. An asymmetric UL/DL operation introduces inter-BS interference, which can be alleviated by successive interference cancellation (SIC) based on CSI acquired from pilots (without quantization error) and encoded data exchanged via backhaul.

Figure 14(a) illustrates a typical interference situation, where two UEs are located close to the same cell border. In this case, the model of the interference channel can be applied such that the two-way communication is a cascade of the same interference channel in UL and DL (but with different transmit powers). By contrast, consider Figure 14(b) where the left BS operates in DL and the right BS receives data in the UL. This asymmetric UL/DL operation changes the interference situation such that one BS receives interference from the other BS, and both UEs may interfere with each other. Hence, the two-way communication consists of two different interference channels each involving one BS and one UT as transmitters.

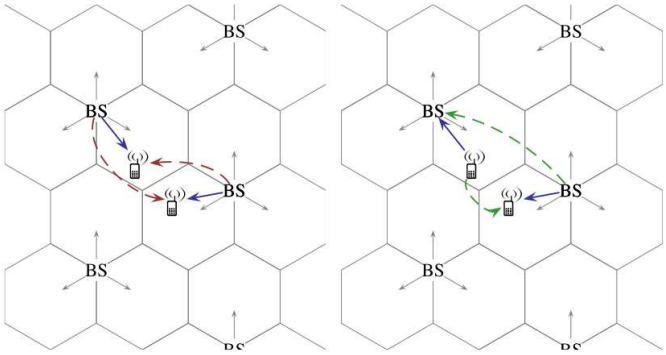

Figure 14: Comparison of symmetric and asymmetric UL/DL frames for two UEs connected to different cells.

This additional degree of freedom can be used to redesign cells or to more efficiently operate existing cellular networks. Instead of applying complex multi-cell MIMO methods, we avoid interference using an asymmetric UL/DL operation.

2.2.3 The two-way Interference channel

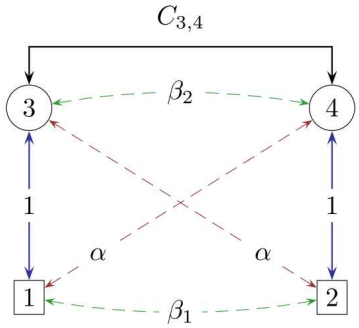

Figure 15: The two-way interference channel.

In order to obtain analytical results, we consider the two-way interference channel. It is fully connected and consists of four half-duplex nodes with i.i.d. zero-mean circularly symmetric Gaussian channel inputs and AWGN. The channel is illustrated in Figure 15. It shows the inter-cell interference quantified by α as well as the inter-terminal/node interference quantified by β. Our model further assumes that both BSs are inter-connected and may coordinate their transmission and detection. By contrast, we do not assume any direct communication between both UEs. In the following, denote the rate with which terminal n communicates with terminal n' as R(n, n'). Then, we constrain all results in this work such that a given ratio η = R(3,1)/R(1,3) = R(4,2)/R(2,4) of DL to UL rates is satisfied. This ratio is of particular importance in mobile communication networks as very high DL-data-rates require a minimum UL-data-rate for signaling.

Our initial analysis assumes that the system is divided into two phases using fraction τ and 1-τ of the available resources for UL and DL, respectively. Without loss of generality, the following discussion relates to a TDD system.

2.2.4 Protocols for the two-way interference channel

In the following, we describe protocols that are applicable to the two-way channel. Our description relies on existing literature on the one-way interference channel for which a variety of approaches has been published. So far, the best known inner bound for the weak interference channel divides each transmitter's message in a private part and common part which are jointly decoded. The common part, however, is decoded at both receivers while the private part is only decoded at the intended receiver. We omit a detailed description of the achievable rates for the sake brevity and refer the interested reader to [20].

If both transmitters are connected with an unlimited backhaul-link, the resulting channel can be understood as a broadcast channel. Costa showed in [21] that by using the dirty paper coding technique one of both nodes can receive its transmission as it was without interference. Similarly, both BSs can exchange received signals with a central entity such that the capacity region for the UL with unlimited receiver cooperation is given by the multiple access channel capacity. Both cases are the standard scenarios considered by multi-BS MIMO.

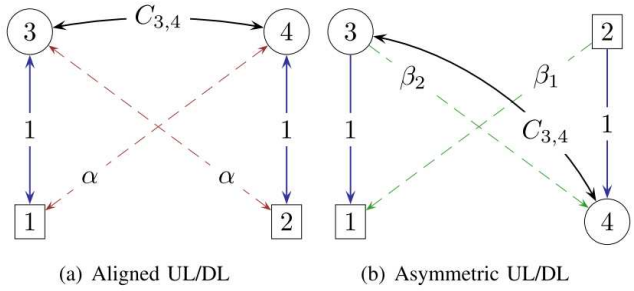

Figure 16: Two cases of the two-way interference channel.

In the two-way interference channel we can extend the previously discussed symmetric scenario. In a scenario with asymmetric UL/DL operation, one BS may be transmitting while another UE of another cell is transmitting. Figure 16 illustrates this scenario. In an aligned UL/DL operation, BSs 3 and 4 are both either in DL or UL at the same. By contrast, in an asymmetric UL/DL operation, BS 3 and UE 2 or BS 4 and UE 1 are transmitting or receiving at the same time.

In the case of asymmetric UL/DL operation and without coordination between BSs we obtain a different interference channel with cross-channel amplitudes β instead of α. This reflects the additional degree of freedom, e.g. either BSs or UEs may be well separated (β<<α) which avoids interference at all or they experience a (very) strong interference channel (β>>1), which allows for simple interference cancellation. Hence, the achievable rates may be increased as the interference situation with β is preferable over α.

Finally, we consider the case that both BSs receive over the backhaul the transmit-message of the other BS in addition to their own transmit-message. Then, under the assumption of CSI at the receiver (which can be acquired using pilots instead of backhaul) we can apply a perfect interference cancellation at both BSs no matter how strong the interference is. By contrast, the other UE still has to cope with the inter-terminal interference. Inter-UE interference may, however, be avoided by an intricate scheduler design and assigning UEs to orthogonal sub-frames.

2.2.5 Results

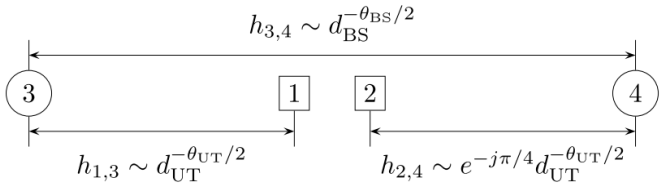

Figure 17: Setup of an exemplary interference channel used for analytical results.

This part discusses preliminary analytical results for the previously described scenario. We use an exemplary interference channel with unlimited backhaul, which is illustrated in Figure 17. Both BSs are placed at distance d_{BS} = 500m from each other and each UE is located at distance d_{UE} from its assigned BS. As indicated in Figure 17, we apply an exponential path-loss model with θ_{UT} = 3 (for BS-UT and UT-UT links) and θ_{BS} = 2.5. Throughout this section we assume a cell-edge SNR at d_{UE} = 250m of $|h_{1,3}|^2P_3 = |h_{3,1}|^2P_1$= 0dB (and similar for the second communication pair).

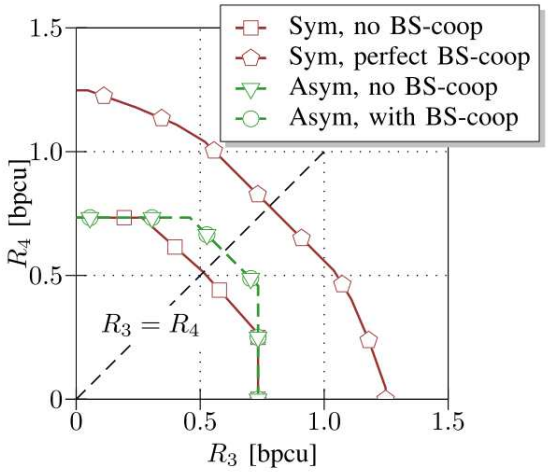

Figure 18: Achievable rate region for d_{UE} = 230m.

Figure 18 shows the results if both UEs are located close to the cell-edge, i.e. d_{UE} = 230m which corresponds to α=0.8 in the standard interference channel and DL-UL-ratio η=5/3 which is commonly used in IEEE 802.16m. In this scenario, the asymmetric UL-DL assignment creates two interference channels with strong interference between both paths. If we do not allow for BS

cooperation, the asymmetric case clearly outperforms the symmetric case. Due to the strong interference between both UTs and both BSs (β>>0), both asymmetric cases provide the same performance. However, one might expect the rate region to be rectangular but it is a pentagon due to the asymmetric ratio η = 5/3. All protocols are outperformed by symmetric assignment and perfect BS cooperation (multi-cell MIMO) which, however, is much more complex and a theoretical outer bound for the symmetric case.

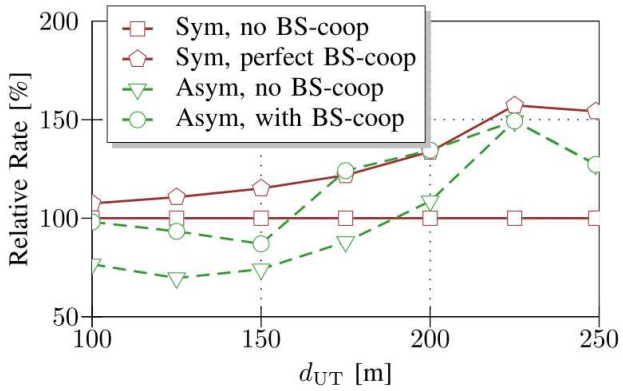

Figure 19: Achievable common-rate for varying user distances.

Consider Figure 19 which shows the performance for varying values of d_{UE}, η = 1, and rates relative to the symmetric, non-cooperative case (the status-quo as of today). Symmetric, perfect BS cooperation (multi-cell MIMO) outperforms all other protocols due to its ability to cancel inter-cell interference and to exploit multi-cell diversity. Since the inter-BS interference is too strong enough to be ignored and must be alleviated, the asymmetric, cooperative protocol applies SIC and hence outperforms the asymmetric non-cooperative case. An asymmetric assignment of UL and DL improves the rates by up to 50% at the cell-edge while the performance drops below the symmetric non-cooperative case towards the cell-centre. However, asymmetric assignment is much less complex than multi-cell MIMO and therefore provides a better trade-off of complexity and performance for large d_{UE} while towards the cell-centre non-cooperative symmetric assignment provides the best trade-off. This makes a mixed approach attractive where resources are assigned to both symmetric and asymmetric assignment. UTs at the cell centre would then be served in the symmetric part while those at the cell edge would be served in the asymmetric part. Such an approach provides performance close to multi-cell MIMO while being much less complex.

2.2.6 Future work

The next steps within WP5 will include a detailed analysis of implementation aspects in a cellular network, an analysis of the affected MAC functions and how they may be designed to support asymmetric UL/DL assignment, and a system level investigation on the benefits of this approach. Further details on this analysis are given in [22].

2.3 Reliable multicast

2.3.1 Multicast in IEEE 802.16

Multicast is a very popular bandwidth-conserving technology exploited in many multimedia applications such as TV, gaming, videoconferencing, corporate communications, distance learning, news, etc. The technology reduces traffic by delivering the same data stream to multiple recipients simultaneously. In IEEE 802.16 networks, Subscriber Stations (SSs) interested in receiving a multicast data stream are included into the related multicast group and are referred to as multicast group members. At MAC layer, a multicast group is identified by a multicast MAC address. Being the multicast stream sender, the Base Station (BS) sends the packets with the Connection ID (CID) related to the particular data stream with the multicast MAC address.

Most of multicast based applications impose strict Quality of Service (QoS) requirements in terms of minimal throughput, maximal Packet Loss Ratio (PLR) and latency. Having a centralized point-to-multipoint architecture, WiMAX provides efficiently Quality of Service (QoS) differentiation for unicast transmission. As to multicast transmissions, IEEE 802.16 protocol does not support some QoS requirements because conventional Automatic Repeat Request (ARQ) schemes used for unicast are not applicable to multicast connections. However, the protocol has potential tools to implement multicast ARQ schemes. For instance, one can increase the reliability, retransmitting every data frame several times and thus decreasing the PLR, using specific ARQ policy.

By now, there is no any reliable MAC layer multicast solution for IEEE 802.16 networks. It makes us to focus on existing ARQ-based IEEE 802.11 multicast proposals, which aim to achieve multicast reliability and which ideas can be extended and/or adapted to IEEE 802.16 MAC. J. Kuri and S. K. Kasera [23]described the Leader-Based Protocol (LBP), where only one leader is selected from all the multicast recipients. The leader is responsible for sending acknowledgements (ACKs) in reply to data frames. The question how to select the leader was not answered in [23]. H. C. Chao, S. W. Chang and J. L. Chen [24] proposed the Random Leader Technique, according to which the leader is selected randomly among all recipients with equal probabilities. LG Electronics and INRIA used the idea of LBP in their proposal [25] to IEEE 802.11v working group. According to the proposal [25], the recipient operating in worst channel conditions is selected as a leader. Obviously, the only leader may be not enough to provide reliable multicast and thus, to meet QoS requirements for all multicast recipients. Batch Mode Multicast MAC protocol (BMMM) [26], Broadcast Support Multiple Access (BSMA) [27] and Broadcast Medium Window (BMW) protocol [28] represent an alternative approach, according to which all recipients are requested to send ACKs. (Further, we refer to this approach as the BMMM one.)

The LBP and BMMM approaches can be easily adapted to IEEE 802.16 in the following way. IEEE 802.16 network has a point-to-multipoint architecture and consists of one BS and multiple SSs managed by the BS. IEEE 802.16 network operation time is divided into fix-sized frames by means of time division duplexing (TDD) operation mode. A frame consists of a downlink (DL) subframe for transmission from the BS to SSs and an uplink (UL) subframe for transmissions in the reverse

direction. IEEE 802.16 frame structure is shown in Figure 20. In the downlink subframe the Downlink MAP (DL-MAP) and Uplink MAP (UL-MAP) messages are transmitted by the BS, which comprise bandwidth allocations for data transmission in downlink and uplink directions, respectively. The ARQ is provided by allocating a special ACK-Channel (ACK-CH) in the UL for the SSs. The bandwidth allocated for this channel depends on how many stations reply with ACK and cannot be very large because the UL subframe itself is tightly bounded and there are a lot of other data transmissions in it.

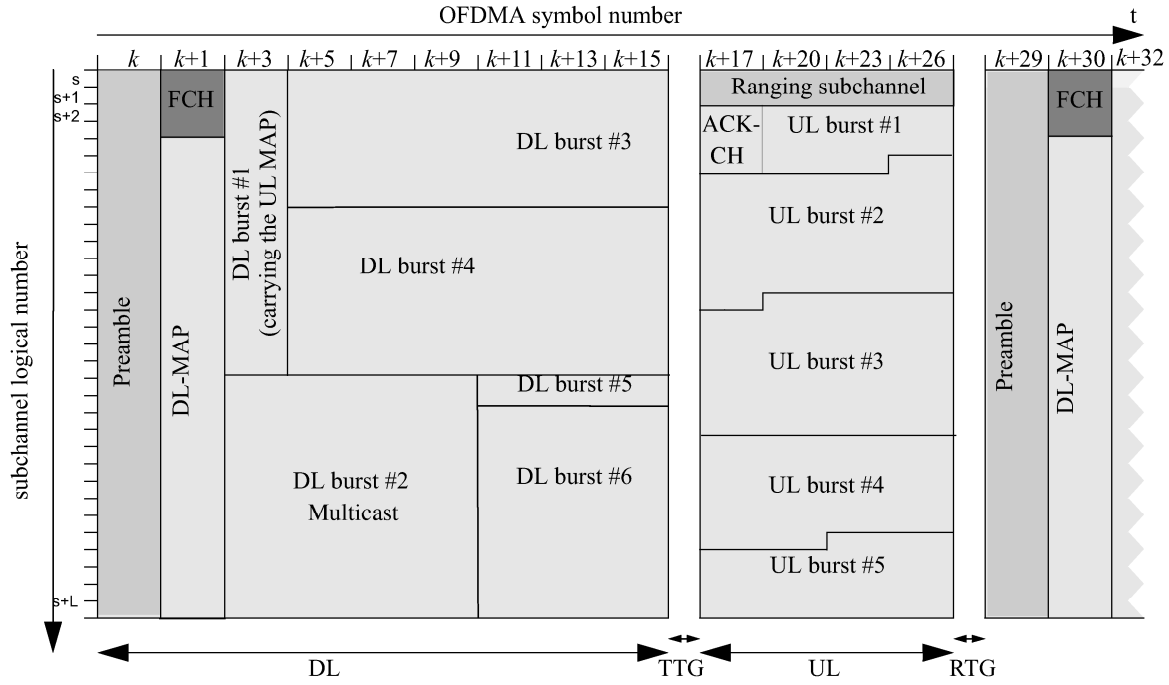

Figure 20: IEEE 802.16 frame structure.

Forming the DL- and UL-MAP, BS allocates a necessary bandwidth to transmit a multicast data burst (a set of data packets related to a given multicast stream and transmitted within one frame) in the DL subframe and to receive the ACK(s) in the UL subframe. In case of LBP, it is enough to include one ACK slot in UL ACK-CH for the multicast stream. In contrast, BMMM requires N ACK slots, where N is the number of multicast recipients in the coverage area. On receiving the DL- and UL-MAP, a recipient becomes aware when the multicast burst is going to be transmitted and if an ACK arrival is expected from the recipient. By the ACK, the BS finds out which of burst packets were corrupted and should be retransmitted.

Obviously, LBP and BMMM in IEEE 802.16 have the same drawbacks as in IEEE 802.11. LBP provides insufficient reliability, while BMMM is reliable, but has a huge ARQ overhead consisting in a lot of ACKs in every frame.

To overcome these drawbacks, we develop new reliable multicast scheme for IEEE 802.16 using the LBP and BMMM approaches as base points. The method we propose takes into account the

trade-off between reliability and protocol overhead and can support QoS. Specifically, to reduce the BMMM overhead, we propose to allocate ACK slots not to all multicast recipients, but only to a part of them. That is, we propose to use several leaders replying with ACK. Further, we refer to them as ACK-leaders and call our proposal the Enhanced Leader Based Protocol (ELBP).

The ELBP works as follows. After a recurrent data burst transmission, the multicast sender, i.e. BS, prepares multicast packets for the burst transmission in the next frame, including both new packets and packets not acknowledged previously by all ACK-leaders and which life times have not expired. BS allocates a bandwidth in DL-MAP for retransmitted packets, first, and then, for the new packets. Then the BS allocates the necessary number of ACK slots in the ACK-CH part of the UL subframe and indicates this allocation in the UL-MAP. Upon receiving a UL-MAP, each recipient becomes aware whether it should reply with an ACK to the multicast burst transmission in the current frame or not. According to IEEE 802.16 standard, ACK message includes a bitmap with a positive or negative feedback on every packet transmitted in the related burst. If the BS receives a negative feedback on a packet from at least one of ACK-leaders, the sender retransmits this packet in the next frame.

This new functionality can be easily added to the existing IEEE 802.16 software, using the novel modular architecture approach developed in the FLAVIA project.

2.3.2 Enhanced leader based protocol adaptation to QoS requirements

In the ELBP, there are two interconnected questions to answer. The first question is how many ACK-leaders should be selected. The second question is which recipients are the best candidates to be ACK-leaders or, in other words, how to select the required number *J* of ACK-leaders from all *N* recipients. We may select them randomly with equal probabilities for every new frame, as in [24]. However, it seems that this equiprobable leader selection is not the best way to support reliability and to meet QoS requirements, because the scheme does not take recipients' PLR, throughput and latency into account. Generally, ACK-leader selection scheme may be a function of QoS requirements, reliability and performance indices, as well as some other metrics, for example, Packet Error Rate (PER).

Usually, multicast based multimedia applications impose the following requirements:

- PLRs η_j among should be not greater than the maximum PLR $\eta_{\max}$ for all *N* recipients;
- The latency defined as the time interval spent to transmit a packet, including possible retransmissions, should not exceed the maximum latency $T_{\max}$. The requirement may be met by setting the MAC layer maximal lifetime of a packet to $T_{\max}$.
- Throughput S_j of recipient *j* defined as the average number of the considered multicast stream payload bits successfully received by the recipient per time unit should not be less than the minimum throughput $S_{\min}$ for all *N* recipients.

Since measures aimed at improving reliability and performance are opposite, some trade-off between PLR, latency and throughput must be found to meet all QoS requirements. To achieve the trade-off, we can tune 3 parameters of the ELBP protocol:

- the burst size *B*, i.e. the number of multicast data packets transmitted in a burst;
- the periodicity *T*, with which the considered multicast stream is allocated with bandwidth, that is, the interval between starts of consecutive bursts; it should be multiple of 802.16 frame duration t_{frame}, that is, $T = M_{frame} t_{frame}$;
- the number *J* of ACK-leaders for every data burst transmission.

In the next subsections, we develop an analytical method that allows to estimate reliability and throughput indices, to look for an admitted region of ELBP parameters values, in which QoS requirements are met for all recipients, and then to optimize the values, remaining in the admitted region, to minimize the bandwidth allocated for a given multicast stream. The optimization criterion is:

$$\min\left\{\beta = t_{OFDM}\frac{Bn_{sp} + Jn_{sa}}{M_{frame}t_{frame}}\right\}, \qquad \textbf{(2.3.1)}$$

where n_{sp} and n_{sa} are the numbers of OFDM symbols per packet and per ACK, respectively, and t_{OFDM} is OFDM symbol duration. Here and further, we assume a fixed packet length *L*.

Leader selection scheme is another ELBP powerful tool. We consider two kinds of schemes. One of them is to fix *J* recipients, based on the experienced PER, and consider them as ACK-leaders for every burst transmission. Specifically, we propose to select the recipients with higher PER and fix them as ACK-leaders. Further, we refer to this ACK-leader selection scheme as ELBP with Fixed ACK-leaders or just Fixed ELBP.

Another scheme is to select recipients as ACK-leaders randomly according to some PER dependent weight function. Every round of multicast transmission, multicast originator selects *J* ACK-leaders out of all *N* recipients according to weights assigned to every recipient by some weight function *W*(). Further, we refer to this ACK-leader selection scheme as ELBP with Weighted ACK-leaders or Weighted ELBP for short. Obviously, the equiprobable leader selection is a special case of the Weighted ELBP, when all recipients are assigned the same weight.

2.3.3 Analytical study

To develop analytical models of these multicast schemes, we need to make some definitions and assumptions, first. The BS transmitting the multicast stream is assumed to work in saturation. Let

p_j be the PER for the *j*-th recipient. We enumerate the recipients in the order of decreasing PERs, i.e. the first recipient has the highest PER p_1 and first *J* recipients serve as ACK-leaders. Since ACK messages, DL- and UL-MAP in IEEE 802.16 are relatively short and are usually transmitted with highest coding gain, we neglect their error probabilities.

As mentioned above, it is reasonable to set the MAC layer maximal lifetime of a packet to $T_{\max}$ to meet the QoS requirement on the maximum latency. Since there may be the only attempt of transmission of a given packet during an interval *T*, the maximum number *K* of transmission attempts of a given packet is:

$$K = \lceil T_{\max} / T \rceil \qquad \textbf{(2.3.2)}$$

where $\lceil\ \rceil$ is a ceiling function. QoS requirement on maximum latency is met if the maximal number of transmission attempts does not exceed *K* defined by (2.3.2). Further, we use $k = 1,\ldots,K$ as the transmission attempt number.

Obviously,

$$p_1 \le \sqrt[\lceil T_{\max}/T \rceil]{\eta_{\max}} \le \sqrt[\lceil T_{\max}/t_{frame} \rceil]{\eta_{\max}}, \qquad \textbf{(2.3.3)}$$

is the necessary condition for reliable multicast. Indeed, if the right inequality in (2.3.3) does not hold, the QoS cannot be supported by the ELBP. In this case, we recommend to decrease p_1 to the necessary value by decreasing the packet length and/or transmission rate.

ELBP with Fixed ACK-leaders. Analytical model of the scheme can be represented with the following theorems which proofs are given in [29]. The first theorem allows to estimate reliability and throughput indices.

Theorem 1: PLRs for an ACK-leader and non-ACK-leader are:

$$\eta_j^{ACK} = p_j^K, \quad j = 1,\ldots,J, \eta_j^{nACK} = p_j - (1 - p_j)\sum_{k=1}^{K-1}\left(\tilde{\pi}_k p_j^k\right),$$

where

$$\tilde{\pi}_k = 1 - \prod_{j=1}^{J}\left(1 - p_j^k\right)$$

is the probability that all ACK-leaders have received a given packet exactly after *k* attempts, i.e. exactly *k* attempts appear to be needed to transmit the packet successfully. Throughput for recipient *j* is:

$$S_j = \frac{8LB}{T\gamma_K}\left(1-\eta_j\right),$$

where η_j equal to η_j^{ACK} for an ACK-leader and η_j^{nACK} for non-ACK-leader,

$$\gamma_K = 1+\sum_{k=1}^{K-1}\tilde{\pi}_k$$

is the average number of transmission attempts of a packet with the limitation K on their maximum number.

Theorem 2: To meet the requirement on the maximal PLR, recipients which PERs are less than

$$p_{bound} = \sqrt{\left(\frac{1-p_1}{2p_1}\right)^2 + \frac{\eta_{\max}}{p_1}} - \frac{1-p_1}{2p_1},$$

should not be selected as ACK-leaders.

Theorem 3: To meet the requirement on the minimal throughput, the following inequality should hold:

$$B \geq B_0(T) = \left\lceil \frac{T\left(1+p_1\right)S_{\min}}{8L\left(1-p_1^2\right)} \right\rceil = \left\lceil \frac{TS_{\min}}{8L\left(1-p_1\right)} \right\rceil.$$

Thus, in the ELBP parameter optimization we need to consider $B \geq B_0(T)$ and $J < J_0$ only, where J_0 is the least recipient number which PER is less than p_{bound} defined by Theorem 2.

ELBP with Weighted ACK-leaders. For the ELBP with weighted ACK-leaders, J ACK-leaders are reselected every frame. The selection is performed from the whole set of recipients, according to their weights w_i, $i = 1,...,N$. Let us partition all recipients into M sets. In set $m = 1,...,M$, there are N_m recipients, which PER is nearly the same and equal to p_m. Obviously, we assign the same weights w_m to all N_m recipients of set m that makes optimization of the weight distribution easier in the case of a large number of recipients. Of course, the partition is not reasonable with a small number of recipients. In this case, we just set $M = N$ and $N_m = 1$.

As J ACK-leaders are to be selected, the selection procedure is carried out in J steps. At step j, a recipient from set h is selected with probability

$$\xi_{h,j} = \left(N_h - u_{h,j-1}\right)w_h \Big/ \sum_{m=1}^{M}\left(N_m - u_{m,j-1}\right)w_m, \qquad \textbf{(2.3.4)}$$

where $u_{m,j}=1,\ldots,N_m$ is the number of recipients selected to be ACK-leaders in set *m* at *j*-th selection step. That is, $\vec{U}_j=\|u_{m,j}\|$, $m=1,\ldots,M$, is a selection vector indicating which recipients have been selected after *j* steps. Obviously, $\vec{U}_0=\vec{0}$ and vector $\vec{U}\propto\vec{U}_J$ indicates all current ACK-leaders responsible for acknowledging the current data burst transmission. The BS stops transmitting a packet when all current ACK-leaders acknowledge the packet and thus, receive the packet successfully.

Taking (2.3.4) into account, the probability distribution $\varphi(\vec{U})\propto\varphi(\vec{U}_J)$ of $\vec{U}$ can be found recursively:

$$\varphi(\vec{U}_1)=\sum_{m=1}^{M}u_{m,1}\xi_{m,1},\ \varphi(\vec{U}_j)=\sum_{\vec{U}_{j-1}\in U_j^{-1}}\sum_{m=1}^{M}(u_{m,j}-u_{m,j-1})\xi_{m,j}\varphi(\vec{U}_{j-1}),\ j=2,\ldots,J,$$

where $U_j^{-1}=\{\vec{A}:\ \vec{A}\le\vec{U}_j,|\vec{U}_j-\vec{A}|=1\}$ is the set of possible selection vectors at step *j*-1 with fixed $\vec{U}_j$. Here and further, for any $\vec{X}=\|x_i\|$ and $\vec{Y}=\|y_i\|$, we assume $\vec{X}\le\vec{Y}$ if $x_i\le y_i$ for all *i* and $|\vec{X}|=\sum_i x_i$.

To find $\tilde{\pi}_k$ in Theorem 1, we consider a process of a given packet transmission. Let us introduce a success vector $\vec{V}_k=\|v_{m,k}\|$, $m=1,\ldots,M$, where $v_{m,k}=1,\ldots,N_m$ is the number of ACK-leaders in set *m*, which successively receive a packet after *k* transmission attempts. Obviously, $\vec{V}_0=\vec{0}$ and $\vec{V}_{k-1}\le\vec{V}_k$. The probability of the success vector change from $\vec{V}_{k-1}$ to $\vec{V}_k$ after *k*-th attempt, given that (*k*-1)-th attempt failed for at least one of recipients which were current ACK-leaders, is

$$R(\vec{V}_k,\vec{V}_{k-1})=\prod_{m=1}^{M}C_{N_m-v_{m,k-1}}^{v_{m,k}-v_{m,k-1}}(1-p_m)^{v_{m,k}-v_{m,k-1}}p_m^{N_m-v_{m,k}}.$$

Let $\pi_k^*(\vec{V}_k)$ be the probability that after *k* attempts (*k*<*K*) the packet transmission process does not complete successfully and the success vector is $\vec{V}_k$. $\pi_k^*(\vec{V}_k)$ is calculated recursively:

$$\pi_1^*(\vec{V}_1)=R(\vec{V}_1,\vec{0})\left[1-\sigma(\vec{V}_1)\right],\quad \pi_k^*(\vec{V}_k)=\sum_{\vec{V}_{k-1}:\vec{V}_{k-1}\le\vec{V}_k}\pi_{k-1}^*(\vec{V}_{k-1})R(\vec{V}_k,\vec{V}_{k-1})\left[1-\sigma(\vec{V}_k)\right],\ k=2,\ldots,K,$$

where

$$\sigma(\vec{V}_k)=\sum_{\vec{U}:\vec{U}\le\vec{V}_k}\varphi(\vec{U})\prod_{m=1}^{M}\left(C_{v_{m,k}}^{u_m}/C_{N_m}^{u_m}\right).$$

is the probability that after *k* attempts the packet transmission process completes successfully with given $\vec{V}_k$. Hence, the probability that not all recipients serving as current ACK-leaders have

received the data packet after *k* attempts, is

$$\tilde{\pi}_k = \sum_{\vec{V}_k} \pi_k^* \left(\vec{V}_k\right).$$

Using probabilities $\tilde{\pi}_k$, we find γ_K in Theorem 1.

To find PLR for a fixed recipient from set *h*, we introduce the probability $R'_h\left(\vec{V}_k, \vec{V}_{k-1}\right)$ that the success vector changes from $\vec{V}_{k-1}$ to $\vec{V}_k$ so that the given recipient does not receive the packet by the end of *k*-th attempt:

$$R'_h\left(\vec{V}_k, \vec{V}_{k-1}\right) = \prod_{m=1}^{M} C_{N_m - v_{m,k-1} - \delta_{mh}}^{v_{m,k} - v_{m,k-1}} \left(1 - p_m\right)^{v_{m,k} - v_{m,k-1}} p_m^{N_m - v_{m,k}},$$

where δ_{mh} is the Kronecker symbol.

Thus, the probability $\pi'_{h,k}\left(\vec{V}_k\right)$ that after the *k*-th attempt , the packet transmission process does not stop, the given recipient from set *h* does not receive the packet and the success vector is $\vec{V}_k$, is obtained recursively for all $\vec{V}_k$ such that $v_{h,k} < N_h$:

$$\pi'_{h,k}\left(\vec{V}_k\right) = \sum_{\vec{V}_{k-1}: \vec{V}_{k-1} \le \vec{V}_k,\, v_{h,k-1} < N_h} \pi'_{h,k-1}\left(\vec{V}_{k-1}\right) R'_h\left(\vec{V}_k, \vec{V}_{k-1}\right)\left[1 - \sigma\left(\vec{V}_k\right)\right],\ \pi'_{h,1}\left(\vec{V}_1\right) = R'_h\left(\vec{V}_1, \vec{0}\right)\left[1 - \sigma\left(\vec{V}_1\right)\right].$$

Now, we can find expressions for probabilities $\rho_{h,k}$ that *k* attempts have been carried out to transmit the packet and the given recipient from set *h* has not received the packet in any of these attempts. We have:

$$\rho_{h,1} = \sum_{\vec{V}_1: v_{h,1} < N_h} R'_h\left(\vec{V}_1, \vec{0}\right)\sigma\left(\vec{V}_1\right), \quad \rho_{h,k} = \sum_{\vec{V}_k: v_{h,k} < N_h} \sum_{\vec{V}_{k-1}: \vec{V}_{k-1} \le \vec{V}_k} \pi'_{h,k-1}\left(\vec{V}_{k-1}\right) R'_h\left(\vec{V}_k, \vec{V}_{k-1}\right)\sigma\left(\vec{V}_k\right),$$

when $k = 2, \ldots, K-1$, and

$$\rho_{h,K} = p_h \sum_{\vec{V}_{K-1}: v_{h,K-1} < N_h} \pi'_{h,K-1}\left(\vec{V}_{K-1}\right).$$

Thus, the PLR for a recipient from set *h* is:

$$\eta_h = \sum_{k=1}^{K} \rho_{h,k}.$$

Throughput for any recipient from set *h* is given by (8), where we substitute η_h for η_j.

2.3.4 Numerical results

In this section, we use our analytical models to investigate and to optimize ELBP multicast schemes in different use cases. As we don't apply any simplifications and assumptions about original ELBP multicast schemes, our mathematical models are accurate and there is no need to validate them via simulation. Although we use some simulation to obtain the input data (the dependence of recipient's PER on distance) for our analytical models.

ELBP with Fixed ACK-Leaders. An IEEE 802.16 Base Station (BS) usually covers a large area with huge number of Subscriber Stations (SSs). To increase the network capacity and QoS provisioning, a BS is equipped with sector antenna. Each sector of this antenna covers a separate area with a part of all SSs in it, achieving spatial diversity. In fact, we can consider each sector as an individual IEEE 802.16 wireless network with its own BS, coverage area and set of SSs. So, further results will concern one of such sectors.

Let us assume that the BS is a multicast sender and multicast data are transmitted in every frame, that is, M_{frame}=1. We also assume that the BS transmits a data burst consisted of multicast multimedia data packets with L=512 Bytes payload at a maximal PHY data rate (R =3/4, 64-QAM) using ELBP mechanism with Fixed ACK-leaders. With this PHY, one 512 Bytes packet takes n_{sp}=16 OFDM symbols, while an acknowledgment takes n_{sa}=2 OFDM symbols. The 802.16 frame duration is t_{frame}= 5 ms and the maximum latency is $T_{\max}$=20 ms. So, the maximal number of retransmissions is K=4, according to (2).

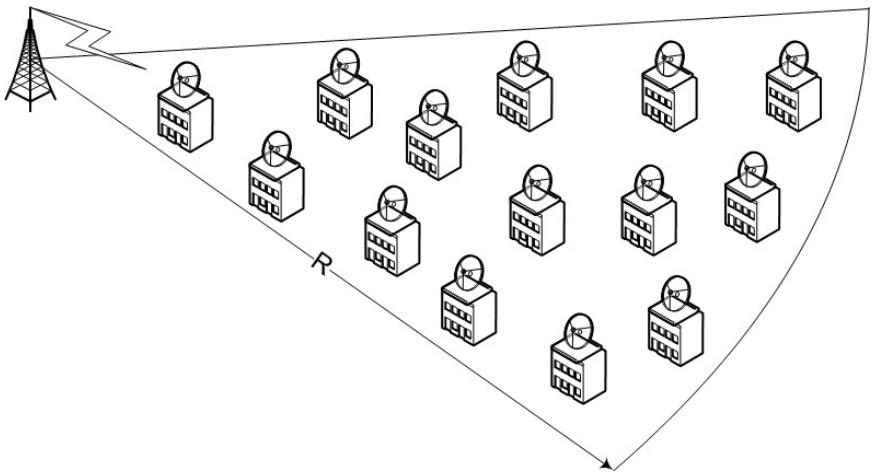

Figure 21: Sector with uniformly distributed SSs.

First, we consider more general case shown in Figure 21. In this use case, the coverage area of the BS is a sector of circle with radius R=1 km and total number N of SSs uniformly distributed across the sector.

To start numerical analysis, we need to derive the dependence of recipient's PER on distance for the investigated network. We divide the process in two steps. First, we obtain the dependence of Signal-to-Noise Ratio (SNR) on distance according to the path loss model in [30] with a critical parameter ν = 3.3. After that we find PER (SNR) by MATLAB [31] simulation of IEEE 802.16 PHY for the highest PHY data rate (R =3/4, 64-QAM), using AWGN channel as a noise source.

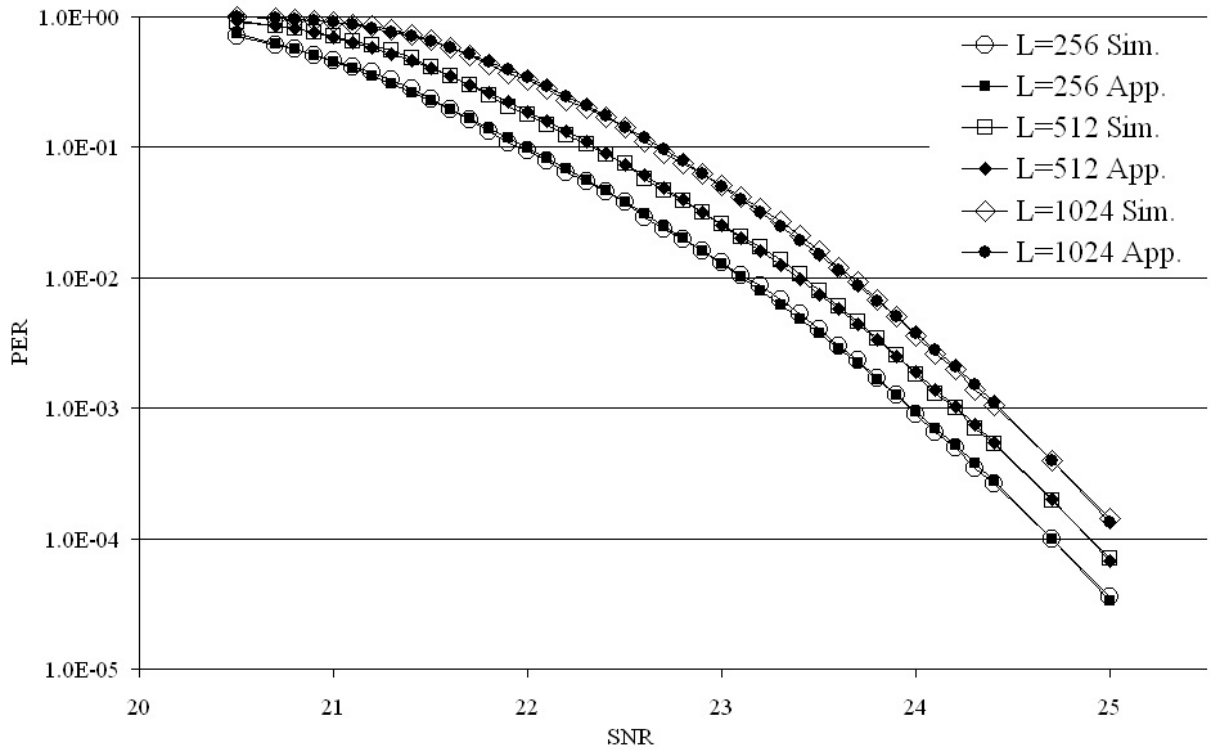

Figure 22: PER vs. SNR.

In Figure 22, we show the simulation data (Sim.) for various packet lengths. We also include the analytical approximation (App.) of the dependencies obtained by simulation. We approximate the simulation data using the formula:

$$PER(SNR, L) = 1 - \left(1 - \frac{1}{2}\right)\exp\left(-\exp\left(\frac{SNR - \zeta}{\alpha}\right)\right)^{8L},$$

where α =4.8355 and ς =10.479. As it is shown in Figure 22, the proposed analytical approximation fits perfectly the simulation data. Using this approximation with L=512, we find PER for every recipient. The PER of the most distant SS is 0.1, that is, 10%. The closest SS has the PER equal to 0.

As follows from Theorem 1, PLR depends on station's PER and the number J of ACK-leaders only. Thus, for a given number N of stations and PER distribution, we can find the optimal number J_{opt} of

ACK-leaders minimizing the bandwidth allocated for a given multicast connection per frame (see (1)), while meeting a certain QoS requirement on PLR for all recipients.

In Figure 23, we show the relationship between J_{opt} and the maximal PLR over the network which contains N = 25, 50 and 100 SSs. The figure shows two of ELBP main advantages.

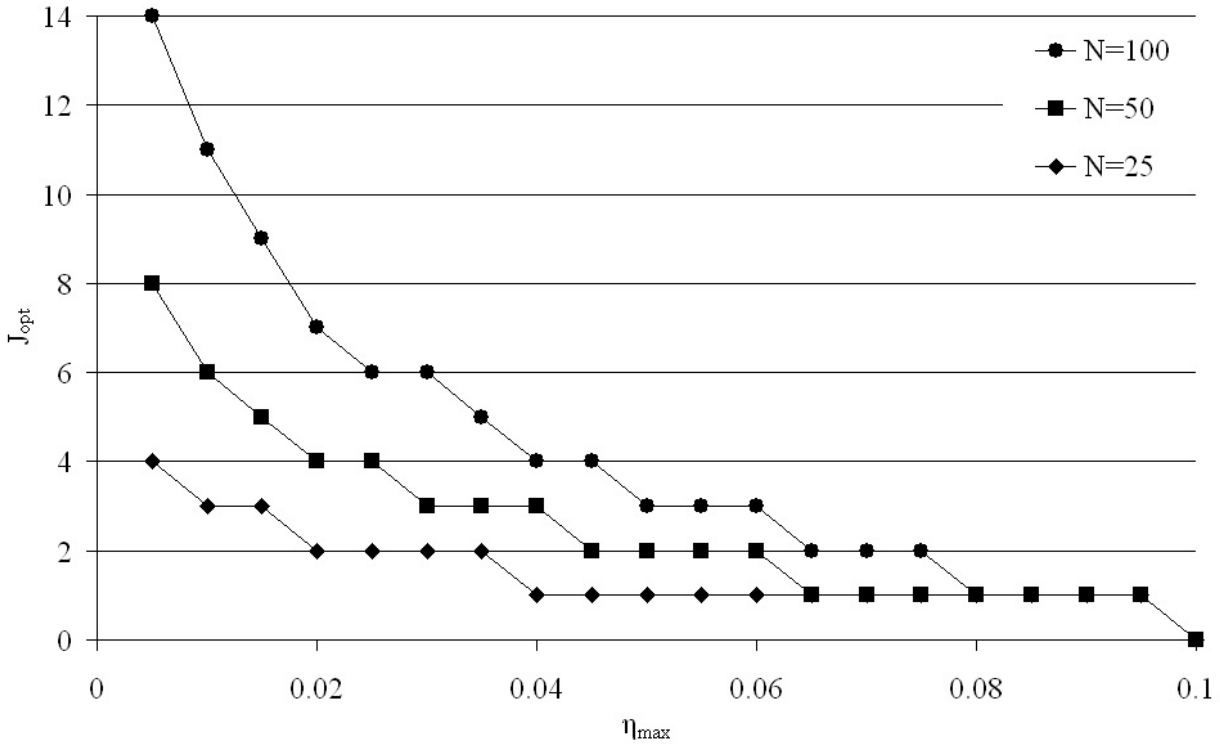

Figure 23: Fixed ELBP: optimal number of ACK-leaders

The first advantage is the scalability. Indeed, even if the number of recipients is quite high (N=100), the optimal number of ACK-leaders is still less than 10 for a wide range of η_{max} values: 2–10%. We can see also that the optimal number J_{opt} of ACK-leaders is nearly proportional to the number N of recipients. So, we can conclude the optimal number of ACK-leaders in the Fixed ELBP scheme is less than 10% over all multicast recipients in wide range of QoS requirements on maximal PLR.

The second advantage is the supremacy over the pure LBP in reliability. Indeed, even if the number of multicast recipients is small (N=25), LBP using only one ACK-leader cannot achieve PLR less than 4%. In contrast, ELBP can meet any pre-assigned QoS requirement η_{max} on PLR (of course, η_{max} cannot be less than p_1^K = 0.01% at the given bit rate, in accordance with (2.3.3)).

ELBP with Weighted ACK-Leaders. Let us consider the case, when there are multiple sets of recipients and recipients of the same set have the same PERs. For certainty, let us assume 3 sets in this use case, which correspond to 3 small settlements covered by a single sector of an IEEE 802.16

BS as it is shown in Figure 24. The total number of recipients is N=25. The first set consists of N_1 = 5 recipients with PER = 0.1; the second set has N_2 = 5 too and PER = 0.075, and the last set has N_3 = 15 recipients with PER = 0.01.

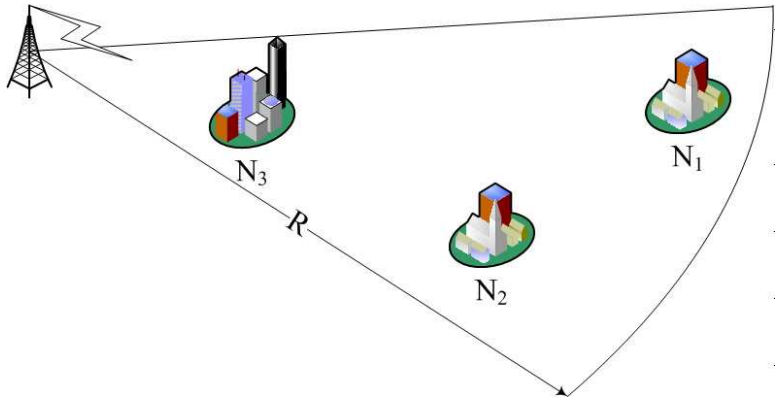

Figure 24: Sector with multiple sets of SSs.

Let us define QoS requirements. Let the maximum latency T_{max} be 15 ms and thus K=3, maximal PLR η_{max} be equal to 0.04, and minimum reserved rate S_{min} be 4 Mbps.

We compare three selection schemes: Fixed ELBP, Weighted ELBP and Full random ELBP. For Fixed ELBP scheme, we limit the range of J and B by B_0=6 and J_0=11, which are obtained by Theorems 2 and 3. For Weighted ELBP, weights are assigned according to the principle of minimizing PLR over all stations in the network. Full Random ELBP is the special case of Weighted ELBP ACK-leader selection scheme with equiprobable weights $w_i = 1/N$.

The PLR characteristics of these multicast schemes are shown in Figure 25. We can see that for Weighted ELBP 4 ACK-leaders is enough to meet QoS requirement on maximal PLR, while minimizing β in (1). In contrast, the other schemes need much more ACK-leaders. Fixed ELBP requires 8 ACK-leaders, and Full Random scheme needs to select 11 ACK-leaders.

The next step of our investigation is to find the optimal burst size B_{opt}. For that, we find how throughput depends on B with optimal numbers J_{opt} of ACK-leaders found at the previous step. The throughput characteristics are given in Figure 26. This figure shows that the optimal burst size which minimizes β in (1) is equal to 7 in the case of Weighted ELBP, while it is equal to 8 for Full Random selection scheme and 9 for Fixed ELBP.

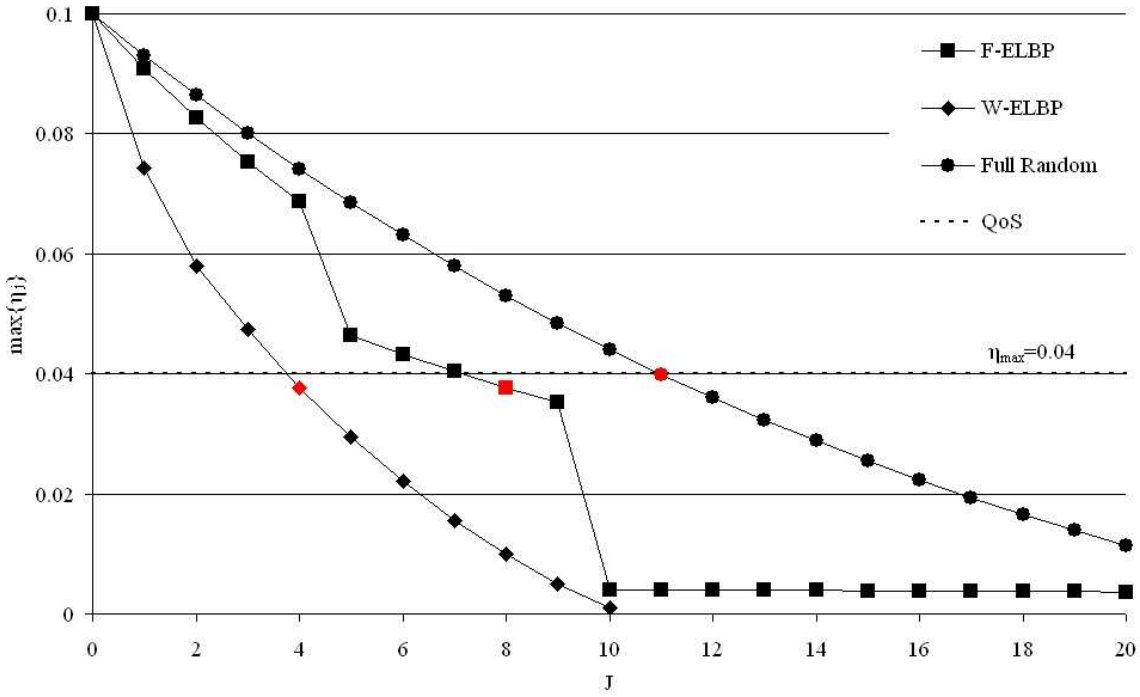

Figure 25: Maximal PLR vs. the number of ACK-leaders

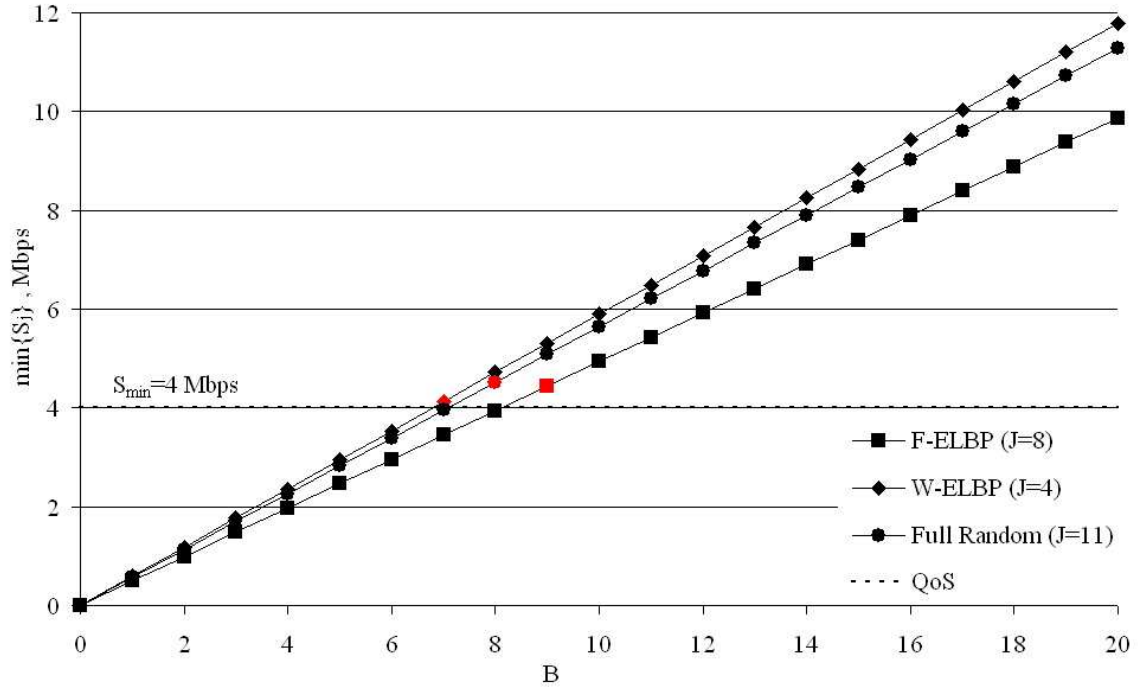

Figure 26: Minimal throughput vs. the burst size

At last, let us show the allocated bandwidth with these selection schemes. In Figure 27, we can see that the optimal Weighted ELBP scheme requires 120 allocated OFDM symbols per frame to meet all QoS requirements of the transmitted multicast stream, while Full Random selection needs 150 symbols and Fixed ELBP require 160 OFDM symbols.

Thus, numerical results obtained by the models show that ELBP can be used efficiently to meet specific multimedia application QoS demands, in contrast with well-known LBP and BMMM approaches when either only one recipient or all recipients acknowledge multicast packets. Both Fixed and Weighted ELBP are scalable multicast solutions: according to our model experiments, even with a large number of recipients it is enough to request a few recipients for acknowledgements to provide reliable multicast for all recipients. Comparing Fixed and Weighted ELBP, we show that Weighted ELBP is more efficient in terms of consumed bandwidth, although its implementation may be more complicated.

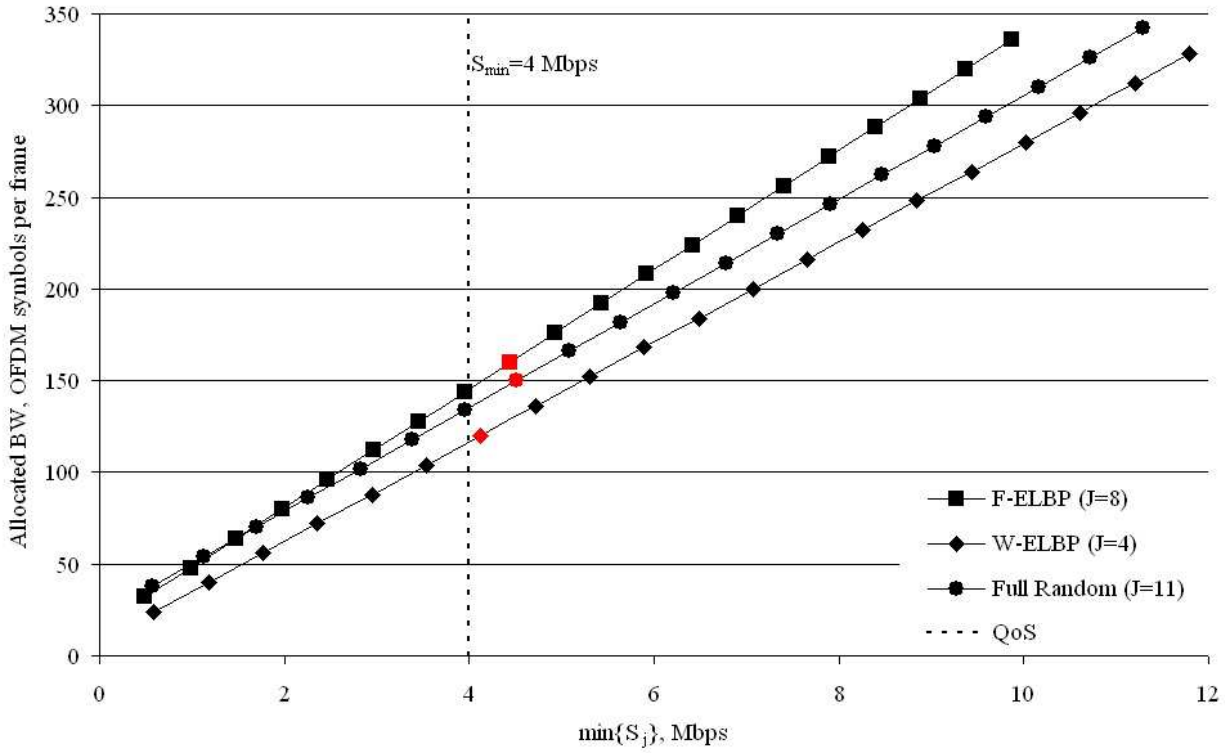

Figure 27: Allocated bandwidth vs throughput.

3 Power save schemes

3.1 Experimental assessment of power-save behavior of commercial IEEE 802.16e network cards

Next generation cellular technology (3.5G going on 4G) is emerging rapidly. For example Clearwire, a leading provider of 4G wireless broadband services in the U.S., has recently reported that the first quarter of 2011 ended with approximately 6.15 million subscribers, which is a 533% growth over the first quarter of 2010 [32]. UQ Communications announced reaching one million subscribers to UQ WiMAX in Japan, i.e., a growth of one million subscribers in approximately two years since starting its commercial service in July, 2009. One of the biggest advantages of such technologies is their ability to provide widespread coverage providing connectivity all over. Consequently, users, mobile or static, can expect high speed mobile broadband services everywhere, even when distant from Access Point (AP) and not necessarily in the proximity of power supply. In addition, due to the portability, devices are expected to be a carry on, hence smaller and lighter with small batteries. Accordingly, in order to fully benefit from remote coverage while extending battery life, 4G technology will necessitate power-save mechanisms. Former cellular technology (e.g. 2G and 3G) utilized power-save mechanisms. However, unlike these technologies which were mainly designed for voice applications, 4th generation cellular technology will integrate voice and data, supporting a variety of applications wherein traditional telephony will only play a secondary role. Accordingly, next generation power-save mechanisms are expected to be more challenging as more applications need to stay tuned regularly (periodically or non-periodically)..

Standards such as IEEE 802.16 and Long Term Evolution (LTE) of the 3GPP recognize two basic mechanisms to reduce power consumption when the device is not fully operational, IDLE and SLEEP. IDLE mode is designed to be activated when the Mobile Station (MS), after connecting to the network, has no data to receive or transmit for a relatively long period. When in IDLE mode, the MS is not expected to transmit or receive data, except for listening, at predetermined frames, for the broadcast MOB_PAG-ADV message which implies whether it has to wake up and exit IDLE mode due to pending data at the network side. The MS context is removed by its Serving Base Station (SBS), but is kept at the level of the paging group. Hence, the procedure of exiting IDLE mode is similar in some aspects to initial network entry (as it begins with a ranging process), but is slightly faster as the MS context is retrieved to the SBS from the network side when the MS exits IDLE.

Unlike IDLE mode, SLEEP mode does not require de-registration from SBS. Using the SLEEP protocol, after network entry, MS and BS negotiate availability and unavailability periods for the MS. SLEEP mode is commonly categorized into three Power Saving Classes (PSC). In all PSCs, while in unavailability period, MS is not expected to transmit or receive data. However, in PSC1 while in availability period, MS shall only receive the MOB_TRF-IND message that indicates whether it has to exit SLEEP as it has pending data at the network side. No other data is expected to be transmitted in PSC1. In PSC2, MS is able to receive and transmit data in the availability periods (therefore it is also known as “SLEEP with traffic”). PSC3 is used to form only one fixed unavailability period, which is not part of a predefined pattern of availability and unavailability periods like in the case of PSC1 and PSC2.

In this paper we summarize a thorough measurement investigation of the power-save mechanisms implemented in current deployed networks, and examine their suitability to various applications. We investigate a different approach for power-save operation termed Intra Frame Power-save (IFPS), in which devices can enter power-save mode for much shorter intervals than the common IDLE/SLEEP modes (i.e., intra-frame resolution). We suggest ways for utilizing IFPS for reducing power consumption. In particular, the contributions of the paper are as follows:
(I) We examine the power consumption of different operational modes (e.g., transmission mode, IDLE mode) on widely deployed WiMAX network cards. We show that the power-save protocols defined in the standard are seldom used when the MS operates in real life scenarios. In particular we show that even though SLEEP PSC2 may be the best theoretical method to save power in some low rate constant bit rate (CBR) applications, neither SLEEP PSC2 nor SLEEP PSC3 are implemented at all by any of the MS devices we examined. Furthermore, we show that IDLE and SLEEP PSC1 were not implemented by all of the examined MS devices, and the devices that did implement them utilized them only in limited instances We show that due to lack of cross layer coordination between the application, the operating system and the network card, even when IDLE and SLEEP PSC1 were implemented, their efficiency was relatively low.
(II) Following these findings, we measure and characterize the power consumption of five commercial WiMAX devices, while performing Rx and Tx for various kinds of signals (control bursts, as well as data bursts). In particular, we identify the power consumption distribution of different operations (e.g., data reception and transmission, map reception, HARQ, CQI, passive listening, etc.) within the common working mode. The data that we collect serve as a basis for comparing SLEEP power consumption to the default online mode.
(III) We examine an intra-frame power-save mechanism termed IFPS, which does not require any modifications in standardization. We show that there are considerable differences between the IFPS mechanisms of the various devices. Based on IFPS, devices stay tuned to receive the maps and can participate in ordinary operations such as transmitting CQI reports and HARQ Ack signals. Nonetheless, when not transmitting or receiving data at all, or transmitting or receiving a data burst that does not occupy the entire uplink (UL) or downlink (DL) sub-frame, an MS limits its power consumption to the actual transmission time, switching off its transceiver at all other times. We evaluate IFPS on four of the examined devices. We show that when compared to SLEEP PSC2, IFPS performs almost the same, but it is free of the BS scheduler complexity to schedule and maintain the SLEEP cycles for all MSs in the cell. These measurements prove that when utilizing the power-save in a single frame, the benefit of applying the standard techniques of SLEEP and or IDLE is relatively small, and can be estimated between 18% to 24% in the best cases. Obviously, IFPS requires no latencies in entering or exiting power-save mode.
Even though our measurements were performed on widely deployed devices running IEEE 802.16e-2009 [33]which has evolved from IEEE 802.16d-2004 [34], the results and conclusions brought in this study not only apply to pre 4G WiMAX networks, but also to 4G networks based on 802.16m and the long term evolution (LTE) of the 3GPP. This is because in both 4G technologies, there are similar protocols, (though not identical) for power-save; SLEEP and IDLE (with small changes in 802.16m), and the mode of discontinuous reception (DRX) in LTE.

3.1.1 Related work

Power-save modes in cellular networks, and particularly sleep mode, attracted attention ever since the introduction of Cellular Digital Packet Data Systems (e.g., [35,36]). The literature presents various studies on power-save modes, mostly in the realm of performance analysis and protocol development.

The power saving mechanism for the UMTS user equipment (UE) has been evaluated in [37]. The performance of IEEE 802.16e power saving has been analytically evaluated in [38], where the authors use a semi-Markov chain approach. Other authors have used queuing theory to analyze power saving. For instance, Seo et al. proposed an embedded Markov chain to model system vacations in IEEE 802.16e, where the base station queue is seen as an M/GI/1/N system [39]. An M/G/1 queue with repeated vacations has been proposed to model an 802.16e-like sleep mode and to compute the service cost for a single user download [40]. However, these works, to allow a tractable analysis, consider models that are not realistic. For example, power saving mechanisms are evaluated under the assumption of Poisson traffic arrival, which is far from reality, especially in high speed data networks. To better validate their analytical models, the authors of [35,38,41] and [42] used simulations with more realistic assumptions. Yet, both analytical and simulation studies require some assumptions on the user equipment power consumption and timing parameters. For example, the authors of [38] borrowed the power consumption values from the IEEE 802.11WLAN because they did not have any power consumption information of IEEE 802.16e, and the authors of [41] just assumed arbitrary values for the energy consumption units in the sleep and listening intervals.

Enhancements to the standard and new power-save protocols have been proposed in numerous studies. Lee and Bahk [43] proposed a sleep mode interval control algorithm that takes into consideration the downlink traffic pattern and the mobility of the mobile station. In [44] a method to approximate idle duration distribution, using a mixture of exponentials, was proposed, and a procedure to optimize the power saving mechanism was developed. The authors of [45] presented another method that determines the length of sleep interval. In [46] a novel approach was suggested for saving power by reducing the modulation scheme and thus the transmission power. However, again, these power-save enhancements were not tested in real-life applications nor in real equipment. Furthermore, to illustrate their advantages, synthetic power consumption values were used. For example, the authors of [45] adopted values measured in wireless LANs for IEEE 802.16e systems. As for another example, the authors of [46] did not present any power measurements to illustrate the potential gain in power consumption from their approach.

Indeed, the importance of real power measurements in IEEE 802.16e have been recognized in [47], which established a power measurement environment for a real WiMAX test-bed. However, the authors of the paper did not assess the power consumption of sleep mode in WiMAX and eventually adopted figures from IEEE 802.11 cards for their simulations.

3.1.2 Measurement setup

In order to fully assess the power-save behavior of different commercial IEEE 802.16e network cards, we ran our measurements on two different setups. The first setup is an operational femtocell network that was used to examine the device behavior in a real environment under operational

conditions. Choosing the femtocell BS rather than a macro BS is encouraged by the fact that operators like UQ and CLWR are deploying this kind of base station for the indoor segment as WiFi replacement. Since in the operational femtocell network we cannot access the BS and in order to better control its behavior (e.g., scheduling, CQI allocations etc.), we conducted a second set of experiments over a second setup based on base station emulator for which we can intervene with the BS behavior.

Both setups were realized based on the setup used in North America. Accordingly, we utilized the same WiMAX frequency bands as the ones used in North America (center frequencies from 2501 MHz to 2691 MHz) and bandwidth of 10 MHz (with FFT set to 1024 and cyclic prefix of 1/8). WiMAX operates in TDD with the frame length set to 5 ms and downlink to uplink ratio of 29/18 [OFDM symbols]. In the sequel we will describe the two setups separately.

3.1.2.1 Femtocell

The set of experiments over real deployed network were conducted over Intel's private WiMAX network in Petach Tikva, Israel. This network is connected to the Internet and serves Intel employees. It operates a commercial Motorola BS (type BCU I, RF head type DAP I. SW version 3.00.10), a commercial carrier access point controller (CAPC) also provided by Motorola (Low Tier, SW bundle version 04.00.01.09.04) and Intel MS embedded in a laptop. The BS transmit power of the PREAMBLE symbol was limited to 24 dBm (over a bandwidth (BW) of 10MHz / FFT 1024), while the maximum Tx power of the MS is 23 dBm, in accordance with regulatory limitations. We utilized this setup mainly to track the BS SLEEP and IDLE performance while activating real life applications. The femtocell setup is described in Figure 28(a).

3.1.2.2 Base station emulator (Pico-Chip)

For measuring and characterizing the power-save behavior in the boundaries of the WiMAX frame, we used a BS emulator (BSE) based on the Pico-Chip development platform PC7203 ([48]) with dedicated BW, as controlling the scheduler and mapper algorithms for data and control bursts in the femtocell setup is very limited. We used the oscilloscope (Tektronix DPO 4054) to measure the current consumption of the MS device by probing its 5 Vcc feed in the USB connector. The oscilloscope also measures the BSE Tx signal. This was done in order to detect the frame boundaries on the same time axis as the power consumption of the MS device (the PREABMLE is easily observed each 5ms). A typical snapshot that depicts the power levels of the MS in IDLE mode and in 'online' mode is shown in Figure 30. The power-meter (Anritsu ML2487A) was used to monitor the actual Tx power, as one of the characterization steps was to test the influence of Tx power on the power consumption. The USB protocol analyzer (Le Croy model 2500H) was used to monitor whether the USB interface was suspended (to save power) or active. The emulator setup is described in Figure 28(b).

We conducted our experiments over five leading commercial MS devices, i.e., we examined devices which are used by Clearwire (USA), UQ (Japan) and Yota (Russia) operators. Table 1 summarizes the specifications of the 5 MS that we used in the measurements.

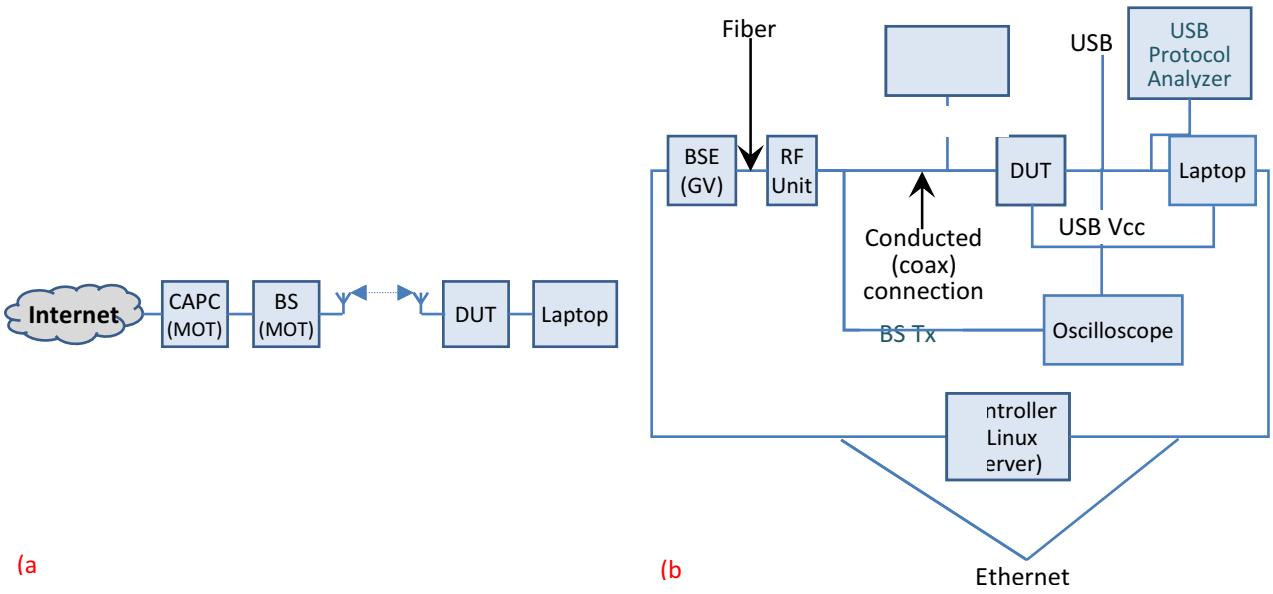

Figure 28: Experimental setup (a) Femtocell setup (b) BSE setup.

Table 1: Specifications of the 5 MS that we used in the measurements (the Beceem device was checked as integrated in two products: Ubee PXU1900 and Alvarion BreezeMax 250)

Product	Intel Centrino WiMAX 6250 (Embedded)	Ubee PXU 1900/ Alvarion BreezeMax 250	Samsung SWC-U200	MODACOM MW-2510
BB Chip vendor	Intel	Beeceem (bece3301 chipset)	Samsung (CMC-730 chipset	GCT (GDM7205K chipset)
Operator	UQ (Japan) CLEAR (US)	CLEAR (US)	YOTA (Russia)	UQ (Japan)
FW/SW	6.5.1037	5.2.2061039/5.2.115.4	Cl14/338	Ver 2
Frequency	2.548[GHz] 2.657[GHz]	2.525[GHz]	2.625[GHz]	2.61[GHz]

3.1.3 Power consumption

Initially we measured the average power consumption of various operational modes. Accordingly, we utilized the BSE setup to operate the commercial mobile stations in various scenarios of receive and transmit signals and measured the average power consumption in milliwatts per frame per

scenario. In addition to the "active" mode measurements, we also measured the average power consumption in IDLE mode as well as in wake-up sequence from offline mode (to receive the MOB_PAG-PLI message).
Specifically we conducted experiments, measuring the power consumption over fourteen different setups. Figure 29 depicts a typical frame in each of the scenarios (both the Rx and Tx). Each experiment lasted a few seconds.
The first setup which serves as a baseline, only the Frame Control Header (FCH) and the map were transmitted on each frame (1+4 symbols), i.e., the BS transmitted the maps with no allocations in the downstream nor in the upstream. In the next three setups the BSE transmits an additional single burst in the DL sub-frame besides the mandatory FCH and map bursts. The transmission is modulated in 16QAM ¾ with no repetition (data = 540 bytes) and is transmitted periodically on each frame. The difference between the three tests is in the location of the burst within the frame. In the first two tests the burst spans the entire BW whereas in Test 2 the burst is adjacent to the DL-map and in Test 3 the burst is located at the last DL slot duration (Figure 29 Test ID2 and Figure 29 Test ID3 respectively). In Test 4 the burst spans over 3 subchannels for 10 slot durations (out of the 12 available) that follow the DL map (Figure 29 Test ID4).
In Tests 5-8 the BSE allocates CQI and HARQ Ack allocations for MS to report CINR or for retransmissions in every frame. Besides the FCH and map bursts and the UL CQI or HARQ Ack transmissions there are no other DL or UL transmissions. Since an MS device that is in the BS proximity (high RSSI) may consume less power for transmitting the CQI signal or HARQ Ack signal than the same MS device located at cell edge (low RSSI), in the next four experiments we examined the power consumption difference between the two cases. Accordingly in Tests 5-6 and Tests 7-8 we experiment with the CQI and HARQ Ack transmissions under two different RSSI levels, -20 dBm/Tone and -10 dBm/Tone (Figure 29 Test ID 5-6 and Figure 29 Test ID 6-7 for the two RSSI levels and for CQI and HARQ ACK, respectively).
Next we examined the UL transmission power under two different RSSI levels. Accordingly, on the DL sub-frames the BSE transmits nothing but the compressed DL-UL map. In the US the BSE allocates either: (i) UL allocation that spans over the available 5 slot durations, over 7 sub-channels (total of 35 slots, which hold 630 bytes when the modulation is 16QAM ¾ with no repetition), Test ID 9 and10 for RSSI levels-20 dBm/Tone and -10 dBm/Tone respectively (Figure 29 Test ID 9-10), or (ii) UL allocation that occupies one slot duration and 35 sub-chanels (total of 35 slots). Test ID 11 and12 for RSSI levels-20 dBm/Tone and -10 dBm/Tone respectively (Figure 29 Test ID 11-12).
In the last two experiments in this set, we examined the power consumption while in IDLE mode (Test ID13), and the power consumption during the wake-up cycle (Test ID 14). Since Samsung MS doesn't support IDLE mode only Intel MS and Beceem MS were used in these IDLE characterizations in Test ID 13-14.

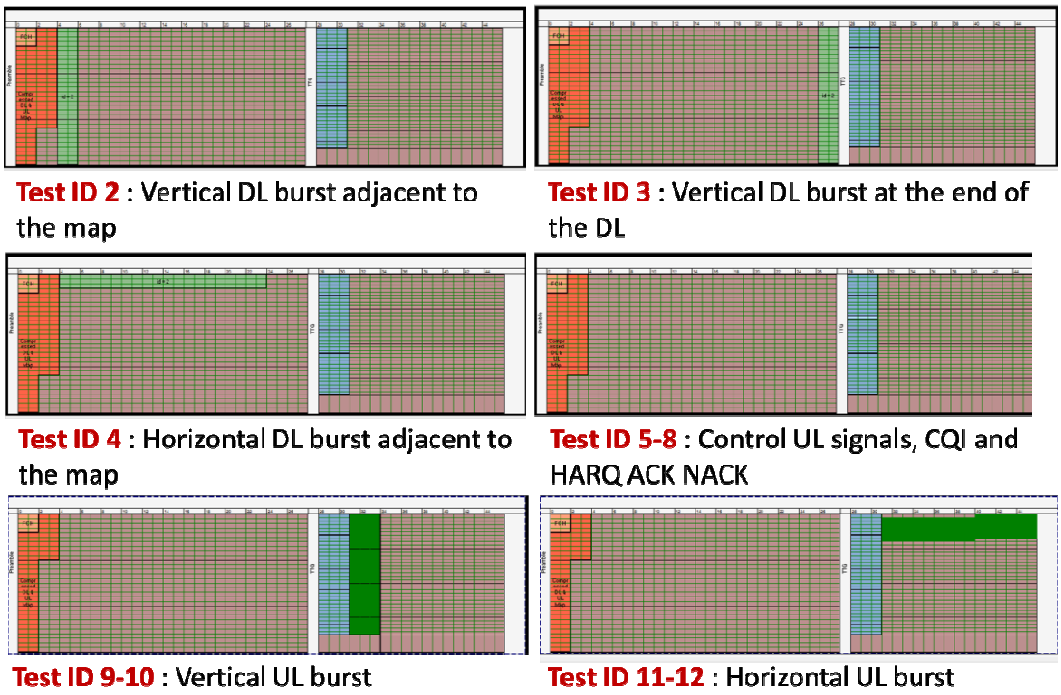

Figure 29: Rx and Tx scenarios in the BSE setup.

Table 2 summarizes the power consumption measurements. Each line in the Rx and Tx sections indicates the average power consumption of a different scenario per WiMAX frame. The result of the IDLE scenario which is presented in Test ID 13 averages the power for a period of 3 seconds (one paging listening interval). The IDLE scenario result which is presented under Test ID 14 averages the power over the time it takes the device to wake up from offline mode, receive the MOB_PAG-ADV message, and go back to offline mode (different times for Intel and Beceem devices). All the power values presented in Table 2 are brought in milliwatt units. The notations NA and NT indicate “Not Applicable” (e.g., Samsung MS doesn’t support IDLE) and “Not Tested” (e.g., the GCT dongle USB 5 Vcc feed was too noisy when we tried to measure with the oscilloscope). Using the USB protocol analyzer we observed that only Intel MS suspends its USB interface while in IDLE mode (this activity can be related to the medium power level as seen in Figure 30).

As can be seen in Table 2, considering the same scenario, there are differences in the power consumption of different mobile stations. Examining the power consumption of each MS along the time axis, we found out that the major reason for this difference is due to different Intra Frame Power-save (IFPS) implementations, in which device is going into a lower power mode after receiving or transmitting its burst. Accordingly, the power consumption of Intel, Beceem and Samsung mobile stations, along the DL sub-frame mostly depends on the location of the DL bursts; for Intel MS, the power consumption rises high to receive the first OFDM symbol of the DL, and decreases to low power level, 6 symbols after the ending of the last burst the MS needs to receive.

Table 2: Power consumption measurements over the fourteen different setups. All the power values are brought in milliwatt units. The notations NA and NT indicate "Not Applicable" and "Not Tested", respectively. Values in IDLE refer to the lowest level for each device.

	ID	Details	Intel	Beceem	Samsung	GCT
RX	1	Only maps (1+4 symbols)	710	500	710	655
	2	2 symbols X30 subchannels burst, adjacent to map	740	510	725	NT
	3	2 symbols X30 subchannels burst, end of DL	935	795	785	NT
	4	20 symbols X3 sub-channels burst, adjacent to map	930	745	750	NT
TX	5	CQI burst @ -20dBm/Tone	770	620	900	705
	6	CQI burst @ -10dBm/Tone	770	615	910	NT
	7	3*HARQ ACK/NACK burst @ -20dBm/Tone	780	640	780	710
	8	3*HARQ ACK/NACK burst @ -10dBm/Tone	785	640	780	NT
	9	3 symbols X35subchannels burst, @ -20dBm/Tone	780	605	895	840
	10	3 symbols X35subchannels burst, @ -10dBm/Tone	825	660	940	NT
	11	15 symbols X7subchannels burst, @ -20dBm/Tone	1050	805	905	840
	12	15 symbols X7subchannels burst, @ -10dBm/Tone	1255	935	1010	NT
IDLE	13	Average power consumption while in IDLE	115	375	NA	NT
	14	Power consumption of wake-up cycle	660	865	NA	NT

The behavior of Beceem MS is further optimized. Its power consumption decreases to low power level only 4 symbols after the burst ending. This power optimization behavior was observed for bursts which are allocated in the first symbols along the DL. For bursts that are not allocated in the first symbols of the DL, its power consumption decreases sharply after the burst ending. As for Samsung MS, its power consumption decreases at the last burst in the DL it has to receive, but not to the minimum level as do the Intel and Beceem mobile stations, but to a medium level. Only when the DL last symbol ends (OFDM symbol 29), does its power level decrease to the lowest level (assuming there's no transmission in the UL).

Checking the mobile stations transmission, we also observed an IFPS behavior; Intel and Beceem mobile stations raise their power consumption to the high level at the beginning of the first burst to be transmitted, and they decrease to the lower power level sharply when the burst transmission ends. Both Intel MS and Beceem MS have the same power consumption behavior with respect to all burst types. This is not the case with Samsung and GCT mobile stations; these devices differentiate the IFPS behavior in the UL sub-frame as follows: for HARQ Ack bursts, both decrease the power consumption sharply after the burst transmission ends. For CQI burst, Samsung MS doesn't change its power consumption level, till the end of the UL sub-frame. GCT MS behaves with CQI as if it was HARQ Ack burst, i.e., decreasing the power consumption level sharply when the burst transmission ends. As for data bursts, both mobile stations do not perform any kind of IFPS, even in the case of vertical data bursts (test Id 9, 10 in Table 2).
An IDLE behavior comparison shows that the average power consumption while in IDLE mode and during the of wake-up cycle for the Intel device are 115, 375 [miliwatt], respectively, and 660, 865 [miliwatt] for the Beceem device, respectively. A typical snapshot of the current consumption of entering and exiting IDLE mode, as measured by the oscilloscope is shown in Figure 30. The current consumption is shown both for the MS device (bottom part of the figure) and for the BSE Tx signal (upper part of the figure). The vertical axis depicts the current consumption measured in milliwatt, while the horizontal axis show the time measured in msec.

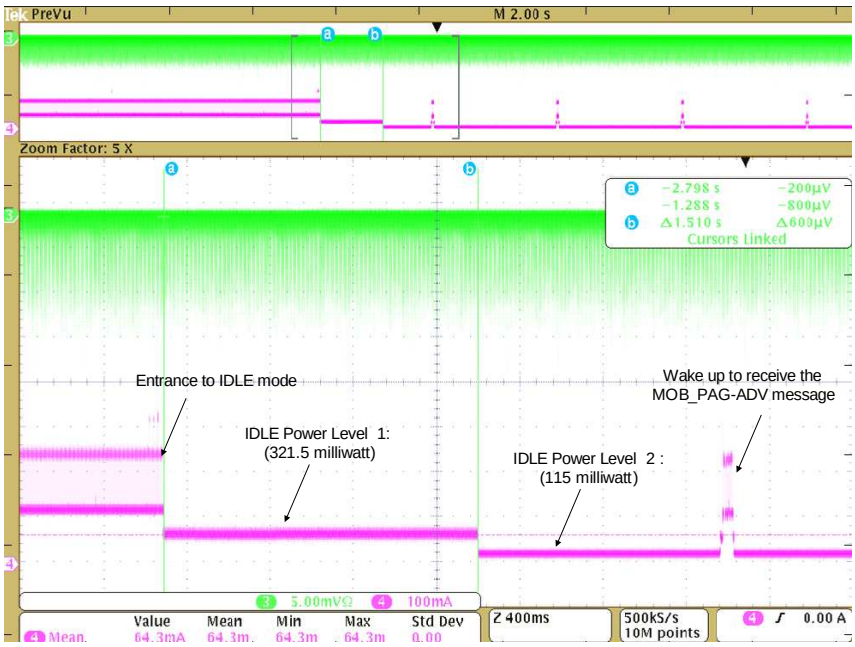

Figure 30: Power levels of the MS in IDLE mode and in 'online' mode.

More IDLE measurements which characterize the times it takes to get into IDLE, and the time it takes to wake-up from IDLE in order to receive the MOB_PAG-ADV message are given in Table 3.

Table 3: IDLE related times

	Intel	Beceem
Time with no traffic to enter IDLE	20 [sec]	>250 [sec]
Time the MS wakes-up before reception of MOB_PAG-ADV	47.5 [msec]	67.5 [msec]
Total time the MS wakes-up before going back to offline mode	63.5 [msec]	84 [msec]

As can be seen in Table 3 it takes a while for the device to decide that it can enter IDLE mode. While Intel's device entered IDLE mode after 20 [Sec] it took the Beeceem device over 250 [Sec] with no traffic to enter IDLE mode.

3.1.4 Sleep and idle behavior

With the power consumption figures at hand, we turn to investigate the cycle of SLEEP and IDLE modes under various traffic patterns, i.e., we examined the adaptation of the SLEEP and IDLE modes to widely used traffic patterns. Particularly, we consider four commonly used mobile applications, namely, Google Earth, Skype (in two operation states), Facebook, and internet radio. In more details, we consider the following application usage:

1. Download Google Earth Application, followed by browsing a map (http://www.google.com/earth/index.html)
2. Conducting a Skype audio call from two MS in the femtocell sector, with and without video.
3. Skype application in online mode (with no incoming/outgoing call or active chat).
4. Web browser with Facebook home page opened (www.facebook.com), with no activity by the user.
5. Web browser playing internet radio stream (http://locator.3dcdn.com/glz/glglzradio/300/200/radio.html)

For each application, we track for several minutes its activity (in terms of packets sent to the network). At the same time, we assess the NIC power-save state (active, idle, sleep, etc.) and the consumed power.
These measurements are performed over the femtocell setup described in 3.1.2.A. We identify the power-save state of the NIC through recorded debug logs. Specifically, the entrance and exit times from SLEEP mode are identified through the MAC messages MOB_SLP-REQ and MOB-SLP-RSP. The entrance and exit times from IDLE are identified through the MAC messages DREG-CMD and RNG-REQ.
Figure 31 shows, for each application, the total percentage of time the device under test (Intel) stayed in each power-save state, namely, online, sleep or idle. We note that, the sleep mode refers to power-save Class 1 (PSC1).

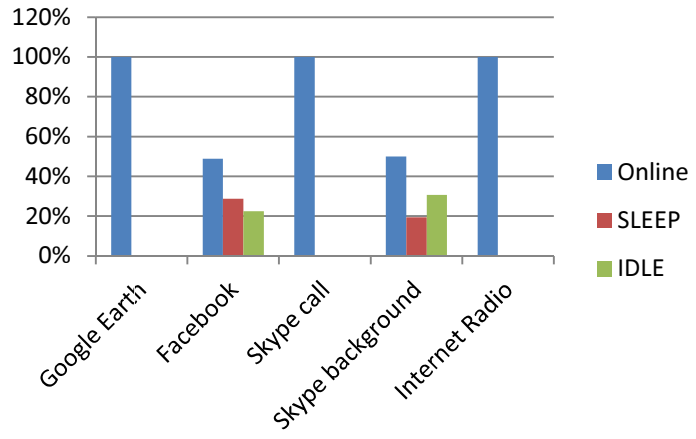

Figure 31: SLEEP and IDLE performance; Values refer to the relative part of the time that the device operation mode was online (to receive and/or transmit data bursts) or offline (in SLEEP or IDLE).

Our measurements show that SLEEP and IDLE modes became operational only in two scenarios, Facebook and Skype background (Figure 31). Although these scenarios are "always-on" they do not involve any interaction by the user. Accordingly, the sporadic packets allowed the NIC to enter SLEEP and IDLE modes. Yet, it is interesting to note that more than half of the time the NIC stayed in active mode, in spite of the low traffic.
In all other cases, neither SLEEP nor IDLE operation was observed due to denser traffic than background Skype and Facebook. The case of internet radio is particularly interesting as the averaged measured traffic was generated by a single burst holding 4500 bytes per 220 frames (which yields around 32 [kbps]); We would have expected the MS to save a lot of power by requesting periodical availability/unavailability periods by activating SLEEP PSC2. However, the MS didn't perform SLEEP at all when operating this scenario.
In the following sections we further examine the above power-save behavior for online applications (Facebook and Skype) as well as for internet radio streaming.

3.1.4.1 Online applications

In this section we further examine "always-on" applications operation with respect to SLEEP and IDLE performance. In order to demonstrate the traffic generated by the MS we draw Figure 32, and Figure 33. Figure 32 depicts about 20 minutes of operation of each application, while Figure 33 focuses only on Skype operation with a zoon in on typical 200 seconds, and 13.5 seconds. In these graphs, the x axis represents the time in units of 5 millisecond (1 WiMAX frame). The y axis represents the burst size; accordingly the level '10' refers to bursts that are up to 100 bytes in size. The level '11' refers to bursts that are 101 to 200 bytes in size, and so on and so forth. Each dot in the Figures represents a burst allocated to the MS for transmission, the time and allocation in bytes assigned to the MS (all the 802.16e MAC messages that do not carry IP information have been filtered out). The solid line at the bottom of each sub figure (below the dots) refers to power-save mode. As can be seen in the Figures, the solid lines composed of 3 levels, each represents the measured MS power consumption. Accordingly, the highest level indicates no power-save mode

(high power consumption), the medium level refers to SLEEP mode (lower power consumption) and the lowest level refers to IDLE (low power consumption).

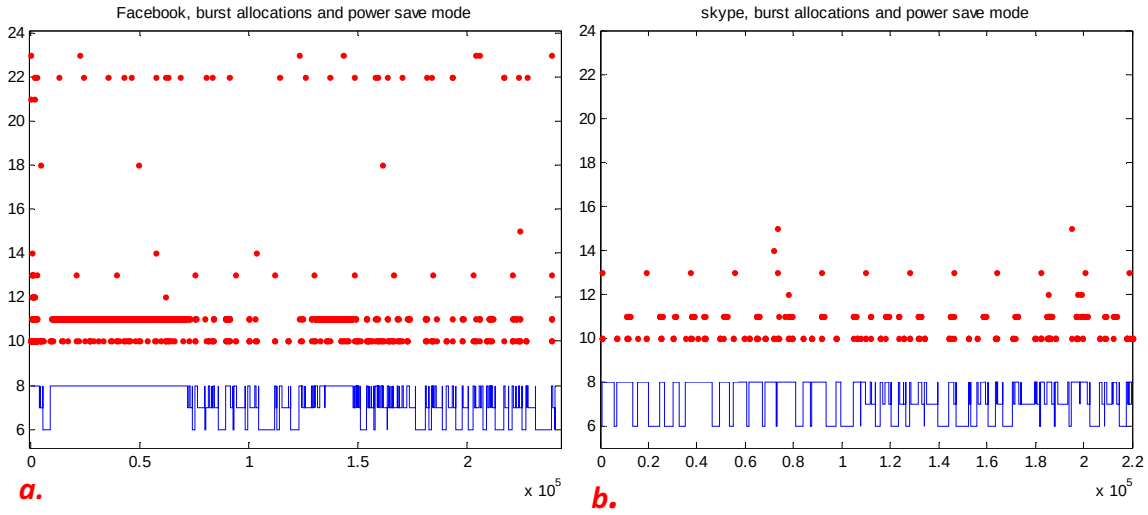

Figure 32: Burst allocations vs. power-save mode for around 16 minutes for a) Facebook b) Skype.

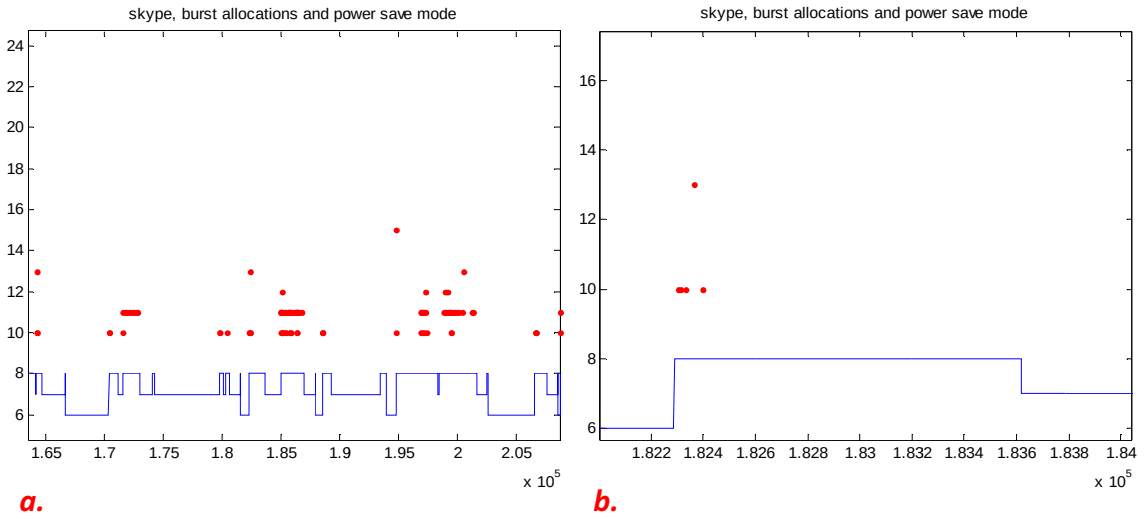

Figure 33: Burst allocations vs. power-save mode for Skype when in online mode for around a) 200 sec b)13.5 sec.

Examining these figures, we observe the following:

- In both tests (Facebook, Skype) there is traffic that we believe is not generated by the application itself, but refers to other processes running unheedingly in the laptop (e.g. operating system processes). Some of this traffic has a periodic pattern for both applications, like the bursts on level '13', repeated every 90 seconds.

- There are conspicuous differences between Facebook and Skype traffic patterns; Facebook seems to generate denser traffic for packets of size 0-200 bytes than Skype does. In two periods (frames 8870-71587 and frames 135000-147482) we observed periodic pattern (bursts of size 118 bytes every 62 or 63 frames) that prevents the MS from getting into SLEEP or IDLE. This behavior was not observed with Skype. In addition, Facebook generates consistently packets of size 2200-2300 bytes while Skype doesn't.
- IDLE mode is always preceded by SLEEP periods.
- Due to the predominance of small packets (up to 100 bytes), both IDLE and SLEEP modes are disrupted in almost all cases by these small packets. In many cases, the power-save period is is very short due to that.
- Most of the frames in online mode are not used for transmission as can be seen in Figure 33(b).

To conclude this evaluation, the power-save modes (SLEEP and IDLE) are not efficient as there is no synchronization mechanism between the data source (OS process / online application) and the WiMAX MAC to preserve their operation. As a result there are multiple instances of short time IDLE and SLEEP, overloading the network with control messages (to enter SLEEP or IDLE) rather than the theoretical alternative of fewer instances of longer duration. For instance, in Figure 33(a) there are 5 instances of IDLE in less than 175 seconds, with about 25 seconds for the longest IDLE duration, and about 5 seconds for the shortest IDLE duration.
Another important finding shows that in online mode the majority of the frames are not used for transmission at all in all five applications; Google Earth only used 71% of all frames for transmit and receive. Similarly, Skype with an active call used 72%. Facebook and Skype as background applications with no user activity used about 99% and the internet radio application used 97% of all frames for transmit and receive. In all these cases, when SLEEP and IDLE were sporadically used (Facebook, background Skype), and when not used at all (Google Earth, Skype call and internet radio), IFPS can be a good alternative for saving power, as the majority of the frames in online mode are neither used for transmit nor receive.

3.1.4.2 Internet radio analysis

We now consider the internet radio measurement we performed with the femtocell setup. The application-required traffic was 32 [kbps], while it started playing only after it buffered 5 seconds of the radio transmissions. For the analysis we will consider two extreme scenarios; the first refers to best radio frequency (RF) conditions and few MS subscribed in the cell. This scenario matches our measurements for the radio internet over the femtocell setup. The second scenario refers to cell edge conditions (only base rate reception is possible) with multiple active subscribers in the cell.
The first scenario, combination of only few MS subscribers in the cell and high signal quality, allows the BS scheduler to allocate the DL burst adjacent to the map and in the highest modulation coding scheme (MCS) in the MIMO zone. In our internet radio measurements, we observed that the required traffic of 32 [kbps] derived a single burst of size 4500 bytes every 220 frames (1.1 seconds). Modulating with the highest MCS in the MIMO zone, such a burst requires 75 physical slots. Due to the low number of MS subscribers registered in the cell, this allocation can be adjacent to the map such that it will span over 6 OFDM symbols. In order to simplify the analysis we assume that in all other frames, there is no DL traffic at all, except for the maps which occupy 4 symbols

(plus one for the preamble). We also assume that there are no data transmissions over the UL sub-frame (meaning that the internet radio is a UDP service which doesn't require TCP Acknowledgement (TCP-Ack) packets to be transmitted in the UL), and that the data bursts in the DL sub-frame have the normal form, rather than HARQ. The only transmission along the UL sub-frame is a CQI burst that precedes the DL burst holding the internet radio data packet.
We now estimate the power consumption for this scenario in two modes; the first one where the MS performs SLEEP PSC2, and the second one where the MS doesn't perform SLEEP. In both cases, the MS IFPS implementation is optimized. We will assume a SLEEP pattern of 116/4 (unavailability/ availability). Note that in order to send CQI signals, the minimum availability period is 4 frames due to protocol limitations. Now, let's assume that the wake-up period we found for IDLE PLI (see Table 2) holds also for SLEEP awakenings, and is equal to 14 frames (70 milliseconds). So, in total, the device performs a cycle comprised of awakening for 14 frames, followed by 4 frames in which it transmits one CQI signal, and receives the DL-burst holding the radio internet data packets, followed by 202 frames the device is in unavailability period, this cycle is repeated periodically. We'll substitute the values for Beceem MS (some of the values can be easily calculated from the table values, though not explicitly brought there):

- Power consumption for the frame containing the DL burst with internet radio packet = 562 [milliwatts].
- Power consumption for the frame containing the CQI transmission = 615 [milliwatts].
- Power consumption for the two frames in which the MS only receives the maps = 500 [milliwatts]
- Power consumption for the 14 frames of wake-up = 865 [milliwatts]
- Power consumption for the 202 frames of SLEEP = 375 [milliwatts]

Substituting these values yields an average power consumption of PSleep = (1*562 + 1*615 + 2*500 + 14*865 + 202*375)/220 = 409 [milliwatts].
Let us now consider that the MS doesn't enter into SLEEP, but only performs IFPS. In this case, we have one frame for receiving the DL burst with radio internet data packet, one frame for transmitting the CQI, and 218 additional frames in which the MS only receives the DL map. Substituting these inputs yields a power consumption of PIFPS = (1*562 + 1*615 + 218*500) / 220 = 500.8 [milliwatts].
The implication of these results is that applying SLEEP PSC2 in a scenario with similar conditions, saves only 18% of the power consumption.
We now analyze the second scenario, where the RF conditions are poor, and the cell is overloaded with MS subscribers. In such a case, the MS receiver is able to correctly demodulate a signal that has been modulated in base rate. In addition, due to the high number of active registered mobile stations in the cell, the map is extended to 8 OFDM symbols (plus one for the preamble). Satisfying the application traffic demand for 32 [kbps] with the base rate MCS requires the data to be modulated in 750 physical slots. Since the maps area occupies now 9 symbols, there are only 20 symbols remaining in the DL sub-frame which form 300 physical slots. Hence, two complete DL sub-frames are needed (assuming we neglect the fragmentation overhead), plus a burst that occupies over 10 more symbols. So now our inputs are as follow:

- Power consumption for 2 full DL sub-frames = 795 [milliwatts]

- Power consumption for the additional sub-frame with the DL burst over 10 symbols = 692 [milliwatts]
- Power consumption for the frame containing the CQI transmission = 667 [milliwatts].
- Power consumption for the two frames in which the MS only receives the maps = 552 [milliwatts]
- Power consumption for the 14 frames of SLEEP awakening = 865 [milliwatts]
- Power consumption for the 200 frames of SLEEP = 375 [milliwatts]

Substituting these values yields an average power consumption of PSleep = (2*795 + 1*692 + 1*667 + 2*552 + 14*865 + 200*375) / 220 = 414.3 [milliwatts].
Substituting similarly to achieve the power consumption for the optimized IFPS case yields PIFPS = (2*795 + 1*692 + 1*667 + 216*552)/220 = 555.3 [milliwatts].
In this case, the benefit of using sleep rises to 25.4%, which is still relatively small (considering the protocol implementation complexity).

3.1.5 Uplink intra frame power-save

Intra frame power-save (IFPS) mechanism has been identified above as a compromise that is both efficient for most applications and relatively simple to implement. Yet, the implementation of IFPS in uplink is not as straightforward as that of in downlink.
Specifically, IFPS in downlink is a viable approach thanks to the frequency-first downlink allocation. Such allocation enables the user to receive its data in a short time relatively to the whole frame duration. However, in uplink, the common approach is to transmit in a time-first manner. This allows the user to span data transmission across longer duration but with lower bandwidth. Lower bandwidth transmission enables the MS to spread its transmission power on fewer sub-carriers and does obtain more reliable communication. Clearly, spanning the transmission over the entire uplink frame prevents the MS from entering an IFPS state while in uplink transmission. Because IFPS is an important mechanism for power saving, we examine the possibility to modify the uplink allocation to support IFPS.
To that end we first examine the MS uplink transmission and in particular the MS power headroom. MS power headroom denotes residual MS power, where zero headroom indicates that the MS transmits at its maximal power. To support uplink IFPS, or in fact, frequency-first allocation, one has to verify that the MS is not in power headroom. A known problem in WiMAX networks refers to the asymmetry between transmission power of macro base stations and that of the mobile stations. As a result, MS at the cell edge typically enters into a zero headroom transmission. Unlike macro BS, femtocells may transmit in relatively low power due to the shorter radius of their cells. Hence the problem of MS zero headroom may be negligible. We verified that indeed users rarely transmit in power headroom (associated with femtocells) through another experiment with our femtocell setup. We found out that along the office floor, there were only two singular locations (the floor area is about 50[m] X 50[m] = 2500 [m2]), where a full bandwidth (BW) transmission of the MS was limited negligibly. In all other locations, a full BW transmission always had significant headroom from the maximal transmission power.
Encouraged by this finding, we used the BSE setup to compare the power consumption of an MS burst transmission that has the horizontal shape (“time-first”) and a burst transmission with vertical shape (“frequency-first”). Note that in order to achieve such a vertical burst, we modified the BSE

mapper module such that it used a zone switch IE (Information Element) to split the UL sub-frame to two zones. The UL allocation was scheduled before the zone switch IE in the map, so according to the standard rules for zones in sub frame, the shape of the burst is derived vertically.
Figure 34 shows the current consumption of the Intel MS scheduled with vertical and horizontal bursts alternately. One can easily observe that the power level for both cases is almost the same, even though the transmit power of the vertical burst is 7 dB higher than that of the horizontal one. (This can be explained due to the inefficiency and non-linearity of the MS power amplifier). However, due to the IFPS behavior in the UL, the duration in time of the horizontal burst is 5 times longer than that of the vertical one. This results in power consumption almost 5 times higher. Table 2 summarizes the numerical results for these tests (Test Id 9-12 in Figure 29).

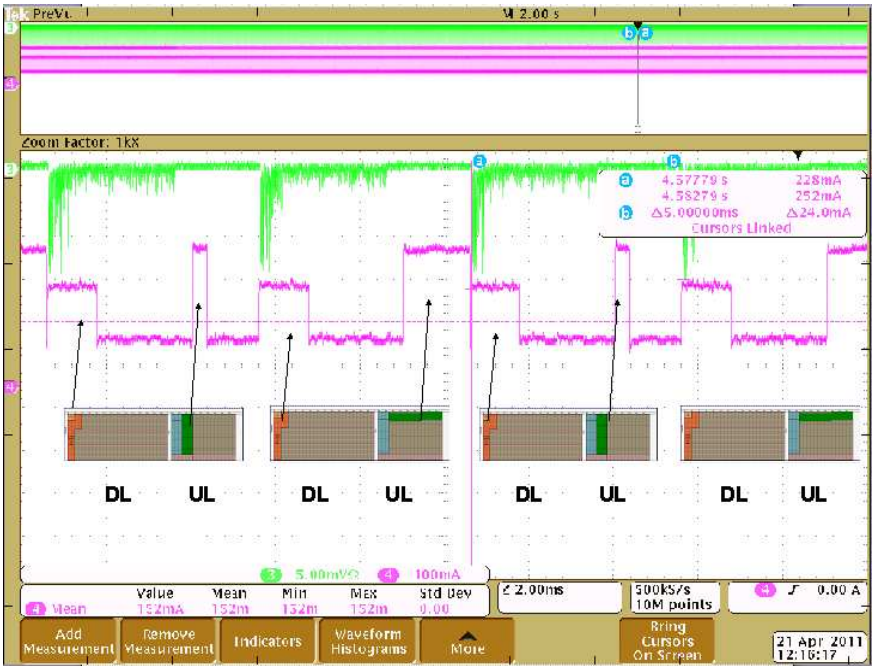

Figure 34: Intel MS DL/UL IFPS behavior of test Id 4, 9,11; in the DL, it takes 6 symbols after the map to reduce the power consumption to the lowest level, while in the UL, the power consumption level depends mainly whether the burst has the vertical shape or horizontal shape.

We believe that this finding justifies a new BS scheduler algorithm that considers MS IFPS capability as well as MS temporal transmission power in order to schedule the MS burst in a way that will allow conservation of power.

3.1.6 FLAVIA architecture support

As previously discussed there are quite a few enhancements which can dramatically reduce the MS power consumption and which are not supported by current state of the art architectures but are

supported by FLAVIA architecture. In particular, the main blocks in FLAVIA architecture that support enhancement for power-save mechanisms are the Scheduler (both the MAC Scheduler and the Scheduling Strategy sub-blocks), the Power-saving block and the Application optimization support block (Figure 35).

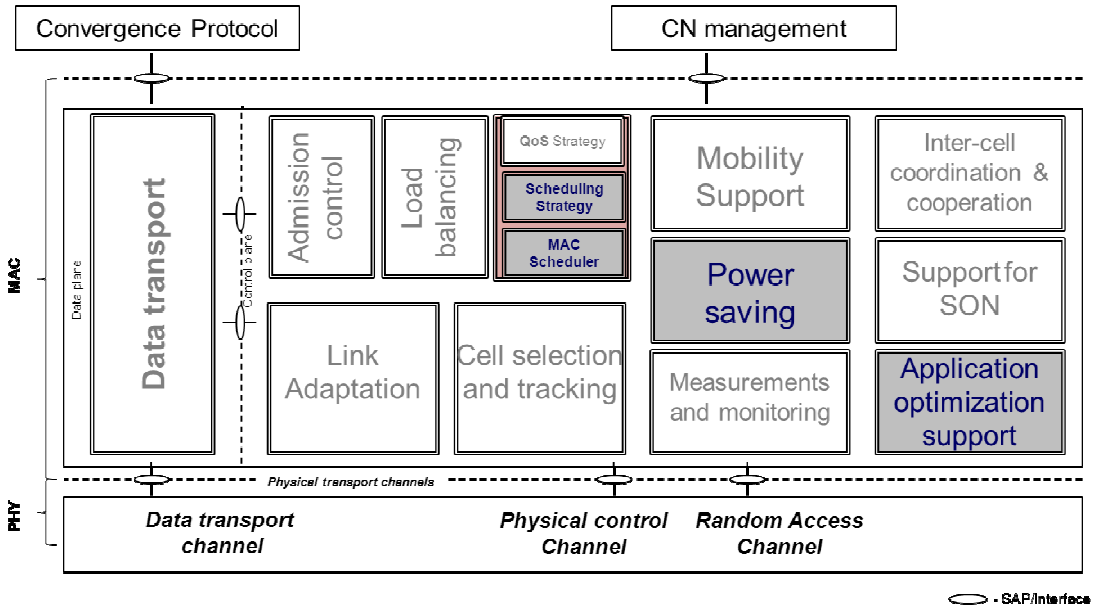

Figure 35: FLAVIA architecture enhancements for power-save mechanisms support.

For example in order to enable opportunistic scheduling which takes into account IFPS capabilities (Section 3.1.3) the scheduler must be modified. Cross layer optimization in which the power-save mechanism is adapted to the application which is running (Section3.1.4) can be implemented in the Application Optimization Support block. Enabling new power-save mechanism which are currently not supported by the standard can be facilitated in the Power-Saving block. Other enhancements which combine diverse mechanisms are also supported by the FLAVIA architecture, through combinations between one or more blocks, e.g. support of IFPS on the upstream, as discussed in Section 3.1.5, can be enabled through the combination of the Measurements and Monitoring block which will examine the MS power constraints (MS power headroom) and the scheduler which will schedule the user taking into account IFPS support and power headroom.

3.2 Power save analysis for base stations and mobiles with continuous connectivity

Here we describe the analytical work that has been conducted in the frame of the FLAVIA project to analyze the power saving that can be achieved by means of Discontinuous Reception (DRX) and Discontinuous Transmission (DTX) in cellular networks. We also show the impact of DRX and DTX on web-traffic performance when customers adopt the continuous connectivity paradigm. To this aim, we provide a model for packet transmission and cost. We model each mobile user's traffic with a realistic web traffic profile, and study the aggregate behavior of the users attached to a base station by means of a processor-shared queueing system. In particular, we evaluate the user access delay, the download time and the expected economy of energy in the cell. The model is validated through packet-level simulations. Our model shows that dramatic energy save can be achieved by both mobile users and base stations, e.g., as much as 70% of the energy cost due to packet transmission at the base station.

3.2.1 Problem statement and related work

The total operating cost for a cellular network is of the order of tens of millions of dollars for a medium-small network with twenty thousand base stations [49]. A relevant portion of this cost is due to power consumption, which can be dramatically reduced by using efficient power save strategies. Power save can be achieved in cellular networks operating WiMAX, HSPA, or LTE protocols by optimizing the hardware, the coverage and the distribution of the signal, or also by implementing energy-aware radio resource management mechanisms. In particular, here we focus on power save in wireless transmissions, which would enable the deployment of compact (e.g., air conditioning free) and green (e.g., solar power operated) base stations, thus requiring less operational and management costs.

An interesting case study is offered by the behavioral analysis of users that remain online for long periods. These users request a continuous availability of a dedicated wideband data channel, in order to shorten the delay to access the network as soon as new packets have to be exchanged. This *continuous connectivity* requires frequent exchange of control packets, even when no data are waiting for transmission. Therefore, in case of continuous connectivity, a huge amount of energy might be spent just to control the high-speed connection, unless power save is enforced.

However, since power save mode affects packet delay, some constraints have to be considered when turning to the power save operational mode. Power save and sleep mode in cellular networks have been analytically and experimentally investigated in the literature, mainly from the user equipment (UE) viewpoint. E.g., power save in the UMTS UE has been evaluated in [50] and [38] by means of a semi-Markov chain model. The authors of [39] proposed an embedded Markov chain to model the system vacations in IEEE 802.16e, where the base station queue is seen as an $M/GI/1/N$ system. In [40], the authors use an $M/G/1$ queue with repeated vacations to model an 802.16e-like sleep mode and to compute the service cost for a single user download.

Analytical models supported by simulations have been proposed by Xiao for evaluating the performance of the UE in terms of energy consumption and access delay in both downlink and uplink [41]. The authors of [44] provide an adaptive algorithm that minimizes energy subject to QoS requirements for delay. The existing work neither tackles the base station (or evolved node B,

namely eNB) viewpoint nor analytically captures the relation between cell load and service rate statistics. Furthermore, for sake of tractability, many of those studies assume that packet arrivals follow a Poisson model. Instead, in real networks, the user traffic can be very bursty and follow long tail distributions [51].
In contrast, in our work use a *G*/*G*/1 queue with vacations to model the behavior of each UE, and we compose the behavior of multiple users into a single *G*/*G*/1 *PS* queue that models the eNB traffic. We analytically compute the cost reduction achievable thanks to power save mode operations, and show how to minimize the system cost under QoS constraints. In particular we refer to the mechanisms made available by 3GPP for *Continuous Packet Connectivity* (CPC), i.e., the Discontinuous Transmission (DTX) and Discontinuous Reception (DRX) [52].
The importance of DRX has been addressed in [53], where the authors model a procedure for adapting the DRX parameters based on the traffic demand, in LTE and UMTS, via a semi-Markov model for bursty packet data traffic. A description of DRX advantages in LTE from the user viewpoint is given in [54] by means of a simple cost model. In [55], the authors use heuristics and simulation to show the importance of DRX for the UE.
Our contribution is threefold: (*i*) we are the first to provide a complete model for the behavior of users (UEs) and base stations (eNBs) in continuous connectivity and with non-Poisson traffic, (*ii*) we provide a cost model that incorporates the different causes of operational costs, and (*iii*) we show how to use the model to minimize operational costs under QoS constraints. Our model has been validated through packet-level simulations, and our results confirm that a tremendous cost reduction can be attained by correctly tuning the power save parameters. In particular, eNB transmission costs can be lowered by more than 70%.
In the following subsections we first review power save operations in continuous connectivity mode; then we describe a model for cellular users generating web traffic, we illustrate a model for downlink transmissions, and describe how to evaluate flow performance and transmission costs. Finally we report our model validation experiments, and numerically show the power saving that can be achieved under the assumption of the 3GPP2 web traffic evaluation model [56].

3.2.2 Continuous connectivity

Cellular packet networks, in which the base station schedules the user activity, require the online UEs to check a control channel continuously, namely for T_{ln} seconds per system slot (i.e., per subframe T_{sub}).For instance, CPC has been defined by 3GPP for the next generation of high-speed mobile users, in which users register to the data packet service of their wireless operator and then remain online even when they do not transmit or receive any data for long periods [57].
A highly efficient power save mode operation is then strongly required, which would allow disabling both transmission and reception of frames during the idle periods. The UE, however, has to transmit and receive control frames at regular rhythm, every few tens of milliseconds, so that synchronization with the base station and power control loop can be maintained. Therefore, idle periods are limited by the mandatory control activity that involves the UE. To save energy, when there is no traffic for the user, the UE can enter a power save mode in which it checks and reports on the control channels according to a fixed pattern, i.e., only once every *m* time slots. Relevant energy economy can be achieved, as we show later in this document.

In change, the queued packets have to wait for the *m*-th subframe before being served. In the following we formally define DRX and DTX through the 3GPP specifications originally meant for HSPA systems. However, both DRX and DTX operations can be easily mapped onto WiMAX and LTE operations that involve the frame duration instead of the subframe, hence our work applies to HSPA as well as to WiMAX/LTE systems.

3.2.2.1 Discontinuous transmission

DTX has been first defined by 3GPP release 7. It is a UE operational mode for discontinuous uplink transmission over the Dedicated Physical Control Channel (DPCCH). With DTX, UEs transmit control information according to a cycle. There are actually two possible DTX cycles. The first cycle is used when some data activity is present in the uplink (normal operation), and it is a short cycle (one or very few subframes).The second cycle is longer (up to tens of subframes), and is triggered after an inactivity timeout in the uplink data channel expires (power save mode operation). The threshold *M* for inactivity period is typically a power of 2 subframes. Since transmissions on uplink data channel can only start in parallel with DPCCH transmissions, DTX also regulates data transmissions.

3.2.2.2 Discontinuous reception

DRX is an operational mode defined by 3GPP release 6 for the UE to save energy while monitoring the control information transmitted by the eNB. It also affects data delivery, since no data can be dependably received without an associated control frame. 3GPP specifications define a cycle, which is the total number of subframes in a listening/sleeping window out of which only one subframe is used for control reception. Suggested values for this cycle are 4 to 20subframes (i.e., using a 2-ms subframe in HSPA yields a cycle of 8 to 40 ms). DRX is activated only upon a timeout expiry after the last downlink transmission, and like DTX, the timeout threshold specified in the standard is *M* subframes, with *M* being a power of 2.

3.2.3 Power save model

We focus on the power consumption due to wireless activity on the air interface of mobile users (UEs) and base station (eNB). On the one hand, we assume that uplink control transmission follows the DTX pattern. On the other hand, the UE has to decode the downlink control channel according to the DRX pattern, and receive packets accordingly [57]. Thus, uplink power save can be enabled by means of a long DTX cycle, with a timeout whose duration can be of the same order of the subframe size. Setting DRX cycle and timeout similarly enforces downlink power save. Thereby, power save issues in uplink and downlink can be modeled in a similar way, and there is little difference between the cost computation of a single UE and the one of a base station. In practice, the evaluation of the costs at the eNB, can be seen as the collection of costs over the control and data channels towards the various UEs, plus a fixed per-cell operational cost that the eNB has to pay to notify its presence and maintain the users synchronized. Therefore, here we focus on the downlink only, and begin our analysis with the behavior of a UE receiving a data stream.

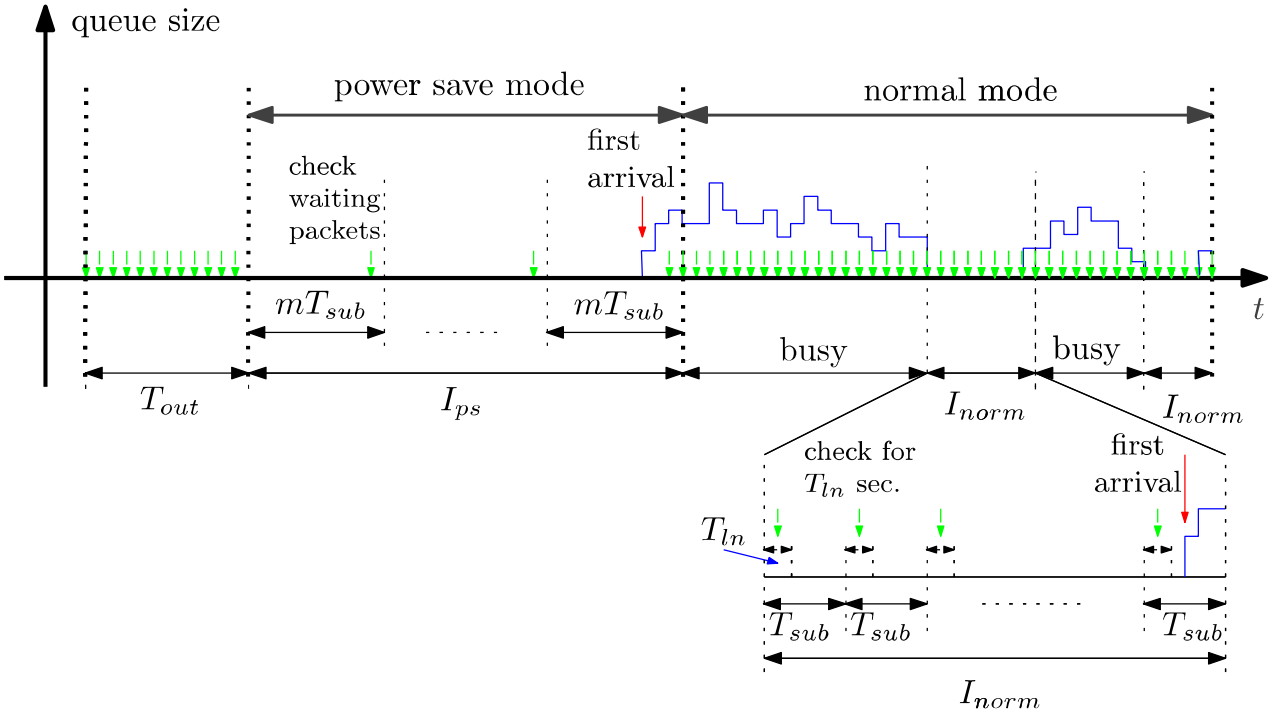

Figure 36: Downlink queue activity with power save and normal operation.

3.2.3.1 Power save in downlink

As illustrated in Figure 36, downlink power save can be obtained by alternating between two possible DRX cycles: after any downlink data activity there is a short cycle in which the UE continuously checks the control channel at each subframe (normal operation mode); instead, upon the expiration of an inactivity timeout T_{out}, consisting of M subframes, there is a longer cycle in which the UE checks the control channel periodically, with period m subframes (power save mode).[1]In power save mode, the UE samples the downlink control channel every m subframes, and returns to normal mode as soon as the channel sampling detects a control message indicating that the downlink queue is no longer empty. Note that UEs do not receive any service during: (*i*) I_{norm}, i.e., idle intervals in normal operation, (*ii*) timeout intervals, and (*iii*) I_{ps}, i.e., idle intervals spent in power save mode. To quantify the power save that can be achieved at the UE, in the following subsections we model the behavior of downlink transmissions with DRX operations enabled and users generating web traffic. After that, we also discuss the tradeoff between per-packet performance and per-UE cost. Our model can be adopted for systems using slotted operations, and in particular LTE and HSPA [57]. The model can be applied to both uplink and downlink. However, forsake of clarity, we explicitly deal with the downlink case. Achievable cost saving and performance metrics will be expressed as a function of the subframe length T_{sub} and the DRX

[1] The actual system timeout is M-subframe long. However, since the UE checks for new traffic at the beginning of a subframe, the UE switches to power save mode if it does not receive any traffic alert at the beginning of the M^{th} idle subframe. Therefore, it is enough to have no arrivals for M-1 subframes and the UE will not receive any packet for M subframes.

parameters, namely the timeout duration, through the parameter M, and the DRX power save cycle duration, through the parameter m.
We assume fixed-length packets, and the server capacity is exactly one packet per subframe. However, no packet is served for UEs in power save mode, and the server capacity is shared, in each subframe, between the UEs operating in normal mode. Therefore, we model a system that behaves as a $G/G/1$ PS queue with repeated fixed-length vacations of mT_{sub} seconds. Before proceeding with the model derivation, we introduce the traffic model adopted in this study.

3.2.3.2 Traffic model

We assume that downlink traffic is the composition of users' web browsing sessions. Traffic profile is the same for all users and is as follows. The size of each web request is modeled as suggested by3GPP2 in [56]: a web page consists of one main object, whose size is a random variable with truncated lognormal distribution, and zero or more embedded objects, each with random, truncated lognormal distributed size. The number of embedded objects is a random variable derived from a truncated Pareto distribution. Each web page request triggers the download of the packets carrying the main object only. Then a *parsing time* is needed for the user application to parse the main object and request the embedded objects, if any. The parsing time distribution is exponential with rate λ_p. After having received the last packet of the last object, the customer *reads* the web page for an exponentially distributed *reading time*, whose rate is λ_r. If no object is embedded, the reading time includes the parsing time. Finally the customer requests another web page. Figure 37 depicts the downlink queue size for one UE, during a generic web page cycle. Table 4 summarizes the parameters used for the generation of web browsing sessions. Note that the probability $\psi_0$to have no embedded objects in a web page can be computed through the distribution of the truncated Pareto random variable Y described in Table 4. Note also that the downlink of the web page experiences a small access delay due to the completion of the current DRX cycle before the first packet of the new burst could be served.

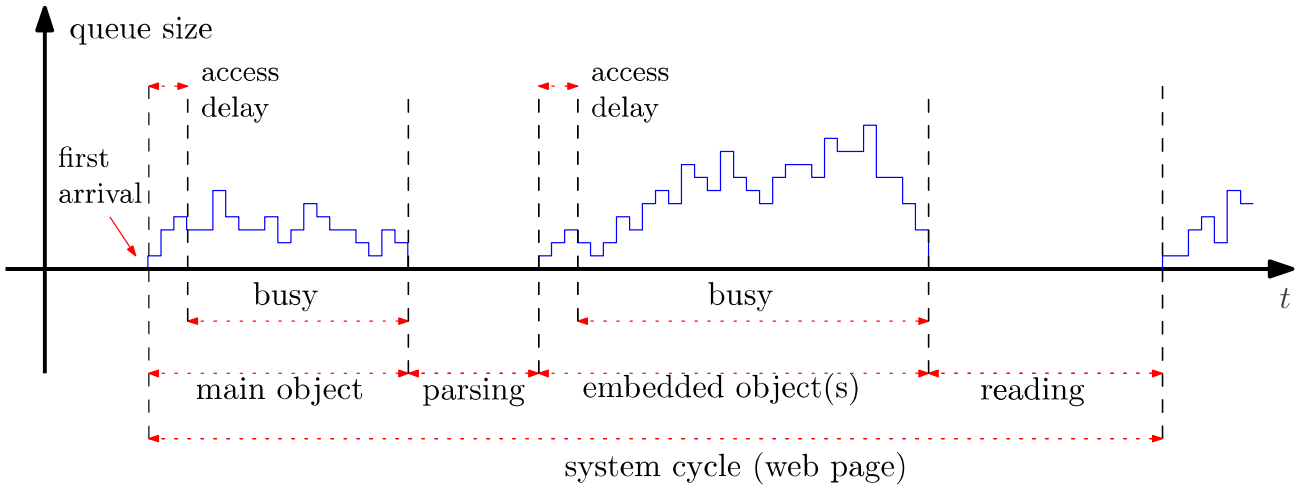

Figure 37: System cycle with web traffic as defined in [56].

Table 4: Parameters suggested by 3GPP2 for the evaluation of web traffic

Quantity	Derivation	Probability distribution	Parameters
Main object size	$S_{mo} = \lceil X \rceil$	$f_X(x) = \frac{\left(2\pi\sigma_X^2\right)^{-\frac{1}{2}} e^{-\frac{(\ln x - \mu_X)^2}{2\sigma_X^2}}}{\int_{x_{\min}}^{x_{\max}} \left(2\pi\sigma_X^2\right)^{-\frac{1}{2}} e^{-\frac{(\ln t - \mu_X)^2}{2\sigma_X^2}} dt}$ $x \in [x_{\min}, x_{\max}]$	$\mu_X = 8.35$, $\sigma_X = 1.37$, $x_{\min} = 100$ bytes, $x_{\max} = 2 \cdot 10^6$ bytes
Number of embedded objects	$N_{eo} = \lfloor Y \rfloor - y_{\min}$	$f_Y(y) = \alpha \frac{y_{\min}^{\alpha}}{y^{\alpha+1}}, \quad y \in [y_{\min}, y_{\max}[$ $f_Y(y_{\max}) = \left[1 - \left(\frac{y_{\min}}{y_{\max}}\right)^{\alpha}\right] \delta(y - y_{\max})$	$y_{\min} = 2$, $y_{\max} = 55$ $\alpha = 1.1$
Embedded object size	$S_{eo} = \lceil Z \rceil$	$f_Z(z) = \frac{\left(2\pi\sigma_Z^2\right)^{-\frac{1}{2}} e^{-\frac{(\ln z - \mu_Z)^2}{2\sigma_Z^2}}}{\int_{z_{\min}}^{z_{\max}} \left(2\pi\sigma_Z^2\right)^{-\frac{1}{2}} e^{-\frac{(\ln t - \mu_Z)^2}{2\sigma_Z^2}} dt}$ $z \in [z_{\min}, z_{\max}]$	$\mu_Z = 6.17$, $\sigma_Z = 2.36$, $z_{\min} = 50$ bytes, $z_{\max} = 2 \cdot 10^6$ bytes
Reading time	Λ_r	$f_{\Lambda_r}(t) = \lambda_r e^{-\lambda_r t}, t \geq 0$	$\lambda_r = 0.0\overline{3}$
Parsing time	Λ_p	$f_{\Lambda_p}(t) = \lambda_p e^{-\lambda_p t}, t \geq 0$	$\lambda_p = 7.69$

In our model, we assume that the time to request a web object with an http GET command is negligible in comparison with the time needed to parse the main object, and therefore also in comparison with the time needed for a customer to read the web page. Hence we incorporate this request delay in the parsing time and in the reading time. In this way, we clearly focus our study on the sole impact of the wireless technology on the system performance and costs. Furthermore, packet arrivals are supposed to be bursty after each GET request, so that no power save mode can be triggered after an object download begins, i.e., all power save intervals are contained in either parsing or reading times. With these assumptions, we study the system performance through the analysis of a generic web page download and its fruition. More precisely, we study the system cycle defined as the time in between two consecutive webpage requests. Therefore, the system cycle can be decomposed in four phases, as depicted in Figure 37: (*i*) download of the main object of the web page, (*ii*) parsing of the main object, (*iii*) download of embedded objects, and (*iv*) web page reading. The first three phases represent the web page download time, from the first packet arrival in the eNB queue to the last packet delivery to the UE. Access delay and download time characterize the service experienced by the customer.

3.2.4 Model derivation

Here we derive the time spent by the system in the various cycle phases. For ease of notation, we define β_p=*exp*(-$\lambda_p T_{sub}$) and β_r=*exp*(-$\lambda_r T_{sub}$) as the probabilities that, respectively, the exponentially distributed parsing time and reading time are longer than one subframe. Hence the timeout probability is β_r^{M-1} in reading time, and β_p^{M-1} in parsing time.

3.2.4.1 Timeouts in a cycle

Each cycle always includes one reading time, while the parsing time is present with probability 1-ψ_0, i.e., only if there are embedded objects. Therefore, the average number of timeouts in a system cycle is:

$$E[N_{to}] = \beta_r^{M-1} + (1-\psi_0)\,\beta_p^{M-1}.$$

Hence each cycle includes, on average, $E[N_{to}]$ (M-1) T_{sub} seconds due to timeout occurrences.

3.2.4.2 Idle time in power save mode

The average time per cycle during which the system is in power save mode, denoted as I_0, is computed by summing up the time spent in power save mode (the intervals I_{ps} as in Figure 36) occurring in the reading time and in the parsing time, if any is present in the cycle: $I_0 = I_{ps|\text{reading}} + I_{ps|\text{ parsing}}$. Thanks to the memoryless property of exponential arrivals, the interval between the timeout expiration and the arrival of the next data packet is exponential too, and has the same exponential rate. In particular, the power save interval that begins in the reading time lasts a multiple number of checking intervals $m\,T_{sub}$, with the following distribution and average:

$$\begin{aligned} &P\left(I_0 = jmT_{sub} \middle|\ \text{reading timeout}\right) \\ &= P(0 \text{ arrivals in } (j-1)mT_{sub})[1-P(0 \text{ arrivals in } mT_{sub})] \\ &= (\beta_r^m)^{j-1}\,(1-\beta_r^m), \qquad j \geq 1; \end{aligned}$$

$$E[I_0|\text{reading}] = \beta_r^{M-1}\frac{mT_{sub}}{1-\beta_r^m}.$$

where we also removed the conditioning on the timeout occurrence. Similarly, for the parsing time:

$$E[I_0|\text{parsing}] = \beta_p^{M-1}\frac{mT_{sub}}{1-\beta_p^m}.$$

Therefore, the expected value of the time spent in power save mode in a system cycle is given by the following average:

$$E[I_0] = \beta_r^{M-1}\frac{mT_{sub}}{1-\beta_r^m} + (1-\psi_0)\,\beta_p^{M-1}\frac{mT_{sub}}{1-\beta_p^m}.$$

Note that $E[I_0]$ is a function of m and M, the web traffic parameters being fixed. It is easy to find that the power save interval I_0 monotonically grows with the duration of the DRX cycle, and decreases with the duration of the timeout.

3.2.4.3 Idle time in normal mode

The amount of time spent in normal mode without serving any traffic is the sum of the normal mode idle intervals due to parsing and reading times. Since we counted apart the time spent in timeouts, here we only count the intervals I_{norm}, whose sum over a system cycle is denoted by $I_1 = I_{norm|\text{ reading}} + I_{norm|\text{ parsing}}$. Considering that I_{norm} is always a multiple of T_{sub} but smaller than a timeout, and since the component of I_1 in reading time is $I_{norm|\text{ reading}}$, the conditional distribution of I_1 in reading time is as follows:

$$\begin{aligned} & P(I_1 = jT_{sub}|\text{reading}) \\ = \;& P(I_{norm} = jT_{sub}|\text{ exp. arrivals with rate } \lambda_r) \\ = \;& \begin{cases} \beta_r^{M-1} & j = 0; \\ \beta_r^{j-1}(1-\beta_r) & 1 \le j \le M-1. \end{cases} \end{aligned}$$

Hence the conditional expected value of this interval I_1 is:

$$E[I_1|\text{reading}] = T_{sub}\frac{1 - M\beta_r^{M-1} + (M-1)\beta_r^M}{1-\beta_r}.$$

Similarly, the expected value for the time spent in normal mode with no traffic to be served during parsing, without counting the timeout, is given by:

$$E[I_1|\text{parsing}] = T_{sub}\frac{1 - M\beta_p^{M-1} + (M-1)\beta_p^M}{1-\beta_p}.$$

Therefore, on average, the time spent in normal mode without serving any traffic during a system cycle is given by the timeout intervals plus $E[I_1|\text{reading}]$, plus 1-ψ_0 times $E[I_1|\text{parsing}]$. So, the expected value of I_1 increases with the timeout duration, through M.

3.2.4.4 Cumulative idle time

The cumulative amount of idle time I in a cycle is the sum of timeouts,I_0, and I_1. Its expected value is then as follows:

$$\begin{aligned} E[I] \;=\; & \beta_r^{M-1}\frac{mT_{sub}}{1-\beta_r^m} + T_{sub}\frac{1-\beta_r^{M-1}}{1-\beta_r} \\ & +(1-\psi_0)\left(\beta_p^{M-1}\frac{mT_{sub}}{1-\beta_p^m} + T_{sub}\frac{1-\beta_p^{M-1}}{1-\beta_p}\right). \end{aligned}$$

$E[I]$ is a decreasing function of M, and increases with m. However, with our model assumptions, $E[I]$ is slightly larger than the sum of reading and parsing times. More precisely, its value is bounded as follows:

$$\frac{1}{\lambda_r} + \frac{1-\psi_0}{\lambda_p} < E[I] < \frac{1}{\lambda_r} + mT_{sub} + (1-\psi_0)\left(\frac{1}{\lambda_p} + mT_{sub}\right).$$

Given that m can be as high as few tens, and T_{sub} is only few milliseconds, the product mT_{sub} is negligible in comparison with the average parsing and reading times. Hence, for all realistic values of m, the per-cycle idle time can be considered constant and equal to its lower bound.

3.2.4.5 Busy time

The expected time spent to serve the packets of a web page, i.e., the busy time in a cycle, is given by the expected number of packets $E[N_p]$ per web page times the expected service time $E[\sigma]$. The

number of packets depends on the distribution of the web page objects, and it is 39.47 with the 3GPP2 traffic model reported in Table 4.[2]
The service time depends on the number of active UEs and on the server capacity, as we show later in this section.

3.2.4.6 System cycle duration

Putting together the results for the time spent in timeouts, idle intervals, and busy periods, the expected duration of a cycle is given by:

$$\begin{aligned} E[T_c] &= E[N_{to}](M-1)T_{sub}+E[I_0]+E[I_1]+E[N_p]E[\sigma] \\ &= E[I]+E[N_p]E[\sigma]. \end{aligned}$$

The relation between $E[T_c]$ and $E[\sigma]$ is linear with a coefficient that is determined by the web page object distribution. Since $E[\sigma]$ too will be shown to grow with m and decrease with M (see next paragraph), the entire expected system cycle increases with m and decreases with M. Furthermore, as the expected service time increases with the number N_u of UEs attached to the eNB, the system cycle behaves likewise. However, both $E[I]$ and $E[\sigma]$ are barely affected by m and M, thereby $E[T_c]$ is mainly affected by N_u only.

3.2.4.7 Service time

We assume that there are N_u homogeneous UEs in the cell. The activity factor of each UE is:

$$\rho = \frac{E[N_p]E[\sigma]}{E[T_c]} = \frac{E[N_p]E[\sigma]}{E[N_p]E[\sigma]+E[I]} < 1.$$

Equivalently, we can interpret ρ as the probability that a UE is under service. Note that $E[\sigma]$, $E[N_p]$, and $E[I]$ assume always positive values, and thus $E[T_c] > 0$ and $0<\rho<1$. From the point of view of a generic queue, the service time in the l^{th} subframe only depends on the number $N_a(l)$ of queues which transmit in that specific subframe. In fact, the downlink bandwidth is shared between the active and backlogged queues, the total serving capacity being fixed to one packet per subframe. Thus, given that the i^{th} queue has a packet under service in the l^{th} system subframe, the service time for the i^{th} queue is $T_{sub}\ N_a\ (l)$. Since we are interested in the service time for the i^{th} queue, we condition the observation of the service time to the transmission of a packet queued in the i^{th} queue. Hence, considering all queues as i.i.d., the number of active queues is a random variable $N_a = 1 + \nu$, with ν being a random variable exhibiting a binomial distribution between 0 and N_u-1 with success probability ρ.Thereby, the average service time is:

$$E[\sigma] = T_{sub}E[1+\nu] = T_{sub}[1+(N_u-1)\rho].$$

Hence, considering the expression of ρ as a function of $E[\sigma]$, we have a system of two equations intwo variables, from which we can compute $E[\sigma]$.

[2]We use 1500-byte packets and consider each object as an integer number of packets. Hence, after having computed the number of bytes N_b in an object, we consider that object as consisting of $ceil(N_b/1500)$ packets.

Proposition 1: The expected packet service $E[\sigma]$ is the unique positive solution of the following quadratic equation:

$$E[N_p]\,E^2[\sigma]+(E[I]-E[N_p]\,N_uT_{sub})\,E[\sigma]-E[I]T_{sub}=0.$$

Proof: the equation is obtained by combining the expressions for $E[\sigma]$ and ρ. Since $E[N_p]$ and $E[I]$ are positive numbers, the quadratic coefficient in the equation is always positive, whilst the constant term is negative: this is necessary and sufficient to have one positive solution and one negative solution. However, the negative solution has no physical meaning. Thus, the positive solution is the only acceptable solution candidate.

Corollary 1: The expected packet service $E[\sigma]$ is:

$$\frac{(E[N_p]N_uT_{sub}-E[I])+\sqrt{(E[I]-E[N_p]\,N_uT_{sub})^2+4E[I]\,E[N_p]\,T_{sub}}}{2E[N_p]}.$$

As we stressed before, the term $E[I]$ increases with m and decreases with M, but its variations are quite limited. So, thanks to the corollary, we can conclude that $E[\sigma]$ behaves as $E[I]$, i.e., it is barely affected by m and M. Furthermore, $E[\sigma]$ grows with N_u, i.e., with the number of UEs in the cell. Notably, the impact of N_u on $E[\sigma]$ is amplified by a factor equal to the average page size $E[N_p]$. Since a new web page is requested only after the reading time of the previous request, the number of customers has no theoretical upper bound. In fact, service time and system cycle just keep growing with the number of UEs, and the average cumulative traffic generated and served per subframe is $N_uE[N_p]/(E[N_p]E[\sigma]+E[I])\leq 1/T_{sub}$. Thus, as the system approaches saturation, $E[\sigma]$ tends to N_uT_{sub}, since in saturation the N_u users are always active and receive a fraction $1/N_u$ of the server capacity. The asymptotic distribution of the system cycle duration is constant and equal to $T_c^{up} = E[N_p]N_uT_{sub}+E[I]$, which scales linearly with the number of users and loosely depends on the power save parameters m and M. T_c^{up} is an upper bound for the evaluation of the system cycle, and can be used to limit the maximum number of customers, thus guaranteeing a maximum web page processing time to any customer.

3.2.5 Performance and cost metrics

The impact of power save mode on web traffic can be evaluated in terms of access delay and page download time, assuming that all the traffic is served. Costs due to wireless transmission and reception of packets are to be traded off with such indicators. Therefore, we first derive an expression for performance metrics and show how to compute the fraction of time during which power save can be realistically obtained. Then we derive the parametric expressions for cost and power save at both UE and eNB.

3.2.5.1 Performance metrics and power save opportunities

3.2.5.2 Page download time

The time W needed to download a web page includes the time to download each and every page's packet, the time to parse the main object of the page, and the access delay. Hence, we can derive $E[W]$ as the difference between $E[T_c]$ and the expected reading time:

$$E[W] = E[T_c] - \frac{1}{\lambda_r}.$$

3.2.5.3 Access delay

The access delay is the delay experienced after any download request. In our model we consider only that part of the access delay that is due to the wireless access protocol. In particular, we have two epochs within each cycle at which a request can experience access delay: at the end of the reading time, corresponding to a new page request, and at the end of the parsing time, corresponding to the request for the embedded objects. We name D the total access delay experienced within a web page download, thus accounting for the delay accumulated in both reading and parsing times. $E[D]$ can be easily computed by subtracting the parsing time, the reading time and the busy time from the expected system cycle duration (see Figure 37), i.e.:

$$E[D] \quad = \quad E[I] - \left(\frac{1}{\lambda_r} + \frac{1-\psi_0}{\lambda_p} \right).$$

The expected access delay is a function of the power save parameters used in the DRX configuration, plus the traffic profile parameters, through λ_r, λ_p, $E[N_p]$, and ψ_0. However, using the upper bound for $E[I]$, one can conclude that the access delay is upper bounded to $(2\text{-}\psi_0)mT_{sub}$.

3.2.5.4 Power save time ratio

Economy of energy can be achieved by reducing the activity of radio interfaces, including the possibility to turn off radio transceivers, according to the DTX/DRX pattern. Therefore, power save opportunities can be measured through the fraction of cycle during which the transceiver can be deactivated. In practice, UE and eNB can save power during I_0, which is a multiple of mT_{sub}, but for the intervals in which the UE has to check the control channel, i.e., exactly T_{ln} seconds out of m subframes. The power save time ratio is then defined as follows:

$$R \doteq \left(1 - \frac{T_{ln}}{mT_{sub}}\right) \frac{E[I_0]}{E[T_c]}.$$

Considering that $E[T_c]$ is almost insensible to m and M, but increases with N_u, and recalling that $E[I_0]$ increases with m and decreases with M, we conclude that R is an increasing function of m, and it decreases with M and N_u.

3.2.5.5 Cost at the UE

Whenever the UE receiver is active, its consumption rate is c_{on}, and $c_{ps}<c_{on}$ otherwise. Decoding a packet has an *additional* consumption rate c_{rx}, while listening to the control channel has an *additional* consumption rate c_{ln}. The average consumption is a combination of these four consumption terms. Recalling that control channel listening is performed in each subframe in normal mode, but only in one out of m subframes in power save mode, and taking the average over a system cycle, we obtain the following cost per UE:

$$C_{UE}(m, M, N_u) = (1-R)\, c_{on} + R\, c_{ps} + \rho\, c_{rx} + \left(1 - \frac{m-1}{m}\frac{E[I_0]}{E[T_c]}\right)\frac{T_{ln}}{T_{sub}} c_{ln}.$$

Considering a fixed web traffic profile, the cost is a function of the power save parameters m and M affecting R, ρ, $E[I_0]$, and $E[T_c]$, and of the number of users N_u which appears in $E[T_c]$ and hence in R. The cost with no power save mode is computed by plugging $E[I_0]=0$, which is equivalent to setting $m= 1$ and $M \to \infty$ in the UE cost equation:

$$C_{UE}(1, \infty, N_u) = c_{on} + \rho\, c_{rx} + \frac{T_{ln}}{T_{sub}} c_{ln}.$$

Finally, the relative power save gain that can be attained is:

$$G_{UE}(m, M, N_u) \doteq \frac{C_{UE}(1, \infty, N_u) - C_{UE}(m, M, N_u)}{C_{UE}(1, \infty, N_u)} = \frac{\gamma(m)}{C_{UE}(1, \infty, N_u)}\frac{E[I_0]}{E[T_c]},$$

where the quantity $\gamma(m)$ is a cost reduction factor which increases with the DRX power save cycle length, that is:

$$\gamma(m) \doteq \left(1 - \frac{T_{ln}}{m T_{sub}}\right)(c_{on} - c_{ps}) + \left(1 - \frac{1}{m}\right)\frac{T_{ln}}{T_{sub}} c_{ln}.$$

We can conclude that the relative gain is a function that increases with the duration of the DRX power save cycle (i.e., with m), and decreases with the timeout (i.e., with M) and with the number N_u of users in the cell.

3.2.5.6 Cost at the eNB

The discontinuous reception and transmission is defined on a per-UE basis, and thereby the eNB power save can be expressed as the sum of power save over all users. However, the eNB experiences some additional cost for cell management (synchronization, pilots, etc.). Hence, the eNB cost per associated UE, namely C'_{UE} is expressed similarly to the UE cost computed earlier in this subsection, where the reception cost rate c_{rx} is replaced by a transmission cost rate c_{tx}, and the listening cost c_{ln} is replaced by the signaling cost c_{sg}. The additional per-eNB fixed cost c_f does not depend on the transceiver activity and it is normally huge. Recent works show that it can be as high as 10 times the average cost for transmitting data over the air interface [58]. In sum, the total base station cost rate with homogeneous users is:

$$C_{BS}(m, M, N_u) = N_u C'_{UE}(m, M, N_u) + c_f.$$

The relative power save gain is then as follows:

$$G_{BS}(m, M, N_u) = \frac{\gamma'(m)}{C'_{UE}(1, \infty, N_u) + \frac{c_f}{N_u}} \cdot \frac{E[I_0]}{E[T_c]},$$

where γ' is obtained from γ by replacing c_{ln} with c_{sg}. Note that with few users the main eNB cost is represented by the fixed cost c_f, thereby the gain increases with the number of users until the per-user cost becomes the predominant term in the denominator of G_{BS}.

3.2.6 Evaluation

In this section we first evaluate the model using a packet-level simulator that reproduces the behavior of downlink transmissions. Second, we use the model to perform the optimization of power save parameters m and M in order to minimize the transmission/reception cost, subject to an upper bound for access delay $E[D]$ and download time $E[W]$.

3.2.6.1 Simulating the *G/G/1 PS* queue with web traffic

We developed a *C++* event-driven simulator that reproduces the behavior of a time slotted *G/G/1 PS* queue with N_u homogeneous classes. In the simulator, each class can be in two different operational modes, namely normal mode and power save mode. The shared processor resources are allocated equally to all classes in normal mode at the beginning of each time slot of duration T_{sub}. The traffic is homogeneously generated, in accordance to the 3GPP2 evaluation methodology discussed before. Furthermore, all simulated packets have the same size, i.e., 1500 bytes, and the processor capacity is 1500 bytes per slot. Hence, if only one class is under service, a packet is served completely in one slot. Otherwise, since the processor is shared, all classes in normal mode have a fraction of packet served in that slot. The fair per-class share is computed as one over the number of classes in normal mode. However, if a class has not enough backlog to use all its processor share, unused resources are redistributed amongst the remaining classes. The service process can last one or more time slots per packet, and packet service is considered complete at the end of its last service slot. Simulations are performed for different numbers of classes N_u, duration of the timeout (through M), and duration of DRX power save cycle (through m). Each simulation consists of a warm-up period lasting 10,000 seconds (5,000,000 slots), followed by 100 runs, each lasting 10,000 seconds. Statistics are separately collected in each run. At the end of a simulation, all statistics are averaged over the 100 runs and 99% confidence intervals are computed for each average result. Simulations have to be run for such a long time to have statistics with relatively small confidence intervals: due to heavy tailed distributions involved in the generation of web traffic, the number of packets per cycle has a huge variance. Furthermore, simulations with a high number of users require very long CPU time (in our specific case, a single simulation point requires up to 12 hours of a 3 GHz Intel Core2^{TM} Duo E6850 CPU), which makes it prohibitive to explore in detail all possible values of the input parameters. As a reference, our model can be run with the Maple software in as few as 30 seconds on the same machine used for simulations.
The model, however, neglects the correlation between the activity of different users, e.g., in the computation of $E[\sigma]$. However, the comparison between model and simulation shows that the model approximates the system performance with a good accuracy. In particular, here we compare

three performance indicators: system cycle duration $E[T_c]$, power save time ratio R, and service time $E[\sigma]$. $E[W]$ could be easily computed from $E[T_c]$. For clarity of presentation, we show only a subset of the results obtained. In particular we selected some extreme cases that well depict the variability of performance with the parameters m, M, and N_u.

Figure 38 compares the estimates of $E[T_c]$ obtained with the model (lines with marks) and with the simulator (marked points) for two very different values of m (4, which is the minimum in the 3GPPrecommendations, and 100). The lower part of the figure contains the results obtained with one user, and the upper part reports the results with N_u=400 users. The results of the simulation are highly variable due to the heavy tailed distribution in web page size statistics, hence 99%-confidence intervals appear large over the zoomed y-scale used in the figure. Though the average values show some small difference, both simulations and model behave similarly. The maximum relative difference between model and simulation with one user is within 1%, and it is below 2% with N_u=400. However, model estimates are within the 99%-confidence intervals of simulation estimates. The main cause of the difference between the results of the model and the ones obtained via simulation is in the estimation of the service time, which linearly affects the cycle duration. By observing Figure 39, it is clear that the model slightly overestimates the service time for high values of N_u, i.e., when the correlation between multiple users, in terms of probability to share the same transmission slot, becomes relevant. As predicted, m and M do not significantly affect $E[\sigma]$. Figure 40 illustrates the power save time ratio R. Model's and simulation's results are very close in all cases, and confidence intervals are very small, so we omitted them in the figure. The results are sensitive to m and N_u, while the effect of M is almost negligible for short timeouts. In conclusion, simulations suggest that we can safely use the model to estimate the system performance and evaluate its potentialities for power save with good accuracy.

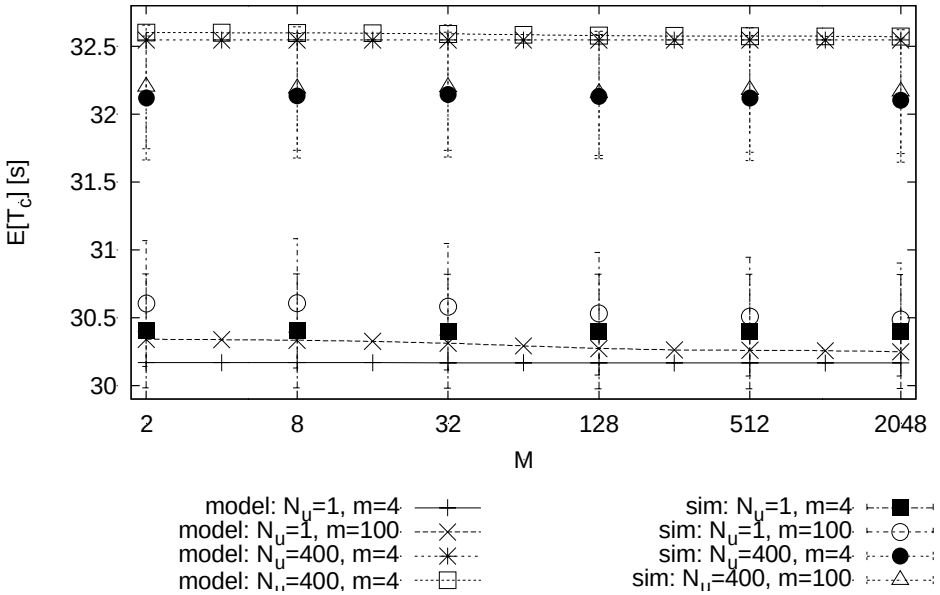

Figure 38: System cycle duration is affected by the number of users. It slightly grows with m and is almost insensitive to M.

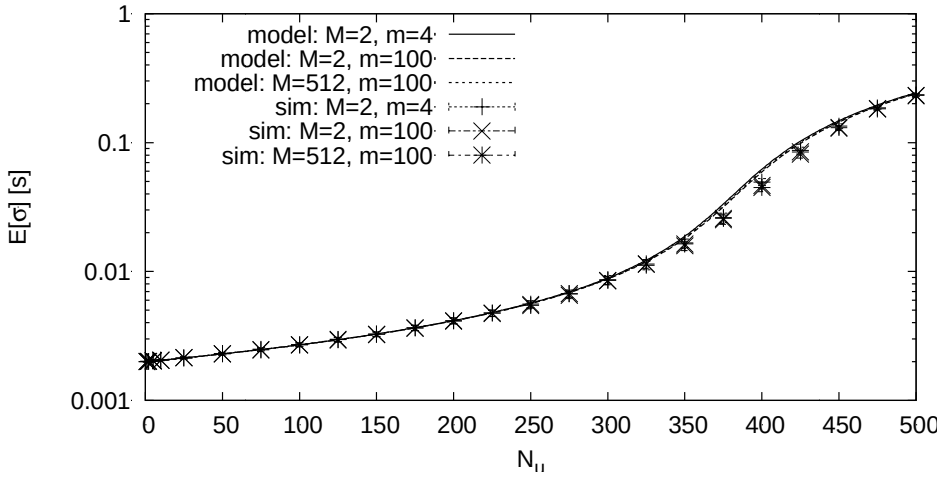

Figure 39: The service time grows with the number of users and is almost not affected by the timeout and the DRX power save cycle durations.

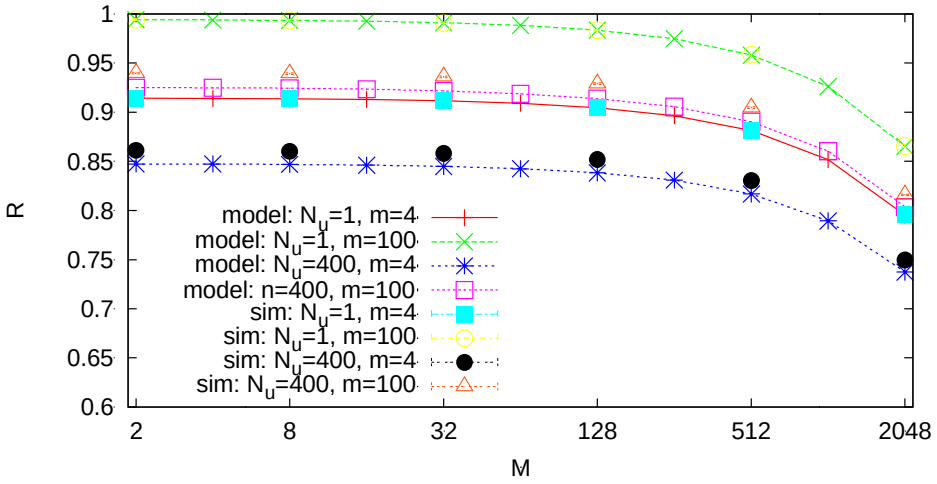

Figure 40: The power save time ratio computed for $T_{ln}=T_{sub}/3$.

3.2.6.2 Model-based parameter optimization

Here we want to compute the optimal values of *m* and *M* that yield the highest gain while keeping low the access delay and the download time. We consider the eNB cost only, but the results can be easily extended to the UE. Reasonably, the cost for transmitting a data packet is larger than the cost for transmitting a control packet, which usually takes less bandwidth. Both transmitting and signaling costs are much higher than the cost to stay on, which, in turn, is at least one order of magnitude greater than the cost to stay in power save mode. As an example, we use the following values: c_{tx}=100, c_{sg}=50,c_{on}=10, and c_{ps}=1. Additionally, as suggested by experimental measurements [58], we consider a base station cost one order of magnitude higher than the transmission cost: c_f=1000. We assume that control packets have duration $T_{ln} = T_{sub}/3$, e.g., the UE has to listen to the control channel only during the first of the three slots composing an HSPA subframe.

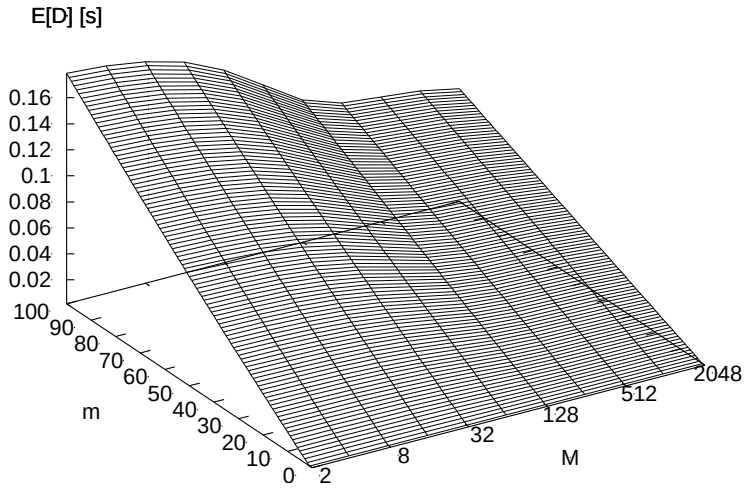

Figure 41: Access delay (independent on the number of users).

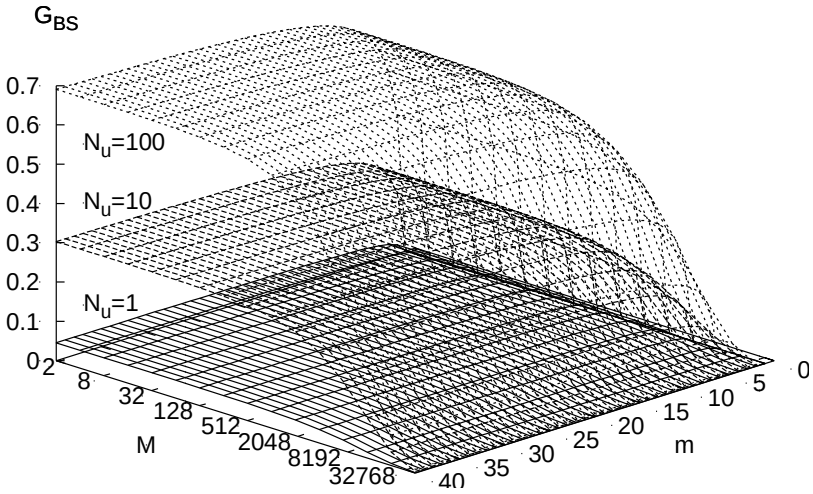

Figure 42: Relevant power save gain can be obtained with small timeouts, even for power save intervals lasting few subframes.

The access delay experienced in the network is reported in Figure 41.$E[D]$ is sensitive to m, especially with low timeout values. However, reasonable values of m, e.g., below 20, yield access delay times not higher than 40ms. With the chosen cost parameters, the function $\gamma'(m)$—not depicted here for lack of space—grows very fast for small m, but it quickly saturates. In practice, values of m larger than 20 do not give substantial gain advantages with respect to m=20, that is the maximum value suggested by 3GPPfor CPC. The relative gain at the eNB is reported in Figure 42 for a few values of N_u. One can notice that low to medium values of the timeout, jointly with moderately high values of m, allow to obtain a relevant gain as soon as the number of users reaches 10. In fact, when few users are attached to the eNB, the main cost figure becomes c_f, which is fixed. However, as shown in Figure 43, if the number of users grows above 350, the gain recedes. In fact, with too many users, the system saturates and the power-save opportunities diminish.

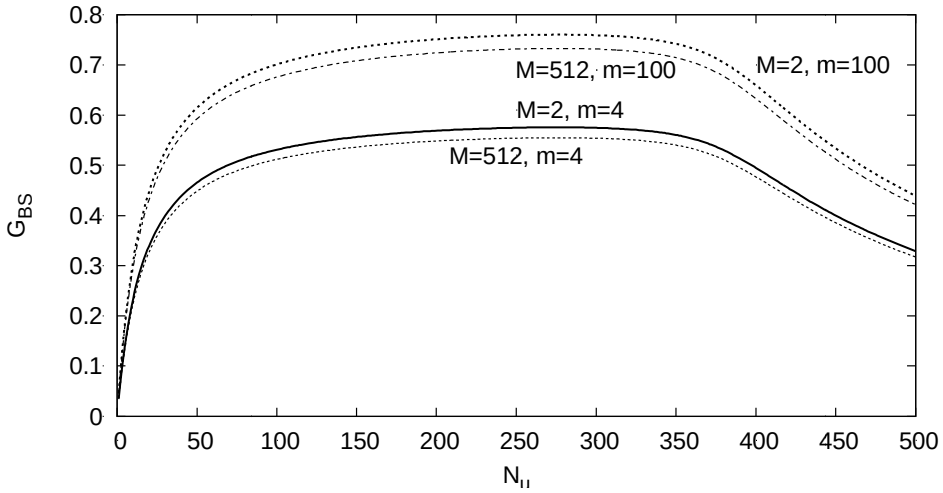

Figure 43:A large gain can be obtained over a wide spectrum of number of users as soon as m grows to few tens.

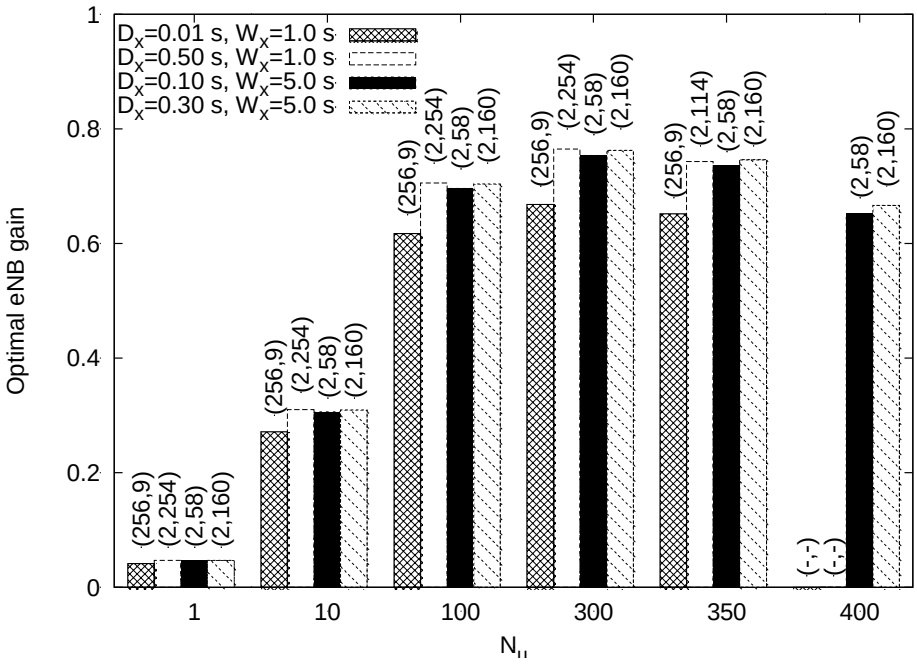

Figure 44: Relative gain for different number of users, optimized over bounded download time and access delay.

Last, Figure 44 shows some particular cases of system optimization. In the figure, D_x and W_x denote the maximum allowable access delay and download time, respectively. Each optimization is performed over m and M, given a fixed number of users N_u. Each optimized value of the gain is labeled with the pair (M,m)that corresponds to the optimum. The figure shows that the gain can exceed 70% while keeping the access delay bounded to less than half second, and the total web page download time below one second. However, with 400 users, the minimum download time grows above one second and the system cannot be optimized unless W_x was raised to a few seconds. Note also that the optimization with very small values of the access delay can only be obtained by

setting a long timeout and short power save intervals (e.g., M=256 and m=9 with 100 users yields about 60% gain, with no more than 10 ms of access delay). With higher access delay bounds, e.g., as high as 100 ms, the optimal timeout is the shortest possible, i.e., M=2. Almost in all cases, the optimization suggests to use very large values for m. However, observing Figure 42, it is clear that near-optimal gain can be obtained with values of m as low as 20.

3.2.7 Summary and remarks on the implementation by means of FLAVIA

We have shown how to model a *G*/*G*/1 *PS* system representing the download transmission queues of cellular users adopting the continuous connectivity model. The model, which has been validated through simulation, is based on two basic assumptions: (*i*) users can receive traffic according to the DRX paradigm, and (*ii*) the user-generated traffic is a realistic sequence of web page requests. We model the per-user activity and evaluate the service share that the base station processor can grant to each user. Furthermore, we proposed a cost model and show how to optimize the power save parameters to minimize the cost under bounded access delay and page download time. Remarkably, we show that up to 70% or more of the downlink transmission cost can be saved while preserving the quality of packet flows.

In order to implement the proposed optimization in a scheduled system, the FLAVIA architecture has to provide, on the one hand, the tools to measure user traffic activity and estimate the parameters that characterize such activity. To achieve this goal, the *Measurements and Monitoring* service of the FLAVIA architecture, as defined [59], has to permit the definition of a few specific filters to collect the needed measures at both the base station and the terminal. On the other hand, the FLAVIA architecture contains a Power Saving service [59], that manages the parameters used to enforce the idle mode of WiMAX devices as well as defines the activity/inactivity cycle of the radio interface. Therefore, the Power Saving service has to permit the definition of activity/inactivity cycles and the manipulation of their parameters. Finally, in order to enforce the dynamic tuning of the optimal power saving parameters, in accordance to the estimated traffic activity, the FLAVIA architecture can either interconnect directly the Power Saving service to the Measurements and Monitoring service, or use the FLAVIA control plan to initiate the monitoring activity and fetch the measures, and then compute the optimal power saving parameters and enforce them via the control interface available to the Power Saving service.

4 Summary

In this document we summarized the research results achieved in the first part of the project and described some of the ongoing research. The research results were classified according to four different aspects of scheduled access technology, namely (i) radio resource allocation, which suggests schemes for both intra cell resource allocation and inter-cell resource allocation; (ii) cellular architecture and scenarios, which propose new paradigms for organizing cellular systems; (iii) power-save schemes, in which, based on a comprehensive measurement study of the power consumption of different operational modes, we analyze the performance and tradeoffs between various power-save modes, and suggest protocols and algorithms to reduce the power consumption of mobile devices and base stations; (iv) scheduled solutions for contention-based technology, which suggest enhancements that support schedule-based operations over contention-based technologies.

Throughout the document we examined the support of FLAVIA's architecture for each suggested solution, highlighted the functions and modules that support each such solution or mechanism and thus proved FLAVIA's architecture flexibility.

5 References

[1] J. M. Holtzman, "Asymptotic analysis of proportional fair algorithm," in *PIMRC*, 2001.

[2] K. Wongthavarawat and A.Ganz, "Packet scheduling for QoS support in IEEE 802.16 broadband wireless access systems," *International Journal of Communication Systems*, 2003.

[3] J. Chen, W. Jiao and Q. Guo, "Providing integrated QoS control for IEEE 802.16 broadband wireless access systems," in *Vehicular Technology Conference (VTC)*, 2005.

[4] Y. Cao, V.O.K. Li and Z. Cao, "Scheduling delay-sensitive and best-effort traffics in wireless networks," in *IEEE International Conference on Communications (ICC)*, 2003.

[5] J. Sun, E. Modiano and L. Zheng, "Wireless channel allocation using an auction algorithm," *IEEE Journal on Selected Areas in Commun.*, vol. 24, no. 5, pp. 1085-1096, May 2006.

[6] S. Han and Y. Han, "A competitive fair subchannel allocation for OFDMA system using an auction algorithm," in *IEEE Vehicular Technology Conference (VTC)*, 2007.

[7] H. Deng, Y. Wang and J Lu, "Auction Based Resource Allocation for Balancing Efficiency and Fairness in OFDMA Relay Networks with Service Differentiation," in *IEEE Vehicular Technology Conference (VTC)*, 2010.

[8] Y. Gai, P. Gong, J. Lv and W. Wu, "Auction-Based Radio Resource Allocation for OFDMA Systems," in *WiCOM*, 2009.

[9] Z. Kong, Y. Kwok and J. Wang, "Auction-Based Scheduling in Non-Cooperative Multiuser OFDM Systems," in *IEEE Vehicular Technology Conference (VTC)*, 2009.

[10] M. Dramitinos, G. Stamoulis and C. Courcoubetis, "Auction-based resource allocation in UMTS high speed downlink packet access (HSDPA)," in *NGI Netw*, 2005.

[11] S. Pal, S. R. Kundu., M. Chatterjee, and S.K. Das, "Combinatorial Reverse Auction-Based Scheduling in Multirate Wireless Systems," *IEEE Trans. On Computers*, Oct 2007.

[12] N. Nisan, T. Roughgarden, E. Tardos, and V.V. Vazirani, *Algorithmic Game Theory*.: Cambridge Univ. Press., 2007.

[13] R. Agrawal and V. Subramanian, "Optimality of Certain Channel Aware Scheduling Policies," in *Allerton Conference*, 2002.

[14] A. L. Stolyar, "On the asymptotic optimality of the gradient scheduling algorithm for multiuser throughput allocation," *Operations Research*, vol. 53, no. 1, pp. 12–25, 2005.

[15] H. Kushner and P. Whiting, "Asymptotic properties of proportional-fair sharing algorithms," in *Allerton Conference*, 2002.

[16] P. Pileggi, G. Iazeolla, and P. Kritzinger, "Demonstrating the Synergy between CAC and Scheduling in Wireless Networks," *International Journal of Modeling, Simulation and Scientific Computing (To appear)*, 2011.

[17] P. Pileggi and P. Kritzinger, "Traffic-Centric Modelling by IEEE 802.11 DCF Example," in *ASMTA'11: 18th International Conference on Analytical and Stochastic Modelling Techniques and Applications*, 2011, pp. 219–233.

[18] P. Pileggi and P. Kritzinger, "Traffic-Centric Modeling Paradigm for Complex Wireless Systems," in *IFIP Wireless Days, Short paper*, Niagara Falls, Ontario, Canada, 2011.

[19] O. Arnold, F. Richter, G. Fettweis, and O. Blume, "Power consumption modeling of different base station types in heterogeneous cellular networks," in *Future Network and Mobile Summit*, Florence, Italy, 2010.

[20] T. Han and K. Kobayashi, "A new achievable rate region for the interference channel," *IEEE Trans. Inform. Theory*, vol. 27, no. 1, pp. 49–60, January 1981.

[21] M. Costa, "On the Gaussian interference channel," *IEEE Trans. Inform. Theory*, vol. 31, no. 5, pp. 607–615, Sep. 1985.

[22] P. Rost, "The two-way interference channel: Towards a re-design of mobile communication systems," in *IEEE Vehicular Technology Conference, accepted for publication*, 2011.

[23] J. Kuri and S. K. Kasera, "Reliable Multicast in Multi-access Wireless LANs," *Wireless Networks*, vol. 7, no. 4, pp. 359 – 369, Aug 2001.

[24] H.C.Chao, S.W.Chang, and J.L.Chen, "Throughput Improvements Using the Random Leader Technique for the Reliable Multicast Wireless LANs," in *Networking- ICN 2001, LNCS 2093*, 2001, pp. 708-719.

[25] Y. Seok, D. Dujovne, T. Turletti and P. Cuenca, "Leader based Multicast Proposal," IEEE 802.11-07/0144r2 2007.

[26] M.T. Sun, L. Huang, A. Arora and T.H. Lai, "Reliable MAC Layer Multicast in IEEE 802.11 Wireless Networks," in *ICCP*, 2002.

[27] K. Tang and M. Gerla, "Random Access MAC for Efficient Broadcast Support in Ad Hoc Networks," in *IEEE WCNC*, 2000, pp. 454-459.

[28] K. Tang and M. Gerla, , "MAC Reliable Broadcast in Ad Hoc Networks," in *IEEE MILCOM*, 2001, pp. 1008-1013.

[29] A. Lyakhov and M.Yakimov, , "Analytical Study of QoS Oriented Multicast in Wireless Networks," *EURASIP Journal on Wireless Communications and Networking*, vol. 2011, p. Article ID 307507, 2002.

[30] B. Bing, *Wireless Local Area Networks. The new wireless revolution.*: John Wiley & Sons, Inc., 2002.

[31] MATLAB, http://www.mathworks.com/.

[32] Clearwire Reports Record First Quarter, 2011, http://corporate.clearwire.com/releasedetail.cfm?ReleaseID=574512.

[33] IEEE 802.16e-2009, IEEE Standard for Local and metropolitan area networks Part 16: Air Interface for Broadband Wireless Access Systems, May, 2009.

[34] IEEE 802.16-2004, Part 16: Air Interface for Fixed Broadband Wireless Access Systems, Standard for Local and metropolitan area networks, Oct.,2009.

[35] Y.B. Lin and Y.M. Chuang, "Modeling the sleep mode for cellular digital packet data," *IEEE Commun. Lett.*, vol. 3, no. 3, pp. 63-65, 1999.

[36] S. J. Kwon, Y. W. Chung, and D. K. Sung, , "Queueing model of sleep-mode operation in cellular digital packet data," *IEEE Trans. Veh. Technol.*, vol. 52, no. 4, pp. 1158-1162, 2003.

[37] S. Yang and Y. Lin, "Modeling UMTS discontinuous reception mechanism," *IEEE Transactions on Wireless Communications*, vol. 4, no. 1, pp. 312–319, Jan. 2005.

[38] K. Han and S. Choi, "Performance analysis of sleep mode operation in IEEE 802.16e mobile broadband wireless access systems," in *IEEE Vehicular Technology Conference (VTC) 2006*, Melbourne, Australia, 2006, p. 1141—1145.

[39] J. Seo, S. Lee, N. Park, H. Lee, and C. Cho, "Performance analysis of sleep mode operation in IEEE 802.16e," in *IEEE Vehicular Technology Conference (VTC)*, Los Angeles, California, 2004, p. 1169—1173.

[40] S. Alouf, E. Altman and A.P. Azad, "M/G/1 queue with repeated inhomogeneous vacations applied to IEEE 802.16e power saving," in *CM Sigmetrics*, Annapolis, Maryland, 2008.

[41] Y. Xiao, "Performance analysis of an energy saving mechanism in the IEEE 802.16e wireless MAN," in *IEEE CCNC*, 2006, p. 406—410.

[42] G. Dong, C. Zheng, H. Zhang, and Jufeng Dai, "Power Saving Class I Sleep Mode in IEEE802.16e System," in *The 9th International Conference on Advanced Communication Technology*, 2007, pp. 1487-1491.

[43] N. H. Lee and S. Bahk, "MAC sleep mode control considering downlink traffic pattern and mobility," in *Vehicular Technology Conference (VTC)*, 2005, pp. 2076-2080.

[44] J. Almhana, Z. Liu, C. Li, and R. McGorman, "Traffic estimation and power saving mechanism optimization of IEEE 802.16e networks," in *IEEE ICC*, Beijin, China, 2008, p. 322—326.

[45] J. R. Lee, and D. H. Cho, "Performance Evaluation of Energy-Saving Mechanism Based on Probabilistic Sleep

Interval Decision Algorithm in IEEE 802.16e," *IEEE Trans. on Vehicular Techn.*, vol. 56, no. 4, pp. 1773-1780, 2007.

[46] J.P. Yoon, W.J. Kim, J.Y. Baek and Y.J. Suh, "Efficient Uplink Resource Allocation for Power Saving in IEEE 802.16 OFDMA Systems," in *IEEE Vehicular Technology Conference (VTC)*, 2008, pp. 2167-2171.

[47] S.L. Tsao and S.Y. Lee, "Evaluating the Energy Efficiency of TCP Transmission over a WiMAX Network," in *19th International Conference on Computer Communications and Networks (ICCCN)*, 2010.

[48] picoChip Designs Ltd., PC720x ADI Radio interface for 802.16e TDD, 2007, https://support.picochip.com/picochip-resource-folder/Nexu5utu/4598jf4897f/app_037_wimax-radio-integration.pdf/download.

[49] Nujira Ltd., State of the art RF power technology for defense systems, 2009, http://www.nujira.com/_uploads/whitepapers/State_of_the_Art_RF_Power_Technology_for_Defence_Systems_EU.pdf.

[50] S. Yang and Y.Lin, "Modeling UMTS discontinuous reception mechanism," *IEEE Transactions on Wireless Communications*, vol. 4, no. 1, p. 312—319, 2005.

[51] H. Choi and J. Limb, "A behavioral model of web traffic," in *ICNP*, Washington, DC, 1999.

[52] 3GPP TS 25.214, Physical layer procedures (FDD), rel. 8.

[53] L. Zhou, H. Xu, H. Tian, Y. Gao, L. Du, and L. Chen, "Performance analysis of power saving mechanism with adjustable DRX cycles in 3GPP LTE," in *IEEE Vehicular Technology Conference (VTC)*, Calgary, Alberta, Cananda, 2008, p. 1—5.

[54] C. Bontu and E. Illidge, "DRX mechanism for power saving in LTE," *IEEE Communications Magazine*, vol. 47, no. 6, p. 48—55, Jun 2009.

[55] T. Kolding, J. Wigard, and L. Dalsgaard, "Balancing power saving and single user experience with discontinuous reception in LTE," in *IEEE ISWCS*, 2008, p. 713—717.

[56] 3GPP2 C.R1002-B v1.0, CDMA2000 evaluation methodology - Revision B, 2009.

[57] E. Dahlman, S. Parkvall, J. Skold, and P. Beming, *3G Evolution: HSPA and LTE for Mobile Broadband*, 2nd ed.: Oxford, UK: Academic Press, 2008.

[58] F. Correa Alegria and F.A. Martins Travassos, "Implementation details of an automatic monitoring system used on a Vodafone radiocommunication base station," *IAENG Engineering Letters*, vol. 16, no. 4, 2008.

[59] FLAVIA Project Deliverable D3.1.1, 802.16 architecture and interfaces specification, 2011, http://www.ict-flavia.eu.

[60] J. Lee and J.Walrand, Design and analysis of an asynchronous zero collision MAC protocol, 2008, Arxiv preprint 0806.3542v1 [cs.NI].

[61] J. Barcelo, B. Bellalta, C. Cano, and M. Oliver, Learning-BEB: Avoiding Collisions in WLAN, 2008, Eunice Summer School.

[62] I. Rhee, A. Warrier, M. Aia, J. Min, and M.L. Sichitiu, "Z-MAC: a hybrid MAC for wireless sensor networks," *IEEE/ACM Transactions on Networking (TON)*, vol. 16, no. 3, 2008.

[63] M. Fang, D. Malone, K. R. Duffy and D. J. Leith, Decentralised Learning MACs for Collision-free Access in WLANs, 2011, arXiv:1009.4386v2.

APPENDIX – A scheduled solution for contention-based technologies

Scheduled MAC approaches such as 802.16 or LTE have the advantage of better utilizing the physical resources by precisely controlling when users access the medium, inherently avoiding simultaneous transmission and channel idle periods, which often occur with contention based technologies such as 802.11. However, current TDMA systems suffer from some limitations. First of all, they require a central controller and non-negligible signaling overhead for acquiring complete information about the demand of the users and the network conditions. Second, they are typically deployed in licensed spectral bands; therefore, they involve significant deployment costs. In contrast, contention-based access schemes, such as the CSMA/CA protocol used in 802.11 WLANs, operate in non-licensed ISM bands (2.4GHz and 5GHz in Europe) and are decentralized by nature, i.e. stations do not need to signal to their peers prior to transmission attempts. Given the advantages and shortcomings of the two approaches highlighted above, hybrid solutions that combine the best features of contention-based and scheduled schemes have been proposed [60,61,62,63]. We aim to assess how we could implement such contention-free MAC protocol in the context of the FLAVIA architecture.

A.1 Collision-free learning media access control

The Binary Exponential Backoff (BEB) implemented by the Distributed Coordination Function (DCF) specified in the IEEE 802.11 standard involves counting down a random number of slots, uniformly chosen integer in the range [0, CW_i -1], prior to each transmission attempt. This random number is referred to as the backoff counter and CW_i is the contention window used at the i^{th} transmission attempt of the same frame. This approach reduces the probability of collision when two or more stations detect the medium available and attempt to transmit. However, the chance of collision increases with the number of stations and/or their traffic demand.

A number of protocols have been proposed that alter this behavior of the DCF to eliminate the possibility of collisions, converging to a collision-free schedule in a distributed way. For example, Barcelo et al. [61] propose a scheme called Learning BEB (L-BEB), where upon a successful transmission stations choose a backoff a fixed value of the backoff counter, equal to the minimum CW value ($CW_{\min}$) specified by the standard (e.g. 16 for 802.11a/g), while following a failure the value of the backoff counter is chosen randomly as in the case of standard DCF. In a network with a number of stations less than $CW_{\min}$, this scheme converges to a collision-free schedule. In [63], Learning MAC (L-MAC) is proposed, which can be regarded as an evolution of L-BEB incorporating ideas from the self-managed decentralized channel selection algorithms. The advantage of L-MAC is that it preserves some state upon a collision, as opposed to L-BEB. Specifically, each station that has found a slot that previously did not have competition is likely to persist with that slot even after a small number of collisions. To achieve this, a probability distribution is introduced as internal state for each station. It determines the likelihood of choosing each slot in a periodic schedule. The benefit of learning is that it introduces a stickiness that improves the speed of convergence to a collision-free transmission schedule and facilitates quick re-convergence to a new schedule when additional stations join an existing network. While the details

differ, other schemes that operate on similar principles have been proposed [60,62], offering improved performance over the default DCF.
Despite the good properties of these protocols demonstrated by means of simulations, due to the limitations of the current drivers, no implementation that demonstrates their behavior exists. We argue that the FLAVIA architecture will enable an easy integration of such protocols with commodity hardware.

A.2 Prototype implementation

As a first step towards the FLAVIA design, we outline a prototype implementation of L-BEB, which demonstrates the practicality of the technique. Although this prototype is implemented in software and lacks the accuracy of a hardware-integrated solution, it demonstrates that commodity hardware has sensing and timing capabilities that are sufficient to implement L-BEB.
To implement L-BEB we rely on controlling the duration of the 802.11e arbitration inter-frame space (AIFS), a functionality that is available on many of the existing network cards to provide service differentiation. AIFS determines the number of physical idle slots that must be seen after a transmission before the restart of a backoff counter decrement, following a sensed transmission. Our aim is to make use of this functionality in order to reach a scheduled access to the medium by setting different values of the AIFS parameters for the contending stations. As an example, consider two stations, the first with AIFS=4 and the second with AIFS=6, both with a single packet to send after a current ongoing transmission, as shown in Figure 45. If both stations chose a backoff counter of zero, then we will see 4 empty slots, then the transmission of the first station, followed by six empty slots and finally the second station's transmission.

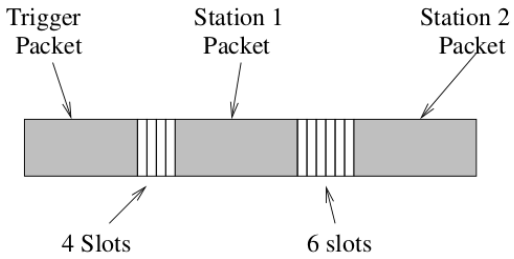

Figure 45: AIFS behavior.

Thus, if we ensure that the backoff counter is zero, we can order the transmissions by selecting appropriate AIFS values and ensuring each station has one packet queued. In our implementation of a learning MAC protocol, we use different AIFS values to identify different slots after a *trigger* packet. Thus the implementation involves the following steps:

1. Initially stations randomly select a slot, and set AIFS accordingly.
2. At the beginning of a schedule, the access point sends a trigger packet.
3. Upon the reception of the trigger packet stations with packets to transmit place a packet in the HW queue.
4. After transmission, if no collision occurred, stations select the same slot. Otherwise a slot is chosen randomly and AIFS is adjusted.
5. Return to step 2.

Several implementation challenges arise with the above mechanism. First, we must ensure that the trigger packet is sent at the beginning of each schedule. For triggering, we rely on the beacon frames sent by the AP and adjust the beacon interval manually. An alternative would be sending trigger packets using a queue that has AIFS set to a large value, such that triggers will be actually sent at the end of each round. However, the first approach has the advantage of using functionality already available with standard hardware and involves no modifications of the AP.
Second, we observed that it is not possible to ensure zero backoff counters, but instead it is possible to determine them to take they take values in {1,2}. To do this, we set CW_{min} to the smallest configurable value and force the CW_{max} to the same value, thereby ensuring the binary increase of the contention window is inhibited. Once we know that the backoff counter will be one or two, we work with AIFS values that are multiples of four in order to schedule the packets.
Finally, packets must be promptly queued after receiving a trigger packet, such that the hardware backoffs of the stations are aligned. To do this, we call the required queuing function immediately when the driver receives the trigger packet.

A.3 Experimental Evaluation

To validate the performance of our implementation, we deploy a testbed consisting of three EeePC 701 netbooks each running Debian Linux with kernel version 2.6.26. Each node is equipped with an Atheros-based 802.11 interface and uses the MadWiFi driver. Stations are configured in the 802.11g mode with the 6Mbps modulation rate. This choice ensures that losses are only due to collisions rather than channel errors. In each experiment, stations are sending saturated UDP traffic towards the AP. Each experiment is repeated 5 times to compute average values of the metrics of interest with good statistical significance.
We compare the performance of L-BEB against DCF with different CW values, in terms of success rate. Note that we set AIFS to a random number from {4, 8, 12, 16} whenever a collision occurs. The results are summarized in Table 5. We conclude that L-BEB effectively convergences to a collision-free state and can potentially boost the performance of 802.11 networks even for larger deployments.

Table 5: Performance comparison of DCF and L-BEB

		Success rate, STA #1	Success rate, STA #1
DCF (AIFS=2)	CW=0	47.9%	69.1%
	CW=1	59.7%	49.2%
	CW=3	66.4%	78.7%
	CW=7	80.7%	88.1%
L-BEB	CW=0	98.1%	98.9%